Universidade de Aveiro Departamento de Engenharia Cerâmica e do Vidro
2007

Flávia Aparecida de Almeida

Diamante CVD nano- e microcristalino para corte de materiais abrasivos

Universidade de Aveiro Departamento de Engenharia Cerâmica e do Vidro
2007

Flávia Aparecida de Almeida

Nano to micrometric grain sized CVD diamond for turning hard and abrasive materials

tese apresentada à Universidade de Aveiro para cumprimento dos requisitos necessários à obtenção do grau de Doutor em Ciência e Engenharia dos Materiais, realizada sob a orientação científica do Dr. Rui Ramos Ferreira e Silva, Professor Associado do Departamento de Engenharia Cerâmica e do Vidro da Universidade de Aveiro.

Apoio financeiro do Programa Alβan – Programa de Bolsas de Alto Nível da União Europeia para a América Latina. Número de identificação: E03D06378BR.

Dedico este trabalho aos meus pais Charles Vítor de Almeida e Regina de Fátima Domingues de Almeida. Estes que, com muita paciência e amor, suportaram minha longa ausência, me apoiando incondicionalmente, sempre.

o júri

presidente

Prof. Dr. Carlos Fernandes da Silva
professor catedrático da Universidade de Aveiro

Profª. Drª. Maria Teresa Freire Vieira
professora catedrática da Universidade de Coimbra

Prof. Dr. Luís Manuel Fernandes Rebouta
professor associado da Universidade do Minho

Prof. Dr. Joaquim Manuel Vieira
professor catedrático da Universidade de Aveiro

Prof. Dr. Rui Ramos Ferreira e Silva
professor associado da Universidade de Aveiro

agradecimentos

À Deus, por colocar no meu caminho as pessoas certas na hora certa, pela força do dia-a-dia,
Ao Prof. Dr. Rui Silva pela oportunidade que me foi dada para a realização do doutoramento em seu grupo de trabalho, pela orientação, paciência, respeito e apoio, minha admiração e meus mais sinceros agradecimentos.
Ao Dr. Filipe Oliveira, nosso "sub-chefe" e braço direito, a pessoa que está connosco na realização dos trabalhos, principalmente na difícil parte dos "testes de fogo" (maquinagem).
À Drª Mercedes Vila, pela ajuda científica, amizade, sorriso sempre estampado em seu rosto e contagiante alegria "à espanhola".
Ao Dr. Manuel Belmonte, pela apoio e incentivo constantes mesmo à distância.
À todos os membros do grupo de diamante, Drª Florinda, António José, João Miguel, Ermelinda, Margarida, Micaela, Jean, Paulo, Filipa, Miguel Ângelo, Diogo, Ana Teresa, pela amizade, respeito e convívio no dia-a-dia.
Aos funcionários do Departamento de Engenharia Cerâmica e Vidro, Engª Conceição, Dr. Augusto, M.Sc. Marta, Eng. Jorge, Engª Célia, D. Maria, Alexandra, Luísa, Sofia, Paula, Sr. Costa, Sr. Otávio e Sr. Jacinto, por todo o apoio técnico e disponibilidade sempre.
À empresa Durit, especialmente ao Eng. Valente, Eng. Carvalho e Dr. Sacramento, por todo o apoio e por manter as portas abertas à investigação.
Aos funcionários Pedro Duarte, João, Pedro (EDM), Andreia (laser), Sr. Alves, Sr. Sá, Sr. Agostinho, Sr. Antunes, Sr. Serafim, Sr. Guerra, Eng. Teresa, Eng. Jorge, Eng. Carlos, que directa ou indirectamente estiveram envolvidos na realização dos trabalhos na empresa.
Aos amigos e ex-colegas de trabalho do Brasil que tiveram papel fundamental na minha vinda à Portugal e também durante meu doutoramento, Dr. Francisco Cristóvão de Melo (AMR/CTA), Ten. Cel. Eng. Cosme Roberto Moreira da Silva (UnB), Dr. Aparecido dos Reis Coutinho (UNIMEP), Dr. Evaldo Corat (INPE), Drª Neidenei Gomes Ferreira (INPE), Drª Mirabel Cerqueira de Rezende (AMR/CTA), Dr. Edson Cocchieri Botelho (UNESP), Drª Alessandra Diniz Ronconi (INPE), Drª Adriana Faria Azevedo, M.Sc. Cláudia R. Miranda, M.Sc. Neila A. Braga, M.Sc. Divani Barbosa, M.Sc. Sandra C. Ramos, M.Sc. Manoel Méndez, M.Sc. Tanila Penteado de Faria (Embraer), M.Sc. João Marcos Kruszinski de Assis (AMR/CTA), Lic. Luciana Baptista e Roberta Marson (AMR/CTA) dentre tantos amigos que não caberiam nessa página, minha sincera gratidão, amizade, respeito e carinho sempre.
Às minhas irmãs, Claudia Domingues de Almeida Dutra e Vanessa Domingues de Almeida, pelo apoio à distância, conversas no msn, por me manterem sempre informada sobre os acontecimentos da nossa família de forma a me sentir mais presente.
Ao meu sobrinho Guilherme de Almeida Dutra, que conheci já com seus 2 aninhos e meio, um super beijo da tia coruja e meu muito obrigada por nossas conversas e canções através da internet e webcam.
Ao meu namorado Manuel António da Silva, pelo seu carinho, ensinamentos científicos valiosos, paciência e companheirismo em todas as fases da realização do doutoramento.

palavras-chave

Diamante CVD, nitreto de silício, adesão, desgaste, rugosidade, ferramentas de corte.

resumo

O presente trabalho consistiu no desenvolvimento de ferramentas de corte de diamante CVD (Chemical Vapour Deposition) obtido na forma de revestimento em materiais cerâmicos à base de nitreto de silício monolítico (Si_3N_4) ou compósitos nitreto de silício-nitreto de titânio (Si_3N_4-TiN). A adição de TiN acima de 23 vol.% conferiu conductividade eléctrica ao compósito, na ordem de $1\times10^{-1}\ \Omega^{-1}.cm^{-1}$, possibilitando a sua maquinagem por electroerosão.

Duas técnicas foram utilizadas para o crescimento dos filmes de diamante: deposição química em fase vapor por plasma gerado por microondas, MPCVD (Microwave Plasma Chemical Vapour Deposition), e por filamento quente, HFCVD (Hot Filament Chemical Vapour Deposition). Previamente os substratos cerâmicos sofreram uma preparação superficial por diversos métodos: rectificação por mós diamantadas; polimento com suspensão de diamante (15μm); ataque da superfície por plasma de CF_4; riscagem manual ou por ultra-sons com pó de diamante (0.5-1.0 μm).

A caracterização das ferramentas revestidas envolveu: o estudo da qualidade e tensões residuais dos filmes de diamante a partir da difracção dos raios X e espectroscopia Raman; a análise da respectiva microestrutura e medida da espessura por microscopia electrónica de varrimento (SEM); a determinação dos valores de rugosidade dos filmes por microscopia de força atómica (AFM); e a avaliação da adesão dos filmes aos substratos por indentação com penetrador Brale.

Foram obtidos filmes com granulometria que variaram da gama do diamante nanométrico (< 100 nm) até ao micrométrico convencional (3-12 μm), com consequências na rugosidade superficial do filme. Os filmes de diamante CVD apresentaram espessuras de 15 a 150μm. Os revestimentos apresentaram elevada adesão ao substrato, sendo que o melhor resultado foi atingido pelo diamante micrométrico, suportando um limite de carga aplicada de até 1600 N.

O estudo do comportamento em serviço das ferramentas foi efectuado na operação de torneamento de metal duro (WC-Co) e de eléctrodos de grafite, com medição de forças de corte em tempo real por meio de um dinamómetro. Os ensaios foram realizados num torno CNC, em ambiente industrial, na empresa Durit (Albergaria-a-Velha), produtora de metal duro. Os modos de desgaste das ferramentas foram avaliados por meio de observação em microscopia óptica e electrónica de varrimento e o grau de acabamento da superfície maquinada por rugosimetria. A influência destes parâmetros foi estudada em termos das forças envolvidas em operações de torneamento, desgaste das ferramentas e do acabamento conferido à peça maquinada.

Os melhores resultados do torneamento de metal duro foram atingidos pelas ferramentas com geometria de aresta em quina-viva, recobertas com os filmes de diamante de 100-200 nm de tamanho de grão, correspondentes às menores forças de corte (<150N), melhor qualidade da peça maquinada (rugosidade aritmética igual a 0,2 μm) e menor desgaste (flanco igual a 110μm). No torneamento de eléctrodos de grafite, as forças de corte foram baixas (< 20N), sendo que o principal modo de desgaste foi a formação de cratera na superfície de ataque (valor máximo igual a 22 μm). O fio da aresta de corte permaneceu inalterado (devido ao mínimo desgaste de flanco), sendo que as diferentes granulometrias do diamante não tiveram influência significativa no comportamento geral das ferramentas.

keywords CVD diamond, silicon nitride, adhesion, wear behaviour, roughness, cutting tools.

abstract This work consisted on the development of CVD (Chemical Vapour Deposition) diamond cutting tools directly deposited on monolithic silicon nitride (Si_3N_4) based ceramics and silicon nitride-titanium nitride composites (Si_3N_4-TiN). A TiN content higher than 23 vol.% confers electric conductivity to the composite in the order of $1\times10^{-1}\ \Omega^{-1}.cm^{-1}$, making possible its machinability by means of electrodischarge machining.
Two techniques were used for diamond growth: Microwave Plasma Chemical Vapour Deposition (MPCVD) and Hot Filament Chemical Vapour Deposition (HFCVD). The substrate pre-treatment steps prior to diamond deposition were: grinding with diamond wheels; polishing with diamond suspension (15μm); chemical etching with CF_4 plasma; manual scratching or ultrasonic bath scratching with diamond powder (0.5-1.0 μm) for seeding purposes.
The diamond cutting tools characterization involved: study of the quality and the residual stress of the films by X ray diffraction and Raman spectroscopy; analysis of respective film microstructure and measurement of film thickness by scanning electron microscopy (SEM); quantification of film surface roughness by atomic force microscopy (AFM); evaluation of adhesion strength of the thin films to Si_3N_4 substrate by the indentation technique with a Brale indenter.
The grain size of the films varied from nanometric (< 100 nm) to conventional micrometric (3-12 μm), therefore giving different surface roughness. The CVD diamond film thickness was in the range of (15-150 μm). The diamond films presented a high adhesion level to the Si_3N_4 ceramic substrates, the best results being achieved by the micrometric grain sized film, which undergo a normal load of until 1600N.

The study of the cutting tool behaviour was performed in turning operations of hardmetal (WC-Co) and graphite electrodes, by real-time acquisition of the cutting forces using a dynamometer. The turning operations were carried out in a CNC lathe, at industrial environment of a hardmetal producer company, Durit (Albergaria-a-Velha). The wear modes of the tested cutting tools were analysed by optical and electronic microscopy observations and the finishing quality of the machined workpiece was measured by surface roughness measurements. The influence of these parameters was studied in terms of the cutting forces developed during turning operations, of tool wear and of the finishing quality of the machined workpieces.

The best results attained in hardmetal turning were achieved by the cutting tools with sharp edges, covered with diamond films of 100-200 nm of grain size, which presented the lowest cutting forces (<150N), the best workpiece surface quality (Ra=0.2μm) and the lowest flank wear (110μm). In graphite turning, the cutting forces were very low (<20N) and the main wear mode was the crater one on the rake face (maximum value of 22μm). The cutting edge remained almost intact (due to the minimum flank wear) while the different diamond grain sizes did not have a significant influence on the overall cutting behaviour.

A worker may be the hammer's master, but the hammer still prevails. A tool knows exactly how it is meant to be handled, while the user of the tool can only have an approximate idea.

Milan Kundera

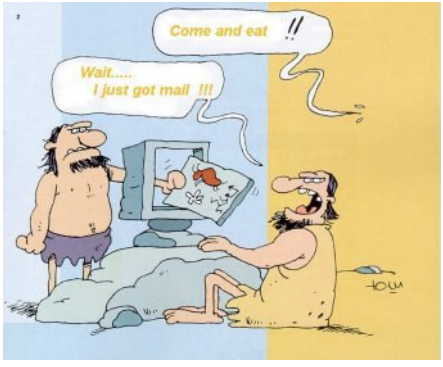

A Idade da Pedra não terminou por falta de pedra… mas pela necessidade de transformação.

Renata Dainese

INDEX

Foreword

The continuous improvement of materials properties leads the cutting tools researchers to find out economical and reliable solutions for the success of their products in today's very competitive markets. For instance, automotive and aeronautic industries are employing lightweight materials such as hypereutectic aluminium-silicon alloys, carbon and glass fibre-reinforced composites and aluminium-silicon carbide metal-matrix composites, which offer better mechanical behaviour, along with economy in energy consumption. However, many of these materials are very abrasive and difficult-to-machine, becoming impractical the use of conventional cutting tools. Another example is the use of hardmetal (mainly WC-Co) for metal forming tools like in deep-drawing or in rolling process, which demands new superhard tools for WC-Co parts shaping. Graphite electrodes for electrical discharge machining (EDM) are difficult-to-shape due to the abrasiveness or their polycrystalline nature and strong anisotropy, requiring the use of adequate cutting tools to ensure the tight tolerances.

The most common superhard tools are polycrystalline diamond (PCD) and polycrystalline cubic boron nitride (PCBN). PCBN tools are used mostly for machining hard ferrous materials whereas PCD tools are used for non-ferrous alloys and composites that are difficult-to-cut. Due to the high costs involved in HPHT (High Pressure High Temperature) manufacturing and in tool finishing, PCD and PCBN tools are very expensive. The relatively new diamond grade manufactured by chemical vapour deposition technique (CVD) uses mainly hydrogen and methane at low pressure and low temperature to produce high quality diamond at lower costs than that with HPHT technique. So, it is being more and more established as an economically and attractive way for diamond cutting tools production. Comparatively to PCD, CVD diamond is harder, better corrosion and wear resistant, and presents higher thermal conductivity since it has no Co binder. To offset these advantages, the absence of Co binder decreases the fracture toughness and also the electrical conductivity. This means that CVD diamond can not be cut by EDM, but by alternative ways, like laser or ultrasound cutting. However, as a consequence of the Co absence, the CVD diamond is more refractory, so higher cutting velocities can be used.

The main objective of the research presented in this thesis is the development and real testing of CVD diamond cutting tools in turning of highly hard and abrasive materials, like hardmetal and EDM graphite. The workpiece surface finishing/tolerances and tool

wear mechanisms, which determine the performance of the cutting tool, are evaluated. The turning tests were done in industry environment, due to the association of a hardmetal producer, Durit, located at Albergaria-a-Velha, district of Aveiro, Portugal.

This thesis is a compilation of scientific papers, published or accepted to publish, in relevant journals of this research area. The introductory Chapter 1 resumes the background on the cutting tools subject. It starts with a brief presentation of the historical evolution of cutting tool materials, followed by a description of the currently available diamond tools. Moreover, an introduction about machining terminology, chip formation, cutting forces and tool wear is given. Chapter 2 reports the preparation of the silicon nitride based ceramic cutting tools, from powder processing to the surface finishing step, and their mechanical, electrical, and microstructural characterization. A detailed description of the chemical vapour deposition (CVD) of diamond is given in Chapter 3, regarding the optimization of deposition parameters and physical characterization. Chapter 4 groups the papers on the cutting behaviour of the diamond coated tools and their wear mechanisms in real turning of different hardmetal and graphite workpieces. Chapter 5 resumes the main conclusions of this thesis and, finally, the perspectives of future work are proposed in Chapter 6.

Background

Chapter 1

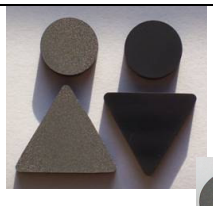

1.1 *A brief history of the evolution of the cutting tools*

Carbon steels were the only tool materials for metal cutting from the beginning of Industrial Revolution until the1860s. These consist essentially of iron alloyed with 0.8 to about 2wt% carbon, the other alloying elements present – manganese, silicon, sulphur and phosphorus – being impurities of additions to facilitate steelmaking[1]. Although these materials display high fracture resistance, the low hardness and low wear resistance limit their wear life in industrial machining of metals and highly abrasive materials[2].

The introduction of the high speed steels (HSS), which use alloying elements to improve the mechanical properties of tool steel, was first made public in 1868 by Robert Mushet[1]. This contained about 6 to 10wt% tungsten and 1.2 to 2wt% manganese and, later, 0.5wt% chromium, with carbon contents of 1.2 to 2.5wt%[3]. By 1906 the optimum composition was: 0.67wt.% C; 18.91wt.% W; 5.47wt.% Cr; 0.11wt.% Mn; 0.29wt.% V; Fe balance. High-speed steel is superior relatively to the older high carbon steel tools as it can withstand higher temperatures without losing its tempered structure. This property allows HSS to cut faster than high carbon steel, hence the name *high speed steel*. At the same time, other cutting tools materials were developed, namely nonferrous cast alloys containing varied amounts of Cr, W, C, and Co.

The development of cemented carbides by the powder metallurgy process at the 1920s led to a revolution of the machining industry[3]. The first industrial production of sintered tungsten carbide (or hardmetal) was in 1926 by the German company *Fredrich Krupp A. G.*, with the name Widia (wie Diamant – "like diamond"). In 1928, the *General Electric Company* (USA) started to produce the *Carboloy* hardmetal. The combination of very hard, high wear resistant tungsten carbide with a tough binder, usually cobalt (WC-Co), results in a completely consolidated material presenting suitable properties for cutting tool applications, such as mechanical resistance, hardness and toughness. To increase the mechanical and tribological properties at high temperature as, for instance, the hot hardness, titanium and tantalum carbide can be added to the WC-Co[3]. Although WC-Co cutting tools have lower fracture resistance than HSS, their mechanical properties are suitable for a very wide range of heavy-duty applications, allowing cutting speeds three to five times higher than that with HSS[2,3].

During the Second World War, the British side used a new cutting tool material, previously studied in Germany and Soviet Union, getting superior cutting speeds than that with hardmetals. This material was a ceramic aluminium oxide, Al_2O_3, with a commercial designation of "Degussit" (Degussa, Germany)[4,5]. The major advantages were: retention of hardness and compressive strength to higher temperatures than with carbides; high resistance do crater formation; much lower solubility in steel than any carbide, as it is practically inert with steel up to its melting point. Opposed to these advantages, its toughness and strength in tension are much lower. Many additives, e.g. MgO and TiO_2, can be used to promote densification while retaining a fine grain size. In order to increase the fracture toughness, ceramic composite tool materials consisting of alumina with 30% or more of a refractory carbide - usually TiC or (Ta,Ti)C – have been commercially available since the 1960s[1]. Also, the addition of ZrO_2 to alumina matrix and, more recently, the use of SiC whisker reinforced alumina are significant alternatives to improve the fracture toughness mechanisms of alumina based cutting tools[5].

Synthetic diamond has been produced since the early 1950s by heating graphitic carbon with a catalyst at temperatures and pressures of the order of 1500ºC and 8 GPa, respectively[1]. This process is usually called the HPHT process (High Pressure-High Temperature), and the credits of this discovering were given to scientists of the General Electric Company[5]. This same process also made possible the transformation of cubic boron nitride (cBN), from hexagonal form to a structure like diamond.

Following the introduction of the synthetic diamond grit, the 1970s yielded the polycrystalline diamond cutting tool material – PCD[6]. PCD tools microstructure consists of randomly oriented diamond particles and a catalytic second phase (metallic and/or ceramic-based system) that forms a solid material by HPHT method. A layer of consolidated PCD, usually 0.5 to 1.0 mm thick, is bonded to a cemented carbide insert. A range of PCD tools is available, with diamond grain sizes from 2 to 25 μm, and the diamond to bonding agent ratio can also be varied for different applications[1]. The introduction of this cutting tool material opened up the field of machining abrasive non-ferrous materials with defined cutting edge tools, for example turning and milling[6].

PCBN (polycrystalline cubic boron nitride) was developed soon after PCD for machining hard ferrous materials, such as hardened steels and grey cast iron[5]. These applications are due to the resistance to chemical dissolution in iron (in contrast to diamond), in addition to the excellent abrasion wear resistance[1]. Likely to PCD manufacture procedure, the resultant microstructure is composed of cubic Boron Nitride (cBN) crystals and a metallic/ceramic second phase consolidated by HPHT process. As the second hardest material after diamond, and possessing a high importance on the manufacture industry, nowadays special attention has been given in the preparation of cBN thin films by less expensive chemical and physical vapour deposition, CVD and PVD routes, respectively[7-9].

The deposition of TiC and TiN hard coatings was firstly developed by the chemical vapour deposition (CVD) process in Germany, in 1953[10]. At the end of the 1960s, TiC-coated cemented carbide and high-speed steel tools become commercially available and at the begging of 1970s coatings of TiN, Ti(C,N), and Al_2O_3 monolayers were presented [2,10]. The high-temperature wear resistance, better corrosion resistance and hardness of these advanced ceramic coatings coupled with superior fracture resistance of the underlying body, played a key role in the furthering performance of commercial cutting tools. The development of multilayer and gradient structures began between 1972 and 1974[10]. The combination of different coating materials, each one appropriated for different applications, enlarged the universal applicability of these coatings and improved the resistance against complex wear loads. Nowadays, since the 1990s, most of these coatings are produced by physical vapour deposition (PVD) method. The PVD process is carried out at lower temperatures, typically around 350-500ºC, avoiding substrate phase transformations that could occur at high CVD coating temperatures[10].

At the 1980s, TiC and TiN cermets (their name derived from *cer*amic materials with a *met*allic binder) started to be commercialized as cutting tools. The production route, the powder metallurgy method, is the same as for tungsten carbide, and uses mainly molybdenum and nickel as binder material[3]. They are more effective material for machining steels at higher cutting speeds than some tungsten carbides, as they are wear and crater resistant to the continuous chip formation of steels[5]. Cermets hardness is superior to the average hardness of tungsten carbides, but their shock resistance is lower[3].

Cost benefits are achieved with higher productivity through higher cutting speeds and longer tool life, besides the fact that cermets are about 20% lower in cost than coated carbide[5].

Also in the 1980s decade, cutting tools made of advanced covalent ceramics as silicon nitride (Si_3N_4), SiALON (Si-Al-O-N) and silicon carbide (SiC), in monolithic form or as composites, were developed. SiC particles are used as second phase in Si_3N_4 tools, improving the creep resistance[11] and increasing the hardness of the composite relatively to the monolithic material[12]. Si_3N_4 is widely used for machining cast iron because of its high abrasion resistance[5]. In addition, Si_3N_4 has a low thermal expansion coefficient (responsible for the high thermal shock resistance), a high thermal conductivity (which confers high resistance to thermal fatigue), good fracture toughness and a very high chemical stability[1,5]. These tools are nowadays of great interest for the CVD diamond film deposition, because of referred low thermal expansion, which is near to that of diamond, together with their chemical compatibility. These are some of the important properties of Si_3N_4, which will be further evidenced in this thesis. SiAlONs are solid solutions between silicon nitride and alumina, where the presence of alumina provides improved resistance to oxidation[5]. These substrates are also used as substrates for CVD diamond coatings[2].

The growth of diamond crystals by low pressure CVD technique was first documented in 1952, almost at the same time of the development of HPHT method, by William Eversole of Union Carbide[13]. Nevertheless, the process was dismissed by most researches because the growth rate was very low, since graphite was co-deposited with the diamond leading to impure mixed phases[14]. In 1968, the Angus' group was able to improve the diamond growth rate by including hydrogen in the carbon-containing gases[15]. They discovered that the presence of atomic hydrogen during the deposition process lead to preferential etching of graphite, rather than of diamond. Initially, the process deposition was restricted only to discrete diamond grains grown over pre-existent diamond grains. Nowadays, a great variety of materials can be used as diamond film substrates. The commercial availability of synthetic diamond cutting tools made by CVD route took place at the beginning of 1990s in two product forms: thick-film freestanding CVD diamond cutting tool tips and thin-film CVD diamond coatings[2,16]. The first form is produced by depositing a thick layer (from 150-1000μm) of diamond on Si or Mo wafers, detached

from the substrate and cleaned with acid solution. The next step is the laser cutting of the free-standing diamond wafer in tool tips that are brazed to a steel or hardmetal body/insert tool. Finishing is made by grinding/polishing procedure of the tool cutting edge with the desired radius and edge angle. The second one is made with fewer steps, by direct deposition of diamond films on a suitable substrate, as silicon nitride, silicon carbide and, the commercially more common, cemented carbide (WC-Co) with Co content lower than 6 wt.%. The thickness is generally in the range of 5 to 50 μm. Although the second form is the simplest one, the problems with adhesion mainly on WC-Co substrates delayed the progress of the diamond direct coated tools. So, this kind of diamond cutting tool fabrication has been much investigated and is in continuous improvement. Some examples of the metallic and non-metallic materials along with their associated machining challenges, which justify the use of the diamond tools, are listed in Table 1.

The development of successful brazing techniques for thick-film diamond in the early 1990s bypassed the adhesion and substrate selection challenges of thin-film CVD diamond tools and it was faster absorbed by the machining industry[2]. One of the biggest diamond producer, De Beers, has been commercializing the free-standing thick-film CVD diamond since 1992, with the name of DIAFILM[17]. Direct coated CVD diamond tools became commercially available as prototypes also in the early 1990's using silicon nitride, silicon carbide or tungsten carbide substrates[18-21]. As said before, the reason for the fairly slow progress of the thin-film CVD diamond coated tools is due to the unsatisfactory and inconsistent adhesion between the diamond coating and the substrate, especially cemented carbide, and great progress on different methods of mechanical and chemical substrate surface pretreatments has been made[22-25].

Table 1. Examples of difficult-to-cut machine composite materials (adapted from [2])

Material	Example	Example of use	Machining issues
Hypereutectic silicon-aluminium alloy	A390 (18 wt.% Si particles in Al matrix)	Reduced-weight, wear resistant, temperature-resistant pistons	Hard silicon particles are extremely abrasive
Metal matrix composites (MMC)	Duralcan (20wt.% SiC in Al matrix)	Brake rotors, light-weight structures	Hard SiC ceramic particles are extremely abrasive
Cemented tungsten carbide	WC- 25wt%Co (sintered WC grain in Co based alloy matrix)	High-fracture-toughness wear parts, mould industries	WC grains are very hard and strong bonded. The Co metal binder can react with the carbon in diamond
Structural aerospace composites	Carbon-epoxy (high density carbon fibres in epoxy polymer)	Stiff and light-weight support structures for commercial aircraft, strong and light-weight sporting goods	Carbon fibres are extremely abrasive
Glass fibre reinforced polymers (GFRP)	G10 (highly compressed fibre glass in epoxy polymer matrix	Light-weight, insulative circuit boards, low-cost structural composites	Glass fibre induce abrasive tool wear; polymer can cause corrosive (chemical) tool wear
Graphite	ISO 88 polycrystalline graphite	Electrodes to electrodischarge machining process (EDM) in mould industries	Abrasive aggregates of polycrystalline graphite are formed during machining and wears the cutting edge parts

There is some divergence about the thin-film CVD diamond coating tool performance, which denotes the need for the improvement of this kind of tool. The tool life would span an order of magnitude in terms of cutting time, with some tools wearing at about the same rate as that of a PCD tool[26]. Shen[26] tested thin film diamond coated indexable WC-Co and Si_3N_4 ceramic inserts from a large number of sources in dry machining of the hypereutectic A390 (18wt.% Si) aluminium alloy. He associated the different adhesion strengths with the reflected differences in the turning performance. Among the tools tested, two or three coatings sources were able to have good film-to-substrate adhesion and a machining performance comparable to that of the PCD inserts. When comparing the flank wear of these tools at the same cutting conditions, he found a great inconsistency even within a batch or among batches by the same coating source. Uhlmann and co-workers[27] compared Si_3N_4 and WC-Co diamond coated tools in turning, milling and drilling of AlSi and AlCu alloys, and a fiber-reinforced polymer. They show that, in turning operations, the diamond coated silicon nitride tools provide the higher wear resistance, increasing the tool life and enlarging the usable cutting speed range. For milling, in some cases, and in all cases for drilling, the diamond coated WC-Co tools presented the best performance because of the high thermo-mechanical stress imposed to the tools in such operations. In a study carried out by Uhlmann and Brucher[28] with thin film diamond coated and thick brazed films tools in machining of the same AlSi alloy, the authors arrived to different conclusions. They found that the thick brazed films could be successfully used with a tool life of 7 min (wear criteria adopted of VB=0.2mm), while it was not possible to conduct tool life tests on both WC-Co and Si_3N_4 ceramic coated tools due to the occurrence of film delamination after cutting times of only 30s. These results contradict the previous work above mentioned, which reports values of 50 min of tool life adopting the same wear criteria. The turning parameters were similar concerning to cutting speed, but differ on feed and depth-of-cut conditions. In the first work, these parameters were: 0.04 and 0.8mm for feed and depth, respectively, while in the second they were: 0.1 and 0.5mm. D'Errico and Calzavarini[16] reported the turning of metal-matrix composites (MMC) based on SiC (20wt.%) reinforced Al matrix (Duralcan) with CVD thick diamond brazed (~500 μm) and thin-film coated WC-Co (20-50 μm) from different sources and compared with PCD tools. They concluded that the thick film can be considered as a competitor for PCD by its superior wear resistance (binder-free, pure diamond

construction), reducing the tendency for diamond grain "pullout" when eroded by the SiC particles. On the other hand, the thin coated tools failed by coating delamination after a very short cutting time (the average was 10 s). More recently, Chou and Liu[29] demonstrated, in turning of the same MMC material with diamond coated WC-Co tools, that adjusting the cutting parameters (mainly diminishing the feed), the film could delay the onset of tool failure by film delamination from few seconds until almost 15 minutes, although all the tested tools failed by this way before reaching a tool life criteria by abrasion. Another problem addressed in that work was the adhesion of the work material on the asperities of the diamond film, which forms a built-up-edge (BUE) formation on the rake face. This can be very harmful to diamond coatings, since it can also cause chipping at the cutting edge of the tool when the adhesive junctions are broken[26].

Nevertheless, direct comparisons and conclusions seems to be very difficult to be assumed since the properties of both diamond coatings and substrates, as well as their manufacturing process (substrate characteristics, surface pretreatments, diamond deposition conditions) certainly differs from producer to producer, affecting the overall quality of the final product. In addition, other factors as cutting parameters, cutting conditions (lathe stability, use and type of lubricant), workpiece characteristics (mechanical properties, homogeneity, dimensions) will direct affect the machining performance of a tool.

Friction between the tool/workpiece contact zones is influenced by the nature of the materials pairs, but also and in a great extent by the quality of the cutting edge, namely the tool surface roughness. A number of techniques were developed to polish the free surface of diamond films, as mechanical[30], thermo-mechanical[31], thermo-chemical[32] and laser[33]. But the stress imposed by some of these techniques as well as the time spent and the complexity of the equipments needed led to the development of diamond film growth with controllable grain texture and/or very small grain sizes, in order to diminish the inherent roughness created by columnar structure of the CVD growth[34]. The development of the "nanocrystalline diamond" (NCD) films is clamed to be the best solution for mechanical and tribological applications. Although just few works concerning the uses as cutting tools are available, they show a very promising prospective in cutting AlSi[35,36] alloys and GFRP[36].

There is a very strong global trend to minimize the use of fluids (lubricants/coolants) in metalworking industries because of industrial pollution, health problems and costs[26]. In this way, CVD diamond tools are the most promising to be used in "dry" conditions, since they gather key properties as low friction, low chemical affinity to non-ferrous materials, high thermal conductivity and anti-sticking properties (because of the absence of Co binder). Nevertheless, the use of coolants is of major importance to control the temperature of the workpiece, especially when high tolerances have to be achieved, at the same time it facilitates chip evacuation and diminishes the tool wear.

The increasing world consumption of industrial diamond justifies the growing investments in research and enlargement of production scale capabilities. The United States remains the world's largest market for industrial diamond, with an increasing of about 21% from 2001-2005 and account almost exclusively for the world growth of about 10%, as can be seen on Table 2 [37]. Among the major consuming industries are: machinery manufacturing, mining services (drilling) and transportation systems (vehicles)[38]. For instance, the manufacturing of every automobile made in USA consumes 1.5 carats of diamond. Other important fields include close-tolerance machining of composite parts for the aerospace industry, heat sinks in electronic circuits, lenses for laser radiation equipment, and products manufacturing for the computer industry[38]. Among the main world sellers of CVD diamond coatings producers and diamond cutting tools are: Element Six, CemeCon AG, DiaCCon, sp^3 diamond technologies, Advanced Diamond Solutions Inc., Diamond Tool Coating, Delaware Diamond Knives Inc., Iljin Diamond Co. Ltd and Crystallume. This last company has an on-line catalogue[39], with direct coated inserts on WC-Co varying from 45 to 200 $ each insert, concerning shape geometry and size.

Table 2. Synthetic diamond: estimated world production by country (thousand carats).[37]

Country	2001	2002	2003	2004	2005
Belarus	25,000	25,000	25,000	25,000	25,000
China	17,000	17,000	17,000	17,000	17,000
Czech Republic	5	5	5	5	5
France	3,000	3,000	3,000	3,000	3,000
Ireland	60,000	60,000	60,000	60,000	60,000
Japan	33,000	34,000	34,000	34,000	34,000
Russia	80,000	80,000	80,000	80,000	80,000
South Africa	60,000	60,000	60,000	60,000	60,000
Sweden	20,000	20,000	20,000	20,000	20,000
Ukraine	8,000	8,000	8,000	8,000	8,000
United States	202,000	222,000	236,000	252,000	256,000
Total	508,000	529,000	543,000	559,000	563,000

1.2 *Some concepts about machining*

In product manufacture processes, such as metal casting and ceramics sintering, there are great efforts to make components with a very near net shape. However, these parts usually need further machining operations to achieve a specified dimensional tolerance, which is dictated by their applications. For example, in the metallic parts submitted to heat treatment, the formed outside layer is generally fragile and need to be removed before utilization. Quality and cost-effective aspects are very dependent on choosing the appropriated machining operations together with adequate tools. Thus, the improvement of the performance of machining operations is an economically important objective. The term *machining* is used for the operations which confer to the workpiece the shape, dimensions, surface finishing, or a combination of these three conditions that involve chip formation[3]. Examples of such process are turning, grinding, drilling and milling, schematically presented in Fig. 1:

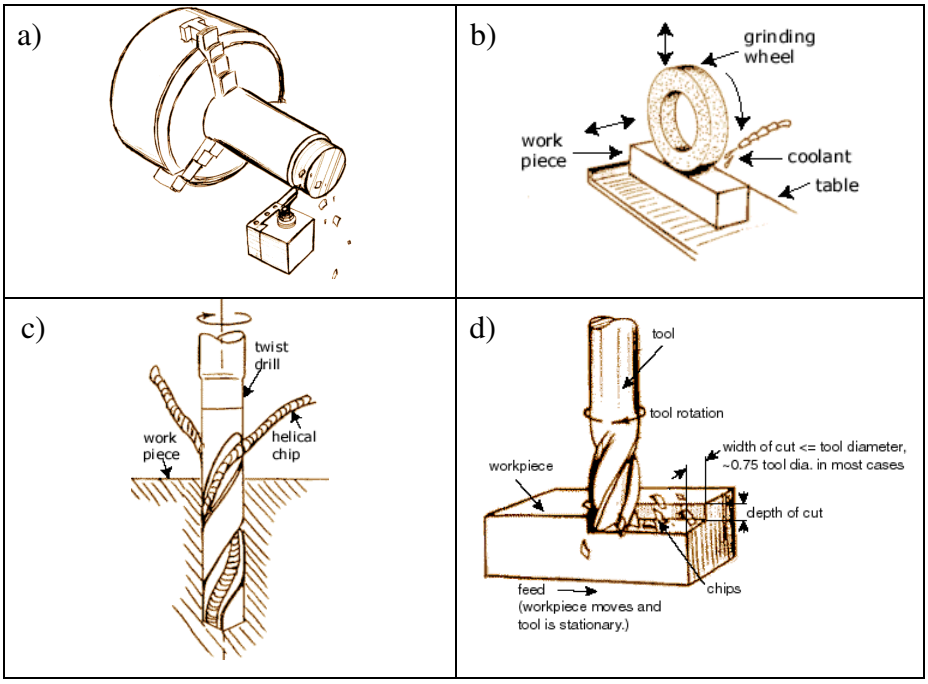

Fig. 1. Examples of machining process: a) turning; b) grinding; c) drilling and d) milling. [40]

The production costs concerned to machining process involve several contributions, like cutting tools, lathe maintenance, cutting fluids, energy/manpower, among others. The distribution of the production costs variables is presented in Fig. 2:

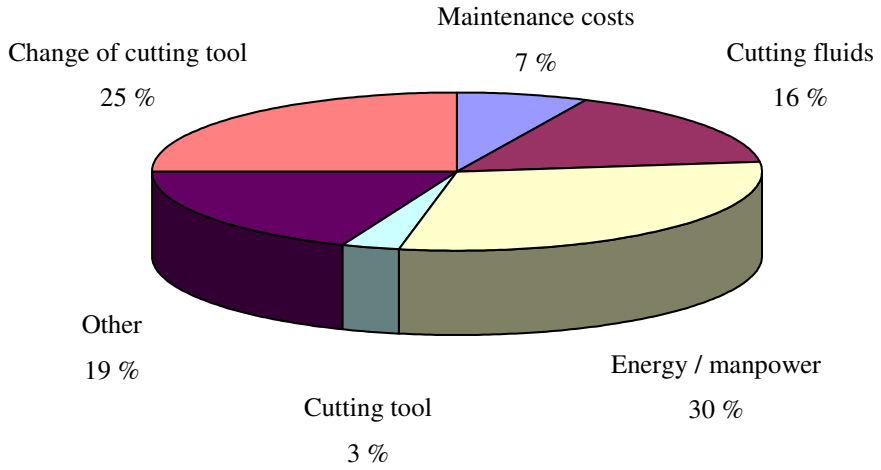

Fig. 2. Division of production costs by machining (adapted from[41]).

Despite the fact that only 3% of the total machining costs are directly related to the cutting tool, costs involving the down-time with the replacement of the cutting tool along with the energy/manpower are the most important factors contributing to the final cost. The use of incorrect cutting tool materials and/or cutting parameters will certainly cause high wear rate, consequently diminishing the tool life and so, the replacement by a new tool has to be made more frequently. It also implicates an undesired workpiece finishing and/or bad tolerances and so, the workpiece is rejected, contributing to the fraction "others" of the total machining costs pie.

The turning process is possibly the more adequated way for studying the thermo-mechanical solicitation suffered by the tools as well as their tribologycal response and was thus chosen for evaluate the quality of the tools developed in this thesis.

1.2.1 - Turning

Turning is used to obtain solids of revolution using a single point cutting tool by the combination of basically two movements: rotation of the workpiece (material to be machined) and feed movement of the tool [3,42]. The workpiece is grasped in the chuck of a lathe and rotated while the tool is held rigidly in a tool post and moved at a constant rate along the axis of the bar, cutting away a layer of material to form a cylinder or a surface of more complex profile[1]. Fig. 3 schematically presents the workpiece and cutting tool position.

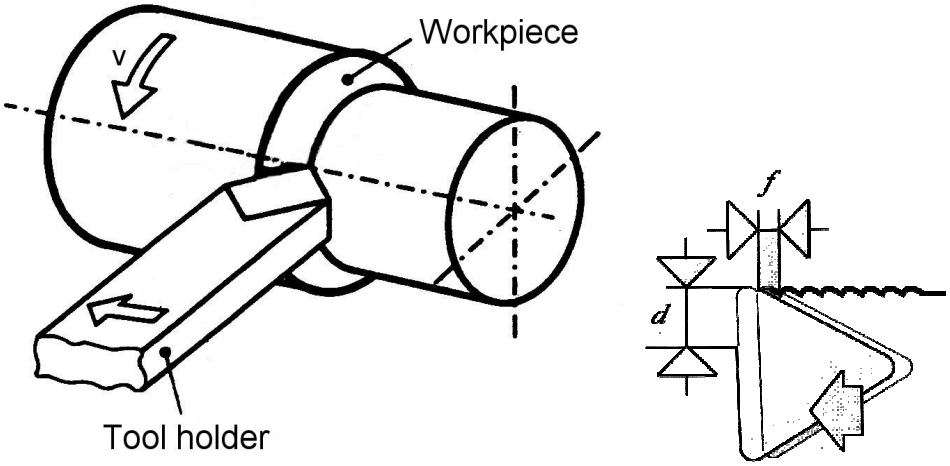

Fig. 3. Turning operation and main process parameters.

Cutting speed (v), *feed (f)*, and *depth of cut (d)* are some of the terminology used in turning operations, constituting the main parameters in the process (Fig. 3). *Cutting speed* is defined as the rate (or speed) at which the uncut surface of the workpiece move passes the cutting edge of the tool [1], expressed in metric units as $m \cdot min^{-1}$. In another words, it is the speed at which the periphery of the cut diameter passes the cutting edge, given by the Eq. 1:

$$v = \frac{\pi \times D \times n}{1000} \qquad \text{Eq. 1}$$

where: v = cutting speed ($m \cdot min^{-1}$);

D = workpiece diameter (mm);

n = number of revolutions per minute (rpm).

A number of factors can affect the cutting speed, including workpiece material, cutting tool material and cooling conditions. The choice of the right cutting speed is also influenced by the economical life of the cutting tool, namely the cost to regrind it or acquire a new one when compared to the quantity of parts produced, always respecting the required tolerances. The rigidity of the lathe is another factor that affects the calculation of the cutting speed, taking into account the reduction in vibration. Some problems that can occur due to the incorrect choice of cutting speed are related in Table 3 [43]:

Table 3. Some problems in the incorrect choose of the cutting speed.

Higher speed	Lower speed
1. Loosening of the mechanical properties, as hardness and toughness, by the overheating of the tool.	**1.** Cut overloading, causing cutting tool failure and even the rejection of the machined workpiece.
2. Changing of the workpiece shape and dimensions accuracy by its overheating.	**2.** Low machine lathe ability due to its underuse, also causing low production efficiency.
3. Premature wear and/or failure of the cutting tool.	

The *feed* is the distance covered by the tool in an axial direction at each workpiece revolution[1], expressed in metric units as $mm \cdot rev^{-1}$. When the tool passes in a given feed rate, feed marks are left on the workpiece. So, the input value of the feed motion is the first parameter to be considered on the determination of the machined surface quality.

The *depth of cut* is the thickness of material removed from the piece in a radial direction[1], given in mm. The product of these three parameters, cutting speed, feed and depth of cut, gives the rate of material removal, a parameter often used to evaluate the efficiency of the cutting operation.

There are four basic turning operations (Fig. 4) [42]: longitudinal turning (1), facing (2), round profiling (3) and copying at angles (4). Turning processes can be used either for roughing and finishing purposes. It is common to start with successive passes using as high feed and depth of cut as permitted by the cutting tool and the workpiece (rough turning), and the last pass with low values of depth of cut and mainly feed (finish turning).

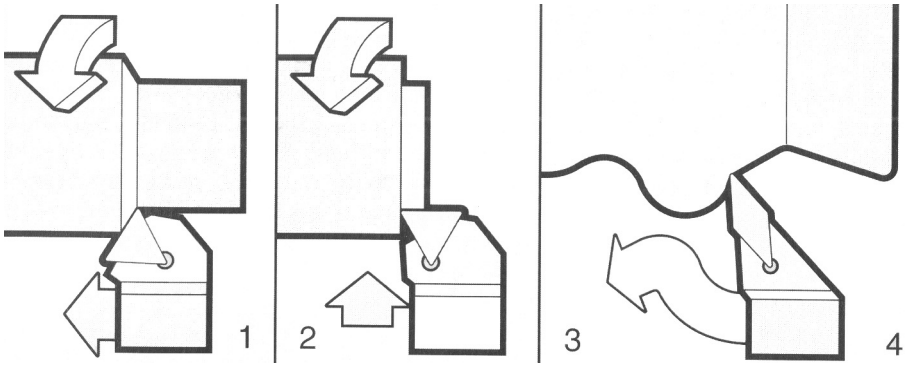

Fig. 4. Four basic turning operations: (1) longitudinal turning; (2) facing; (3) round profiling; (4) copying at angle.[42]

1.2.2 – Cutting tool terminology

The cutting edge of a cutting insert is formed by the intersection of the *rake face* with the *clearance* (or *flank*) *face* (Fig. 5). Rake face is the surface of the tool over which the chip flows, whereas the clearance face is at contact with the freshly cut surface of the workpiece[1]. The tool is positioned in such angle that the clearance face dos not rub against the workpiece. This angle often varies in a range of 6 to 11º. The rake face is inclined at an angle to the axis of the workpiece and can be adjusted to achieve optimum cutting performance for particular cutting tools, workpieces and cutting conditions[1]. The rake angle can be positive, zero or negative, relatively to the line parallel to the axis of rotation of the workpiece, as shown schematically on Fig. 6.a, Fig. 6b and Fig. 6c, respectively.

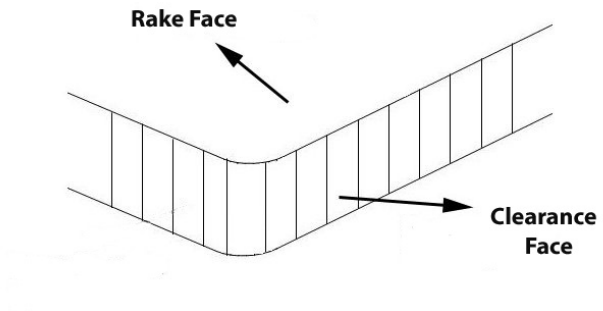

Fig. 5. Rake and clearance faces of a tool.

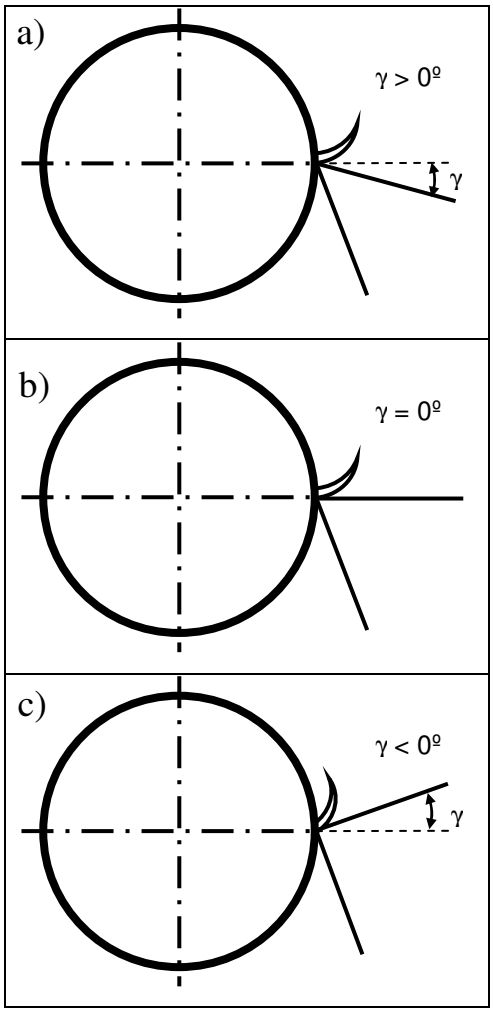

Fig. 6. a) positive; b) zero and c) negative rake angles.

Positive rake angles give a keen cutting edge, but easily damaged and even may lead to fracture. This configuration can be used by tough cutting tools when machining ductile materials, presenting low resistance to cut operation, as is the case of low carbon steel, for instance[44]. In the case of hard, difficult-to-cut materials, a more robust configuration shall be used, as is the case of zero or negative rake angles[1,43]. Negative rake angles also permit a higher feed and depth-of-cut, though increasing the cutting forces and so, demanding higher power and rigidity of the lathe[44].

1.2.3- Chip formation [3,45,46]

During machining, due to the entrance of the cutting tool edge on the workpiece, a layer of workpiece material is stressed against the rake face of the tool (Fig. 7). This stressed layer suffers a progressive plastic deformation, until shear stresses becomes sufficiently high to originate a sliding movement between the stressed material and the workpiece (primary shear or deformation zone). This region can heat up considerably due to the plastic deformation. Afterwards, a partial or complete rupture in this region can occur, depending on the workpiece material ductility and cutting conditions, originating different chip types, from continuous to short, segmented ones. The chip formed flows over a region on the rake face of the tool, called secondary shear or deformation zone (Fig. 7). This is an area where friction and slipping occur, causing crater wear on the tool. Here, additional heat is generated due to the friction between the cutting tool and the chip. At low cutting speeds, friction between the chip and the rake face of the tool can be high enough to cause adherence of the chip to the tool face. This deposit of material is known as *built-up edge*, and has detrimental effects on the tool integrity, tool life and workpiece surface finishing. The tertiary shearing area, between the flank and the machined surface, gives rise to flank wear. The wear modes will be further discussed in the section 1.2.5 of this chapter.

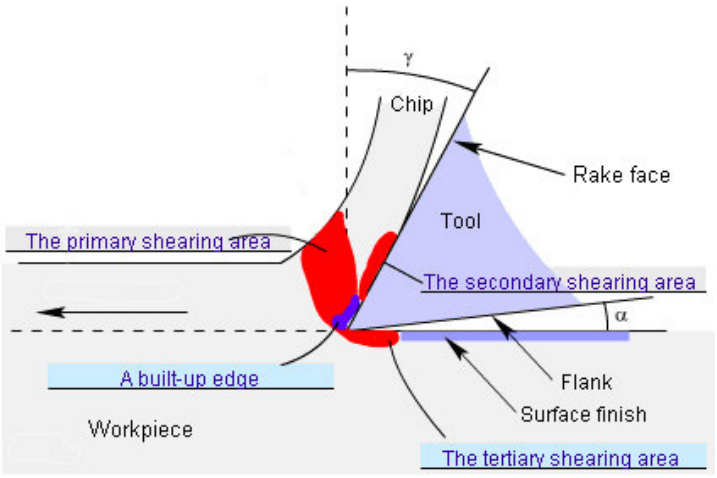

Fig. 7. Chip formation (adapted from [46]).

1.2.4- Cutting forces

The knowledge of the cutting forces that act on the cutting edge during cutting is very important, since they are directly related with required power consumption, wear state and operation progress. The cutting forces are dependent of two main factors[1,47]: tool-chip contact area and shear resistance of the workpiece on primary and secondary shearing areas. As a result, they vary with tool angles, machining parameters, as speed and feed, and wear state of the tool. For instance, the use of positive rake angles or increasing cutting speed leads to lower cutting forces. In this way, an accurate measurement of forces is helpful in optimizing tool design and cutting conditions.

The cutting forces required to shear the workpiece material and move away the chips over the cutting tool, lead to a localized compressive and shear stress state at the contact zone, reaching the highest value at the edge and being reduced to zero where the chip leaves the tool[1,48]. The cutting edge also heats up considerably, and so, it is under a very heavy thermo-mechanical solicitation.

The cutting force is divided into three measurable components (Fig. 8): the tangential or main cutting force (F_c), acting in *Y* direction, the radial or depth-of-cut force (F_d), acting in *X* direction, and the axial of feed force (F_f), which acts in *Z* direction.

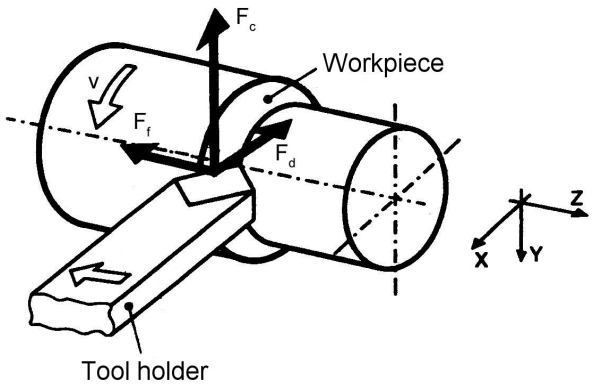

Fig. 8. The three components of the cutting force.

The magnitude of the main cutting force contributes directly to the torque, and so, influences the power required for the cutting process. Theoretically, the product of the main cutting force and the cutting speed corresponds to the power needed[42].

As the cutting edge becomes worn, the area of contact on the clearance face is increased by flank wear, invariably increasing the tool force. The increment in force may be used to monitor the wear on the tool, indirectly guaranteeing the workpiece finish and dimensions and helping to prevent catastrophic tool failure.

The use of lubricants may also affect the contact length and cutting forces magnitude, particularly when cutting at low speed. In this case, the lubricant may restrict the area of seizure between tool and workpiece to a smaller region and thus greatly reducing the forces[1].

1.2.5- Tool wear

Wear is the result of the interaction between tool, workpiece material and machining conditions, which causes changes in tool edge geometry and even its damage. Tool wear is the consequence of a combination of mechanical, thermal and chemical loading, which act simultaneously on the cutting edge. As the result of these load factors, five basic wear mechanisms can develop[42]:

1 – abrasion;

2 – diffusion;

3 – oxidation;

4 – fatigue;

5 – adhesion.

These wear mechanisms cause different modes of wear, as illustrated in Fig. 9:

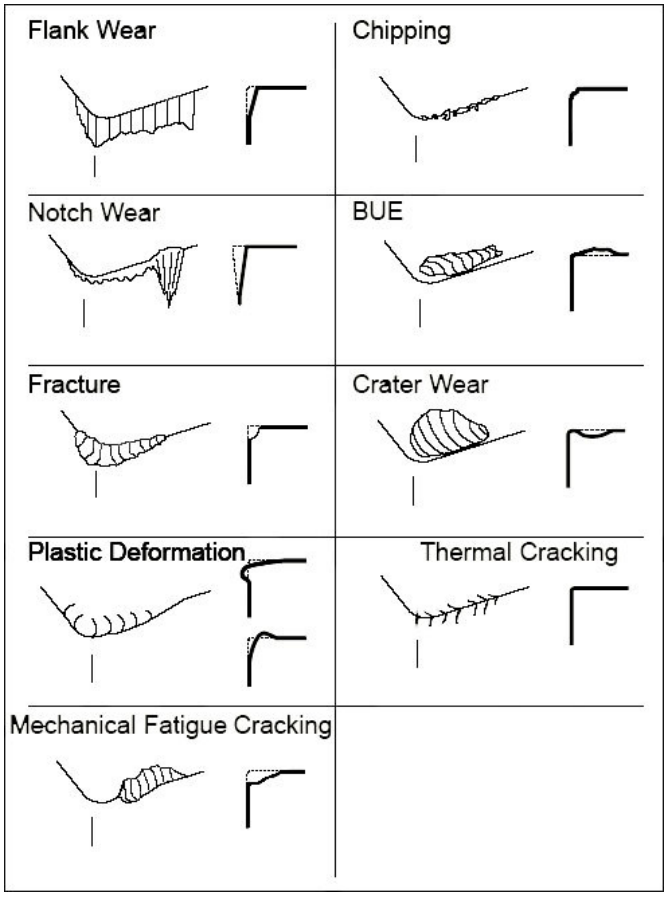

Fig. 9. Different modes of wear that can occur in a cutting tool (adapted from [42,49]).

Abrasion wear is a result of the mechanical load on the insert that leads to the wearing of a flat face on the cutting edge flank (causing *flank wear*, Fig. 9). It is very common and is caused mainly by hard particles of the workpiece material. The most critical property of a cutting tool to resist abrasive wear is hardness, more specifically the "hot hardness". At high temperatures, which invariably are developed during cutting, the tool material becomes soft and thus its ability to resist particle penetration and abrasive wear decreases significantly [48]. This is a problem when using a metallic cutting tool rather than a ceramic tool, since the last is able to much better preserve its hardness at high temperatures.

Diffusion wear is more affected by the chemical loading. The chemical inertness or affinity between the cutting tool material and the workpiece, at elevated temperatures, dictates the appearance of this wear mechanism. Elemental diffusion may take place

between the chip and the top rake surface of the cutting edge, contributing to *crater wear* (Fig. 9) [50]. The mechanism is highly temperature dependent and is thus greatest at high cutting speeds [42]. In fact, diffusion is considered as the dominant process of tool wear in high cutting speed [51]. This kind of wear occurs, as an example, in the case of high speed machining of steels with tungsten carbide inserts, by atoms motion from the tool to the chip, reducing the tool life and being the diffusion type of wear the limiting factor [42,50,51].

Oxidation wear is also a result of chemical loading. The presence of air in high temperature machining results in oxidation for most metals, while the oxide ceramic tools are the highest resistant materials to this kind of wear. In the case of hardmetal inserts, for example, tungsten and cobalt form porous oxide films, easily removed by the chip, exposing a new area for oxidation and further removal in a cyclic process[42]. The more propitious area to oxidation wear is at the interface part of the edge that intersects the workpiece surface (at the depth of cut). This area is accessible to air, leading to *notch wear* (Fig. 9) in the cutting tool[42]. Notch wear can also be caused by workpiece hardening, by the previous pass of the tool[42,52].

Fatigue wear is the result of the combination of thermo-mechanical effects. The cutting edge of a tool is subjected to load-unload cycles of cutting forces and temperature fluctuations, which creates cracks (Fig. 9) on the surface or subsurface of the cutting material. After a number of cycles, these cracks can reach such an extent, that parts of the tool are broken off. Therefore, fatigue wear is a function of loading cycles number and becomes mainly critical in intermittent cutting action, as milling, or even when the workpiece material contains non homogeneous hard particles or pores in a continuous cutting. The main mechanical property of the cutting material to resist the fatigue wear is the fracture toughness.

Adhesive wear occurs at the asperities of the cutting edge material. It occurs mainly at low cutting speeds, when the temperature at the contact is not so high, but enough to weld part of the chip material to the rake face of the tool, causing the *built-up edge* (BUE) (Fig. 9) formation, as referred in the section 1.2.3. It is a dynamic structure, with successive layers from the chip being welded and hardened, becoming part of the edge. An adhesive layer can also be formed at the flank face, by the contact of this area with the

machined workpiece, contributing to the flank wear. So, this kind of wear is caused by the mechanical removal of the tool material when the adhesive junctions are broken [51]. This wear can also cause chipping at the cutting edge of the tool (Fig. 9). In the machining of ductile workpiece materials, like aluminium alloys, it is more susceptible to the occurrence of the adhesive wear.

When analysing the wear modes of a cutting tool, it is difficult to discriminate the contribution of each wear mechanism to the resultant tool wear. Most of the time, the wear in a cutting tool takes place as the sum of two or more wear mechanisms, being their influence the product of workpiece/cutting tool materials, cutting environment/parameters [53]. Some consequences of tool wear are listed below:

- decrease of the dimension accuracy;
- increase of the surface roughness;
- increase of the cutting force;
- increase of the temperature;
- possibly can cause vibration;
- lower of the production efficiency (component quality);
- increase of the material production cost.

The cutting tool and workpiece material properties are the most important factors for withstand the tool wear progress. They are listed as follows [42]:

- hardness;
- strength/toughness;
- chemical stability;
- thermal conductivity;
- thermal expansion;
- coating adhesion (when used).

The study of the wear types and their progress has a great importance in the development of a cutting tool. To understand the causes of tool wear and their consequences is essential to delineate the limits of tool work, respecting some production standards, and not of less importance, the optimization of machining economics. Tool wear

dictates the limit of utilization of a cutting tool. In the next section a description of some tool life criteria, usually adopted in the industry, is given.

1.2.6- Tool life

Tool life can be expressed as the effective cutting time of a tool until its regrind or replacement. It can be also expressed in number of pieces produced, machined length or volume of material removed. The reason why the useful life of a cutting tool is considered to be ended is often changed in different machining operations [52]. The simplest case is that the tool suffers catastrophic failure, as rupture of the edge, for example. There are several factors that could determine when the tool has to be renewed [47]:

- when the tool wear reach high levels that rupture of the edge can occur. This can happen in the case of rough machining, which permits high values of tool wear since no tight dimensional tolerances and good surface finishing are required;

- when the wear at the flank face is high enough to hinder the fabrication of extremely accurate parts or in the case of finishing operations;

- when the wear rate is high and, as consequence, the temperature at the edge exceeds the temperature limit of the tool;

- when the cutting process becomes unstable (vibration) by the action of the augmented cutting forces caused by the tool wear.

By economic and quality reasons enumerated before, it is very important to monitor, directly or indirectly, the wear state of a tool. The direct way consists in optical measurement of the wear with the assistance of a microscope. This is the most common and reliable technique used, but the machining operation needs to be stopped. The indirect approach make a correlation between tool wear and process variables, as cutting force, power, temperature, surface finishing, noise and vibration. Very good relationships can be achieved by the monitoring of these variables. Cutting forces, acquired by means of a piezoelectric dynamometer coupled in the machine lathe, and temperature, estimated by thermocouples fixed near the cutting edge or by an infrared pyrometer, are the most used in laboratory research and in the cutting tool industry. In the present thesis, the study of the

diamond cutting tools behaviour in industry environment is done with the help of cutting forces acquisition. Examples of cutting forces measurements can also be found in Sikdar and Chen [54] in turning a AISI 4340 steel with a coated carbide tool, in Oliveira et al [55] in turning of two different steels with Si_3N_4 based ceramic tools, in Zhou et al [56] in turning of 100Cr6 steel with PCBN insert, and in Belmonte at al [57], the first published work concerning cutting forces measurement in turning hardmetal with a thick CVD diamond tool.

Measurements of the wear marks by optical and SEM micrographs can be correlated with the cutting parameters and developed cutting forces. These measurements may be done accordingly with the ISO 3685 Standard [52], adopting the wear parameters KT (crater depth) and VB (flank wear), Fig. 10.

The tool life criteria for high-speed steel, hardmetal and ceramic cutting tools, accordingly with this standard, are as follows:

- average flank wear (in the case of regular worn flank wear land), $VB_B = 0.3$ mm;
- maximum flank wear (in the case of irregular worn flank wear land), $VB_{Bmax} = 0.6$ mm;
- maximum crater depth in the range of 0.14 to 0.25 mm for a feed of 0.25 to 0.63 $mm \cdot rev^{-1}$.
- catastrophic failure.

Crater wear is not the main mode of tool wear for diamond tools, due to the high thermal conductivity and very low coefficient of friction with most materials. Instead, flank wear is more common and usually determine the tool life[58].

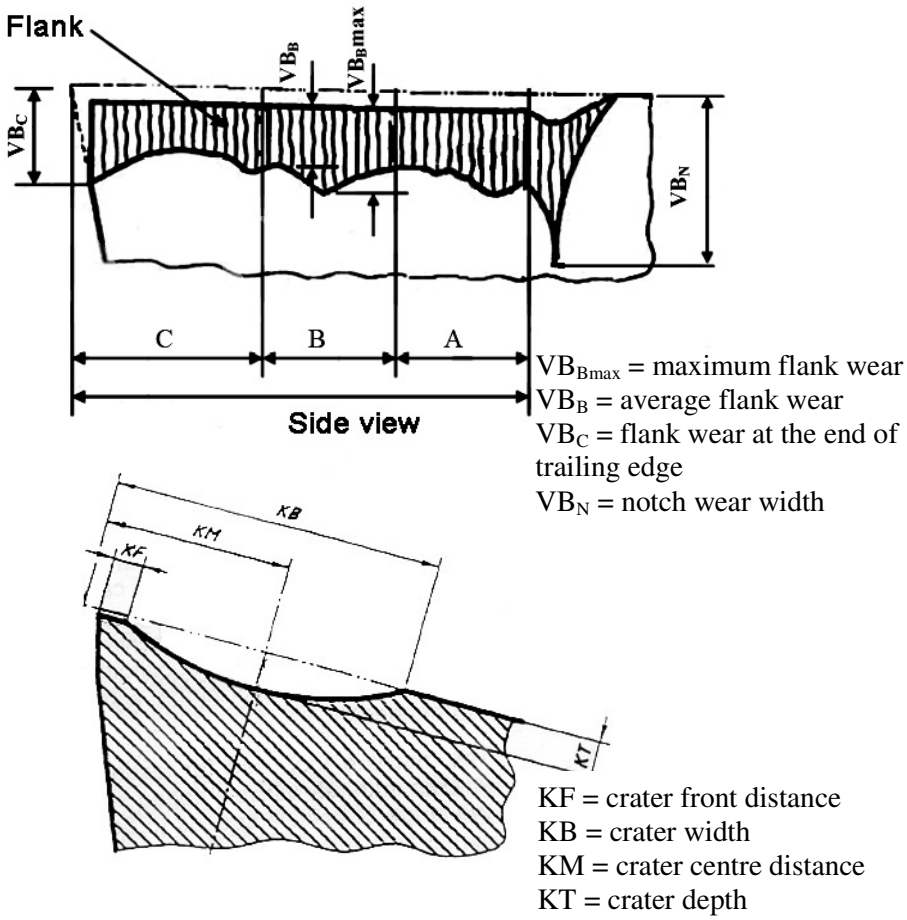

Fig. 10. Measurement of flank and crater wear on turning cutting tools (adapted from[52]).

1.2.7- Diamond coated tools

The use of coatings can significantly improve the tribological properties of the cutting tools, and thus the tool life. By combining and adjusting the necessary properties for a larger applicability of the tool, a *composite* tool is an advantage in extreme requirements. The more frequently property combination is the toughness of the tool centre material with the hardness of the coating shell. Some examples of coatings used in cutting tools include TiN, Al_2O_3, TiC, TiCN, AlN, ZrN, TiB_2, diamond-like carbon, CBN and diamond [10,47,59-62]. Novel protective coatings are deposited in the form of nanocomposite multilayers or compositionally graded coating systems such as that containing a combination of (Ti,Si)N, (Ti,Si,Al)N, Cr/TiN, (Ti/W)N [63-66]. By the adjustment of some

factors, as crystallite size, interface nature/volume, single layer thickness/period, surface and interfacial energy, some of these coatings can exceed the superhardness value of 40 GPa, approaching diamond and CBN values [67,68]. The use of coatings reached a so high importance in cutting tools industry that 90%[59]of tungsten carbide tools, as for example, are used with coatings. Coating processes for cutting tools are CVD (chemical vapour deposition) and PVD (physical vapour deposition) technologies [10].

The main functions of coatings are[10,44]: protection of the tool base material; reduction of friction coefficients at the tool/chip interface, thus lowering the thermal stresses; increase of hardness; rise of thermal conduction rate far from cutting edge; thermal isolation of base tool material, mainly when this has low heat resistance.

Polycrystalline CVD diamond causes a significant decrease of the mechanical strength comparatively to single crystals, as transverse rupture and tensile strength, but presents a higher toughness values. Table 4 shows some properties of the intrinsic superhard materials.

Table 4. Properties of the intrinsic superhard materials [2,6,62,69-73].

Mechanical and physical properties	Single crystal diamond	CVD diamond	CBN (PVD and CVD)
Hardness (GPa)	50-100	75-100	40-60
Coefficient of friction against steel in dry contact	-	-	0.4
Coefficient of friction against AlSi17Cu4Mg in dry contact	-	0.1	-
Maximum working temperature (ºC)	600	600	1200
Fracture toughness (MPa‘$m^{1/2}$)	3.4	5.5-8.5	5
Young’s modulus (GPa)	1000-1100	1000-1100	500-800
Tensile strength (GPa)	1050-3000*	800-1300**	-
Transverse rupture strength (GPa)	2.9	1.3	-
Compressive strength (GPa)	9.0	9.0	-

*Crystallographic orientation dependent. ** Values for the growth face and for nucleation face in tension, respectively, measured by three-point bend test.

CVD diamond coatings are used for cutting tools in machining of abrasive and hard materials, such as metal-matrix composites (MMC's), carbon fiber reinforced carbon materials (CFRC's) and aluminum-silicon alloys [2,16,27]. However, the surface roughness of conventional microcrystalline CVD diamond is a major problem when considering such purposes. Concerning other tribological applications, like mechanical seals, the large grain size of microcrystalline CVD diamond induces extremely long running-in polishing times before the full sealing condition is reached [74]. To overcome this drawback, research efforts have started to focus on nanocrystalline diamond (NCD) coatings, due to its small grain size and very low surface smoothness [75-79]. One of the main advantages of these coatings is the almost constant crystallite size of the diamond through the entire film cross-section, contrarily to columnar growth observed in microcrystalline CVD diamond[75].

When considering tribological and mechanical applications, adhesion of the diamond film to the substrate determines the success of the component in service. The CVD process ideally requires a substrate material with a thermal expansion coefficient similar to that of diamond ($\sim 1 \times 10^{-6} K^{-1}$), in order to reduce the thermal induced stresses developed on the cooling step. Hardmetal is the most common substrate for cutting tools [80,81], but it possesses a higher thermal expansion coefficient ($\sim 6 \times 10^{-6} K^{-1}$), leading to a higher thermal mismatch. A promising solution is proposed in this thesis and consists on the use of silicon nitride ($\sim 2 \times 10^{-6} K^{-1}$) cutting substrates. These ceramics do not induce graphite formation at the interface during deposition and enhance chemical bonding [82].

References

[1] Trent EM, Wright PK. Metal Cutting. 4th ed., Woburn: Butterworth-Heinemann, 2000.

[2] Cline BL, Olson JM. CVD diamond solutions for machining and other mechanical applications. In: Asmussen J and Reinhard DK, editors. Diamond Films Handbook. New York: Marcell Dekker, 2001.

[3] Ferraresi D. Fundamentos da Usinagem dos Metais. São Paulo: Edgard Blücher LTDA, 1977.

[4] Davim JP. Princípios da Maquinagem. Coimbra: Livraria Almedina, 1995.

[5] Whitney ED. Ceramic Cutting tools. Park Ridge, New Jersey: Noyes Publications, 1994.

[6] An introduction to cutting tool materials. Internet information from Element Six Industrial diamond tools. http://www.e6.com/e6/uploaded_files/121_po.pdf

[7] Gimeno S, Munõz JC, Lousa A. Adherence experiments on cBN films. Diam. Relat. Mater. 1998; 7: 853-857.

[8] Yang H, Yoshida T. Mechanical properties of boron nitride films prepared by plasma-enhanced chemical vapor deposition. Surf. Coat. Technol. 2005; 200: 984-987.

[9] Bello I, Chong, YM, Leung KM, Chan CY, Ma KL, Zhang WJ, Lee ST, Layous A. Cubic boron nitride films for industrial applications. Diam. Relat. Mater. 2005; 14: 1784-1790.

[10] Knotek O, Löffler F, Krämer G. Applications to cutting tools. Chapter 7. In: Bunshah RF (Ed.). Handbook of Hard Coatings. New York: William Andrew Publishing, 2001.

[11] Sajgalik P, Hnatko M, Lences, Z. *In situ* preparation of Si_3N_4/SiC nanocomposites for cutting tools application. Int. J. Appl. Ceram. Technol. 2006; 3: 41-46.

[12] Carrapichano JM, Taillaire A, Oliveira FJ, Silva RF. Complete densification of Si_3N_4-SiC ceramic matrix composites (CMC's) by a pressureless sintering route. Mater. Sci. Forum. 2004; 455-456: 225-229.

[13] Angus JC. In: Spear KE, Dismukes JP (Eds.). Synthetic diamond: emerging CVD science and technology. New York: John Wiley & Sons, 1994, cap. 2.

[14] May PW. Diamond thin films: a 21st-century material. The Royal Society. Phil. Trans. R. Soc. Lond. A. 2000; 358: 473-495.

[15] Angus JC, Will HA, Stanko WS. Growth of diamond seed crystals by vapour deposition. J. Appl. Phys. 1968; 39: 2915-2922.

[16] D'Errico GE, Calzavarini R. Turning of metal matrix composites. J. Mater. Process. Technol. 2001; 119: 257-260.

[17] Clark IE, Sen PK. Advances in the development of ultrahard cutting tool materials. Industrial Diamond Review 1998; 2: 40-44.

[18] Hay, RA and Galimberti JM. Cutting and wear applications. In: Prelas MA, Popovici G, Bigelow LK,editors. Handbook of industrial diamonds and diamond films. New York: Marcell Dekker, 1998.

[19] Inspektor A, Bauer CE, Oles EJ. Superhard coatings for metal cutting applications. Surf. Coat. Technol. 1994: 68-69: 359-368.

[20] Peng XL, Liu HF, Gan ZP, Li HQ, Li HD. Characterization and adhesion strength of diamond films deposited on silicon nitride inserts by d.c. plasma jet chemical vapour deposition. Diam. Relat. Mater. 1995; 4: 1260-1266.

[21] Oles EJ, Inspektor A, Bauer CE. The new diamond-coated carbide cutting tools. Diam. Relat. Mater. 1996; 5: 617-624.

[22] Mallika K and Komanduri R. Diamond coatings on cemented tungsten carbide tools by low-pressure microwave CVD. Wear 1999; 224: 245-266.

[23] Mallika K and Komanduri R. Low pressure microwave plasma assisted chemical vapour deposition (MPCVD) of diamond coatings on silicon nitride cutting tools. Thin Sol. Films 2001; 396: 145-165.

[24] Itoh H, Shimura S, Sugiyama K, Iwahara H. Improvement of cutting performance of silicon nitride tool by adherent coating of thick diamond film. J. Am. Ceram. Soc. 1997; 80: 189-196.

[25] Polini R. Chemically vapour deposited diamond coatings on cemented tungsten carbides: substrate pretreatments, adhesion and cutting performance. Thin Sol. Films 2006; 515: 4-13.

[26] Shen CH. The importance of diamond coated tools for agile manufacturing and dry machining. Surf. Coat. Technol. 1996; 86-87: 672-677.

[27] Uhlmann E, Lachmund U, Brücher M. Wear behavior of HFCVD-diamond coated carbide and ceramic tools. Surf. Coat. Technol. 2000; 131: 395-399.

[28] Uhlmann E and Brücher M. Wear behavior of CVD-diamond tools. Manufacturing Technology, Annals of CIRP 2002; 51: 49-52.

[29] Chou YK and Liu J. CVD diamond tool performance in metal matrix composite machining. Surf. Coat. Technol. 2005; 200: 1872-1878.

[30] Zong WJ, Li D, Sun T, Cheng K. Contact accuracy and orientations affecting the lapped tool sharpness of diamond cutting tools by mechanical lapping. Diam. Relat. Mater. 2006; 15: 1424-1433.

[31] Jin S, Chen LH, Graebner JE, McCormack M, Reiss ME. Thermal conductivity in molten-metal-etched diamond films. Appl. Phys. Lett. 1993; 63: 622-624.

[32] Bhushan B, Subramaniam VV, Malshe A, Gupta BK, Ruan J. Tribological properties of polished diamond films. J. Appl. Phys. 1993; 74: 4174-4180.

[33] Ozkan AM, Malshe AP, Brown WD. Sequential multiple-laser-assisted polishing of free-standing CVD diamond substrates. Diam. Relat. Mater. 1997; 6: 1789-1798.

[34] Erdemir A, Fenske GR, Krauss AR, Gruen DM, McCauley T, Csencsits RT. Tribological properties of nanocrystalline diamond films. Surf. Coat. Techonol. 1999; 120-121: 565-572.

[35] Olszyna A, Smolik J. Nanocrystalline diamond-like carbon coatings produced on the Si_3N_4-TiC composites intended for the edges of cutting tools. Thin Sol. Films 2004; 459: 224-227.

[36] Köpf A, Feistritzer S, Udier K. Diamond coated cutting tools for machining of non-ferrous metals and fibre reinforced polymers. Int. J. Refract. Met. Hard Mater. 2006; 24: 354-359.

[37] Synthetic diamond: estimated world production by contry. http://www.indexmundi.com/en/commodities/minerals/diamond_(industrial)/diamond_(industrial)_t6.html

[38] Olson BDW. Diamond, Industrial – 2003. http://minerals.usgs.gov/minerals/pubs/commodity/diamond/diamomyb03.pdf

[39] Crystallume catalog. http://www.crystallume.com/pdf/Crystallume2006Pricelist.pdf

[40] http://www.efunda.com/processes/machining/machin_intro.cfm

[41] Kopač J. Influence of cutting material and coating on tool quality and tool life. J: Mater. Process. Technol. 1998; 78: 95-103.

[42] Sandvik Coromant. Modern metal cutting: a practical handbook. Sandvik coromant: Technical Editoral Dept., 1994.

[43] Aula 02 da Disciplina de Prática de Oficina. Parâmetros de corte. Pontifícia Universidade Católica do Rio Grande do Sul. Faculdade de Engenharia. http://www.em.pucrs.br/~edir/Oficina/Par_corte/ParametroCorte.htm.

[44] Stoeterau RL. Processos de usinagem, aula 03. Universidade Federal de Santa Catarina. Centro Tecnológico. Departamento de Engenharia Mecânica. http://www.lmp.ufsc.br.

[45] Kalhori V. Modelling and Simulation of Mechanical Cutting. Doctoral Thesis. University of Technology. Department of Mechanical Engineering. Lulea, Sweden. 2001.

[46]http://aluminium.matter.org.uk/content/html/eng/default.asp?catid=122&pageid=2144416178

[47] Lanna M. Estudo da usinabilidade do compósito carbono-carbono 2D com ferramentas cerâmicas de nitreto de silício comuns e revestidas com filme de diamante por CVD. Doctoral Thesis. Instituto Tecnológico de Aeronáutica. São José dos Campos, São Paulo, Brasil. 2006.

[48] Abukhshim NA, Mativenga PT, Sheikh MA. An investigation of the tool-tip contact length and wear in high-speed turning of EN19 steel. Proc. Instn. Mech. Engrs. Part B 2004; .218: 889-903.

[49] Castner M. Simplifying turning of stainless steel - Part 2. CNC Machining. 1998; 2 – winter: 28-31.

[50] Kopač J, Sokovic M, Dolinsek S. Tribology of coated tools in conventional and HSC machining. J. Mater. Process. Technol. 2001; 118: 377-384.

[51] Nouari M, List G, Girot F, Géhin D. Effect of machining parameters and coating on wear mechanisms in dry drilling of aluminium alloys. Int. J. Mach. Tools Manuf. 2005; 45: 1436-1442.

[52] International Standard ISO 3685 (1993). Tool life testing with single-point turning tools.

[53] Qiu Y. Hard surface coating experimental evaluation and thermomechanical analysis of a seal with micro heat exchanger. Master Thesis. Faculty of the Louisiana State University and Agricultural and Mechanical College. Louisiana. United States of America. 2002.

[54] Sikdar SK, Chen M. Relationship between tool flank wear area and component forces in single point turning. J. Mater. Process. Technol. 2002; 128: 210-215.

[55] Oliveira FJ, Silva RF, Vieira JM. Improved wear resistance of Si_3N_4 tool inserts by addition of Al_2O_3 platelets. Tribol. Int. 2003; 36: 57-60.

[56] Zhou JM, Walter H, Andersson M, Stahl JE. Effect of chamfer angle on wear of PCBN cutting tool. Int. J. Mach. Tools Manuf. 2003; 43: 301-305.

[57] Belmonte M, Oliveira FJ, Sacramento J, Fernandes AJS, Silva RF. Cutting forces evolution with tool wear in sintered hardmetal turning with CVD diamond. Diam. Relat. Mater. 2004; 13: 843-847.

[58] Andrewes CJE, Feng H-Y, Lau WM. Machining of an aluminum/SiC composite using diamond inserts. J. Mater. Process. Technol. 2000; 102: 25-29.

[59] Choy KL. Chemical vapour deposition of coatings. Prog. Mater. Sci. 2003; 48: 57-170.

[60] Fallböhmer P, Rodríguez CA, Özel T, Altan T. High-speed machining of cast iron and alloy steels for die and mould manufacturing. J. Mater. Process. Technol. 2000; 98: 104-115.

[61] Yuhara DA. Aplicação de revestimentos PVD em ferramentas de corte. http://www.brasimet.com.br/artigos/REVESTIMENTOS.pdf

[62] Keunecke M, Yamamoto K, Bewilogua K. Mechanical and tribological properties of cBN films on silicon and tungsten carbide substrates. Thin Solid Films 2001; 398-399: 142-149.

[63] Carvalho S, Ribeiro E, Rebouta L, Tavares C, Mendonça JP, Monteiro AC, Carvalho NJM, De Hosson JTM, Cavaleiro A. Microstructure, mechanical properties and cutting performance of superhard (Ti,Si,Al)N nanocomposite films grown by d.c. reactive magnetron sputtering. Surf. Coat. Technol. 2004; 177-178: 459-468.

[64] Veprek S, Veprek-Heijman MGJ, Karvankova P, Prochazka J. Different approaches to superhard coatings and nanocomposites – Review. Thin Sol. Films 2005; 476: 1-29.

[65] Ducros C, Benevent V, Sanchette F. Deposition, characterization and machining performance of multilayer PVD coatings on cemented carbide cutting tools. Surf. Coat. Technol. 2003; 163-164: 681-688.

[66] Cavaleiro A, Trindade B, Vieira MT. Influence of Ti addition on the properties of W–Ti–C/N sputtered films. Surf. Coat. Technol. 2003; 174-175; 68-75.

[67] Bauer CE, Inspektor A, Oles EJ. A comparative machining study of diamond-coated tools made by plasma torch, microwave, and hot filament techniques. Sadhana-Acad. Proc. Eng. Sci. 2003; 28: 933-944.

[68] Raveh, A. Zukerman I, Shneck R, Avni R, Fried I. Thermal stability of nanostructured superhard coatings: A review. Surf. Coat. Techol. 2007; 201: 6136-6142.

[69] Novikov NV, Dub SN. Hardness and fracture toughness of CVD diamond film. Diam. Relat. Mater. 1996; 5: 1026-1030.

[70] Yamada Y, Tsuda O, Yoshida T. Microstructure and mechanical properties of cubic boron nitride films prepared by bias sputter deposition. Thin Solid Films 1998; 316: 35-39.

[71] Guruz MU, Dravid VP, Chung YW. Synthesis and characterization of single and multilayer boron nitride and boron carbide thin films grown by magnetron sputtering of boron carbide. Thin Solid Films 2002; 414: 129-135.

[72] Takashi T, Minoru A, Shinobu Y. Mechanical properties of polycrystalline translucent cubic boron nitride as characterized by the Vickers indentation method. J. Am. Ceram. Soc. 1996; 79: 547-549.

[73] Frank M, Breidt D, Cremer R. Nanocrystalline diamond coatings for machining. Vakuum in Forschung und Praxis. 2006; 3:12-16.

[74] Tome MA, Fernandes AJS, Oliveira FJ, Silva RF, Carrapichano JM. High performance sealing with CVD diamond self-mated rings. Diam. Relat. Mater. 2005; 14: 617-621.

[75] Toprani N. Catledge SA, Vohra YK. Interfacial adhesion and toughness of nanostructured diamond coatings. J. Mater. Res. 2000; 15: 1052-1055.

[76] Ferrari AC, Robertson J. Origin of the 1150 cm^{-1} Raman mode in nanocrystalline diamond. Phys. Rev. B 2001; 63: 121405.

[77] Bhattacharyya S. Auciello O. Birrel J, Carlisle JA. Curtiss LA, Goyette NA, Gruen DM, Krauss AR, Schlueter J, Sumant A, Zapol P. Synthesis and characterization of highly-conducting nitrogen-doped ultrananocrystalline diamond films. Appl. Phys. Lett. 2001; 79: 1441-1443.

[78] Gupta S, Weiner BR, Morell G. Synthesizing nanocrystalline carbon thin films by hot filament chemical vapor deposition and controlling their microstrucutre. J. Mater. Res. 2002; 17: 1820-1833.

[79] Catledge SA, Borham J, Vohra YK, Lacefield WR, Lemons JE. Nanoindentation hardness and adhesion investigations of vapour deposited nanostructured diamond films. J. Appl. Phys. 2002; 91: 5347-5352.

[80] Gäbler J, Schäfer L, Menze B, Hoffmeister H-W. Micro abrasive pencils with CVD diamond coating. Diam. Relat. Mater. 2003; 12: 707-710.

[81] Polini R, Barletta M, Delogu M. Fluidized bed micro-machining and HFCVD of diamond films onto Co-cemented tungsten carbide (WC-Co) hardmetal slabs. Thin Solid Films 2006; 515: 87-94.

[82] Amaral M, Oliveira FJ, Belmonte M, Fernandes AJS, Costa FM, Silva RF. Tailored Si_3N_4 ceramic substrate for CVD diamond coating. Surf Eng 2003;19:410-416.

Chapter 2

Processing and characterization of Si_3N_4 and Si_3N_4-TiN substrates

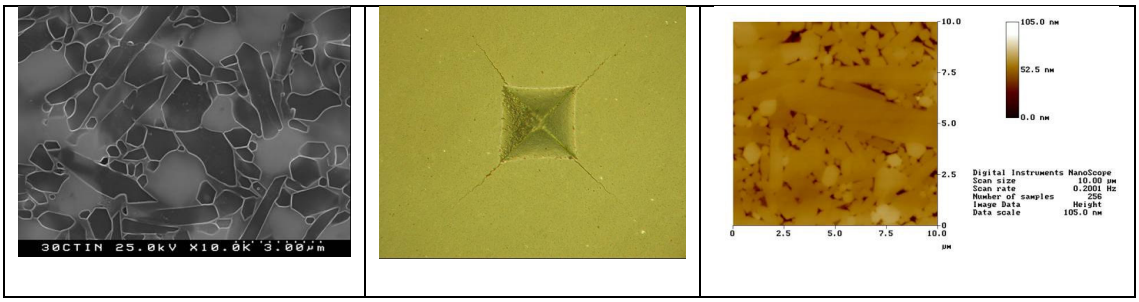

Introduction

The needs for engines operating at high temperatures motivated the development of silicon nitride based ceramics in the 60's and 70's, especially for application in high-efficiency gas-turbine and reciprocating engines[1,2]. Due to the properties of these ceramics as high hardness, good fracture toughness and thermal conductivity, low thermal expansion coefficient, low density and good creep, wear and thermal shock resistance, they have been extensively applied in aerospace, automotive and defence industries[3]. In cutting tools applications, their major advantage is the combination of a high hardness and fracture toughness, even at high temperatures, as well as the chemical stability. The high temperature strength of silicon nitride made possible its use in metal machining applications with significantly increased machining rates[4]. The main physical and mechanical properties of silicon nitride are listed in Table 1.

Table 1 – Typical properties of silicon nitride ceramics[4].

Property	
Bulk density ($g \cdot cm^{-3}$)	3.2-3.3
Flexural strength (MPa)	800-1000
Fracture toughness ($MPa \cdot m^{-1/2}$)	6-8
Hardness (GPa)	15-16
Elastic modulus (GPa)	300-380

In addition to silicon nitride (Si_3N_4), other nitrides such as boron (BN), aluminium (AlN) and titanium (TiN) are used as structural materials. The compound combinations within this group and with other ceramics like SiC, TiC, Al_2O_3, ZrO_2, can result in interesting composites with an even wide range of applications when compared with their monolithic composition[5-9]. For instance, the increment of BN, SiC, TiC and TiN as second phase in the Si_3N_4 matrix confers to the composite the improvement of the high-temperature mechanical properties, due to the higher refractoriness of these ceramics[10]. TiC and TiN also give electrical conductivity to the composite when the percolation

concentration is achieved, which can be around 20-40 vol.% being dependent on the uniformity of the conductive phase network, grain size, shape and the interaction with the matrix[11]. The electrical conductivity of hard ceramics is an important characteristic, since they are able to be machined by electrical discharge machining (EDM), making easier the preparation of pieces with complex geometries that could be very difficult and even impossible to obtain by conventional machining[12-16]. Another aspect is the use of these ceramics as reinforcement of the silicon nitride matrix, increasing the fracture toughness values related to the monolithic material. When the reinforcement has high aspect ratio, as whiskers or platelets, higher values of fracture toughness are achieved. On the other hand, the price of such materials and the difficulty to obtain a fully dense final product are some disadvantages when compared with particulate ones[8,11].

Silicon nitride has two different crystal structures: α and β. They are hexagonal for both phases, differing basically in the lattice parameter "c". Their cell parameters can be found in Table 2. The α-phase is stable only at temperatures below 1450ºC and the irreversibly transition of α → β phase becomes easier during liquid phase sintering by dissolution – reprecipitation mechanisms[17,18].

Table 2 – Crystal structures of α and β- Si_3N_4 [18,19].

Phase	Crystal structure	Lattice parameters (nm)			Unit cell
		a	c	c/a	
α-Si_3N_4	Hexagonal	0,782	0,561	0,717	$Si_{12}N_{16}$
β-Si_3N_4	Hexagonal	0,759	0,291	0,383	Si_6N_8

The low mobility of the atoms, due to the strong covalent chemical bonds, limits the attaining of high densification levels by solid state sintering. As said before, silicon nitride ceramics densification needs sintering aids, generally oxide additives, to promote liquid phase sintering (LPS). These additives, as Al_2O_3, Y_2O_3, MgO and Ce_2O_3, react with the SiO_2 present in the surface of Si_3N_4 grains to form a liquid phase that, upon cooling, forms an intergranular vitreous material or can partially solidify as a silicate or as a silicon oxynitride[8,19].

Basically, the LPS mechanism can be divided into three stages[18,19]: (i) rearrangement of the particles by capillary forces, due to the formation of an eutectic melt consisting of additives and the SiO_2 present on the Si_3N_4 surface; (ii) dissolution of α-Si_3N_4, diffusion of Si and N through the liquid phase and reprecipitation into a more stable β-Si_3N_4 nuclei; (iii) grain coarsening and coalescence of β-Si_3N_4 crystals, elimination or lowering of residual porosity. The final microstructure consists of prismatic β-Si_3N_4 grains, with high aspect ratio (length/diameter ratio), surrounded by an amorphous or partially crystallized intergranular glassy phase. The acicular characteristic of the β-Si_3N_4 grains is responsible for the high fracture toughness of this ceramic, and a close control of the aspect ratio can be used to improve this property[19,20].

Sintering of silicon nitride

The main processes used to sintering silicon nitride are[1,19]: reaction bonded silicon nitride (RBSN), pressureless sintering silicon nitride (PSSN), hot pressed silicon nitride (HPSN) and hot isostatic pressed silicon nitride (HIPSN). In this thesis, two process were used, presureless and hot pressing. The basic process of monolithic Si_3N_4 ceramics production is described below as flow chart in Fig. 1:

The starting powder composition and the production steps were chosen accordingly to previous works of our group[8,21] in order to obtain fully dense materials, combining good mechanical properties. The composition was chosen based on the SiO_2-Y_2O_3-Al_2O_3 ternary phase diagram to form a vitreous phase at approximately 1550ºC and all the SiO_2 is found in the surface of α-Si_3N_4 grains. The production of the Si_3N_4-TiN composites followed the same procedure, with partial substitution of the Si_3N_4 matrix amount, and will be further described in the article presented in this chapter.

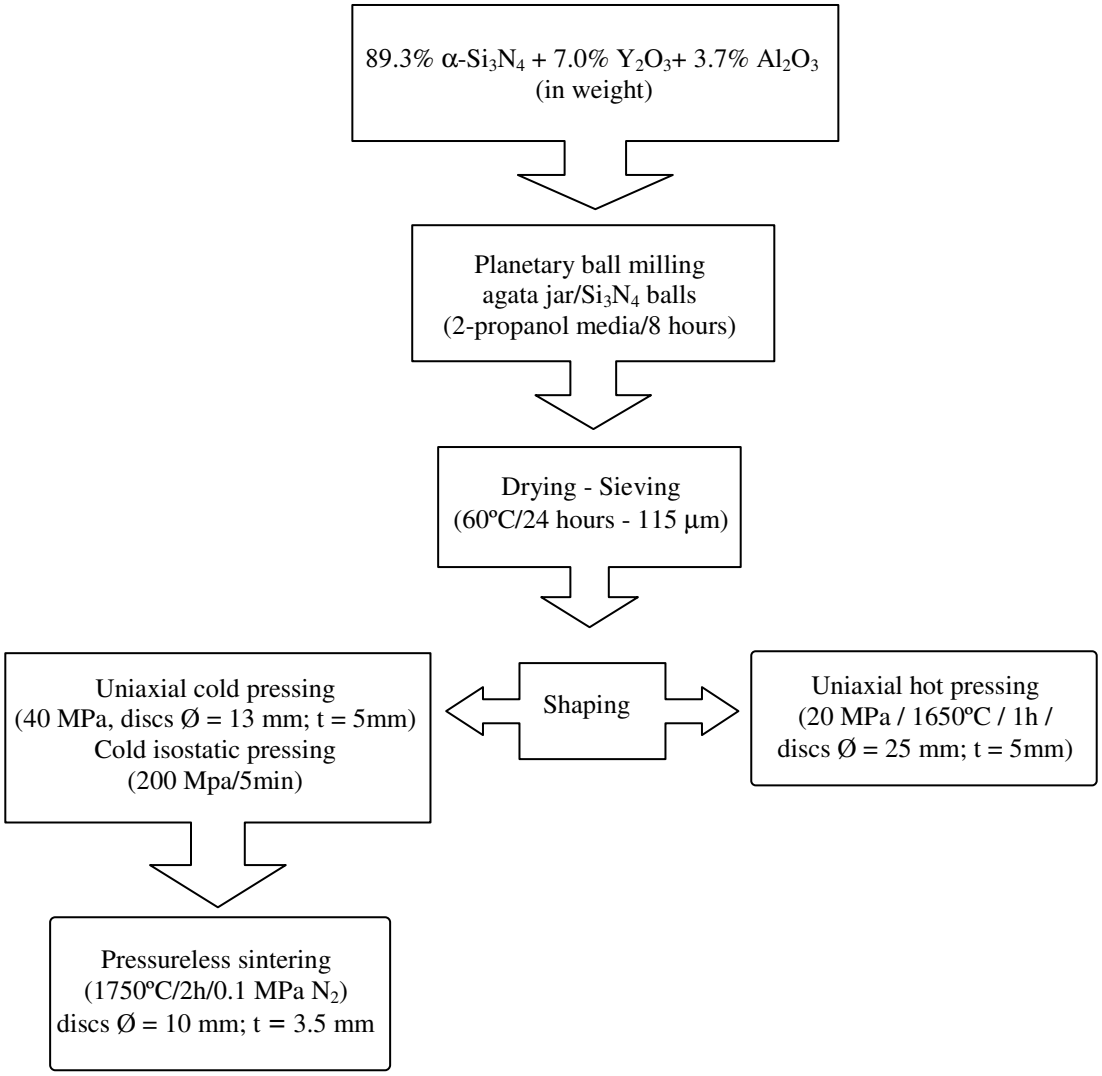

Fig. 1. Flow chart of the production of Si_3N_4 ceramics.

The pressureless sintering step was performed in a graphite furnace (Thermal Technology Inc.), which is able to work in vacuum or controlled atmosphere (N_2, Ar). The near-net shaped silicon nitride ceramics were displaced in a closed graphite container in a mixture of 50% Si_3N_4+additives with 50% BN (powder bed). In this way, the direct contact with the surrounding graphite walls is avoided and also reduces the decomposition of the Si_3N_4 powder. After air evacuation of the chamber, a flow of N_2 was passed performed throughout the sintering cycle to avoid Si_3N_4 thermal decomposition, displacing the equilibrium given by eq. 1 to the left, as follows[1]:

$$Si_3N_{4(s)} \rightarrow 3Si_{(g,l)} + 2N_{2(g)} \qquad \text{(eq.1)}$$

As an alternative for densification, uniaxial hot pressing was done in an induction furnace (Inductelec) using graphite moulds and punches. The moulds were previously covered by a BN layer (brushing it with a suspension of BN powder in ethanol), the powder disposed between two graphite punches and them covered with alumina powder. A small hole on the alumina was open to make possible the reading of the graphite temperature by means of a pyrometer (Mikron M67).

After densification, the samples were cut (in the case of HP samples), ground (47μm diamond wheel), lapped (15μm diamond suspension) and mirror-polished (0.25 μm silica suspension). The samples characterization involved the determination of density by liquid immersion (ethylene glycol), hardness by Vickers indentation and fracture toughness by measurement of the indentation cracks length, crystalline phases detection by XRD, electrical conductivity by four-point probe and morphology by SEM of the surfaces etched with CF_4 plasma (Emitech K1050X). The following article presents the characterizations of the monolithic Si_3N_4 ceramic and Si_3N_4-TiN composites, used as substrates for further CVD diamond deposition.

References

[1] Riley FL. Silicon nitride and related materials. J. Am. Ceram. Soc. 2000; 83: 245-265.

[2] Wiederhorn SM, Hockey BJ, French JD. Mechanisms of deformation of silicon nitride and silicon carbide at high temperatures. J. Eur. Ceram. Soc. 1999; 19: 2273-2284.

[3] Richerson DW. Modern Ceramic Engineering: properties, processing and use in design. 2nd ed. New York: Marcel Dekker, 1992.

[4] DePoorter GL, Brog TK, Readey MJ. Structural ceramics. In: ASM International Handbook. v.2. Properties and selection: nonferrous alloys and special-purpose materials. Materials Park: American Society for Metals, 1990.

[5] Rak ZS and Czechowski J. Manufacture and properties of Al_2O_3-TiN particulate composites. J. Eur. Ceram. Soc. 1998; 18: 373-380.

[6] Oliveira FJ, Silva RF, Vieira JM. Improved wear resistance of Si_3N_4 tool inserts by addition of Al_2O_3 platelets. Tribology Int. 2003; 36: 57-60.

[7] Tangen I-L, Yu Y, Grande T, Hoier R, Einarsrud M-A. Preparation and characterization of aluminium nitride-titanium nitride composites. J. Eur. Ceram. Soc. 2004; 24: 2169-2179.

[8] Carrapichano JM, Tallaire A, Oliveira FJ, Silva RF. Complete densification of Si_3N_4-SiC ceramic matrix composites (CMC's) by a pressureless sintering route. Mater. Sci. Forum 2004; 455-456: 225-229.

[9] Salehi S, Van der Biest O, VleugelsJ. Electrically conductive ZrO_2-TiN composites. J. Eur. Ceram. Soc. 2006; 26: 3173-3179.

[10] Kusunose T, Sung R-J, Sekino T, Sakaguchi S, Niihara K. High-temperature properties of a silicon nitride/boron nitride nanocomposite. J. Mater. Res. 2004; 19: 1432-1438.

[11] Gogotsi YG. Particulate silicon nitride-based composites – Review. J. Mater. Sci. 1994; 29: 2541-2556.

[12] Huang J-L, Lee M-T, Lu H-H, Lii D-F. Microstructure, fracture behavior and mechanical properties of TiN/Si_3N_4 composites. Mater. Chem. Phys. 1996; 45: 203-210.

[13] Lee B-T, Yoon Y-J, Lee K-H. Microstructural characterization of electroconductive Si_3N_4-TiN composites. Materials Letters 2001; 47: 71-76.

[14] Guicciardi S, Melandri C, Medri V, Bellosi A. Effects of testing temperature and thermal treatments on some mechanical properties of a Si_3N_4-TiN composite. Mater. Sci. Eng. A 2003; 360: 35-45.

[15] Liu C-C, Huang J-L. Effect of the electrical discharge machining on strength and reliability of TiN/Si_3N_4. Ceram. Int. 2003; 29: 679-687.

[16] Bracisiewicz M, Medri V, Bellosi A. Factors inducing degradation of properties after long term oxidation of Si_3N_4-TiN electroconductive composites. Appl. Surf. Sci. 2002; 202: 139-149.

[17] Kingery WD, Bowen HK, Uhlmann DR. Introduction to ceramics. 2nd ed. New York: John Wiley, 1976.

[18] Wolfgang D and Riedel R. Progress in silicon-based non-oxide structural ceramics. Int. J. Refr. Metals and Hard Mater. 1997; 15: 13-47.

[19] Petzow G and Herrmann M. Silicon nitride ceramics. In: Jansen M (Ed.). Structure and Bonding. Springer Berlin/Heidelberg, 2002.

[20] Painter GS, Becher PF, Shelton WA, Satet RL, Hoffmann MJ. First-principles study of rare-earth effects on grain growth and microstructure in β-Si_3N_4 ceramics.

[21] Tallaire A, Silva VA, Fernandes AJS, Costa FM, Silva RF. Effect of intergranular phase of Si_3N_4 substrates on MPCVD diamond deposition. Surf. Coat. Technol. 2002; 151-152: 521-525.

Electroconductive ceramic composites for cutting tools

F. A. Almeida[1], H. Bóia[1], C. Santos[1], J. Monteiro[2], F. J. Oliveira[1], R. F. Silva[1]

[1] Department of Ceramics and Glass Engineering, CICECO, University of Aveiro, 3810-193 Aveiro, Portugal

[2] Department of Physics, University of Aveiro, 3810-193 Aveiro, Portugal

(Materials Science Forum 514-516, 2006, 638-642)

Abstract

The addition of titanium nitride (TiN) particles to a Si_3N_4 matrix reduces the intrinsic electric resistivity of this ceramic allowing it to be machined by EDM in cutting tools manufacturing. Gains can be expected given the cost reduction by the increase of productivity when shaping these hard to machine ceramic materials. Si_3N_4 ceramic matrix composites (CMC's) with 0-30vol.% of TiN sub-micrometric particles were produced by uniaxial hot pressing (HP) and pressureless sintering (PS). For the PS samples, EDM tests showed that machining of the composites is possible when they contain at least 23vol.% TiN particles what corresponds to a resistivity of 7.5 Ω.cm. For HP samples at least 30vol.% of TiN is required to get an electroconductive material for EDM machining. This difference is due to the lower temperatures used in the HP process that delays the formation of a conductive network between the TiN particles.

Keywords: *Silicon Nitride, Titanium Nitride, Ceramic Matrix Composites (CMC´s), Electrical Discharge Machining.*

1. Introduction

Silicon nitride (Si_3N_4) is one of the ceramic materials having a strong penetration in the market of applications for structural components due to its low density, high hardness, high bending strength and fracture toughness and excellent thermal shock resistance[1]. The shaping and surface finishing of this ceramic still are time consuming steps. These are usually done by conventional grinding and polishing methods that can induce subsurface flaws to the components and diminish their strength[2]. Within this scope, appropriate amounts of an electrical conductive second phase, such as TiN, TiC or ZrN, can be incorporated into an insulating matrix, making it workable by the EDM (Electrical Discharge Machining) method[3]. This process is based on short duration electric discharges between an electrode and the workpiece that provokes material removal by erosion[4]. This second phase can be incorporated in the form of particles, fibres or whiskers, and may contribute to enhance the fracture toughness relatively to the unreinforced matrix [5,6].

These materials can be densified by several methods such as hot-pressing (HP), gas pressure sintering (HIP, GPS) or pressureless sintering (PS). The latter technique has been used for producing Si_3N_4 cutting inserts, coated with diamond and successfully tested in turning operations of hard materials[7]. The feasibility of such method to produce particle reinforced composites is a less used subject since HP, HIP or GPS are generally required to reach full densification of these composites. The aim of the present work is to produce and characterize electrically conductive Si_3N_4 matrix ceramic composites with TiN particles. Titanium nitride is chemically compatible with the silicon nitride matrix, possesses high hardness, low electric resistivity and has a coefficient of thermal expansion close to that of silicon nitride, what diminishes the residual stresses[5]. PS and HP routes were used to fully densify composites containing up to 30vol.% TiN particles.

2. Experimental Procedure

The matrix of Si_3N_4/TiN ceramic composites is composed by 89.3% of Si_3N_4, 3.7% of Al_2O_3 and 7.0% of Y_2O_3 (in weight). Details on the choice of this composition were

previously reported[8]. TiN replaces the matrix in volume percentages of 9, 23 and 30%, consequently diminishing the amount of additives available for the formation of the glassy phase sintering aid. For the higher volume fraction of TiN, and anticipating lower sintering rates due to this diminution of the glassy phase fraction, another composite was made by replacing 30% of Si_3N_4 with the same volume amount of TiN. In this way the vitreous phase fraction and composition of the sample (called "30C") are equivalent to that of the unreinforced matrix. This composite has effectively 26vol.% of TiN. The composites were densified by HP (1650ºC/20MPa/1h) and by PS (1750ºC/2-5h/0.1MPa of N_2). The phase composition of all samples was analysed by X-ray diffraction (XRD). The dense ceramics were polished, etched by CF_4 plasma and observed by Scanning Electron Microscopy (SEM). Vickers hardness and indentation fracture toughness (K_{Ic}) were measured with 98N of applied load. The electrical resistivity was measured using the dc four-point-probe technique. Samples having low electric resistivity were machined by wire EDM (W-Cu-Zn, 0.25mm diameter wire). The EDM parameters, the duration and time between electric discharges, were fixed at 1.2 and 10µs, respectively, for a current of 16A and voltage of 50V.

3. Results and Discussion

Phase composition. All the samples produced by both the PS and HP processes were fully dense after the adequate sintering cycles. In the case of PS cycles, the sintering time was 2h for the matrix, 3 hours for the additive corrected composite (30C), and 5h for all the other composites to allow them to completely densify. Fig. 1a shows the XRD patterns of the matrix sintered by HP and PS. The two methods yield slightly different materials with respect to composition. For the HP matrix the tailored composition[8] results in β-Si_3N_4 and amorphous intergranular phase. In the case of the PS matrix, and besides β-Si_3N_4, there are minor secondary phases such as Y_2SiAlO_5N, $Y_3AlSi_2O_7N_2$ and $Y_2Si_2O_7$ that formed upon cooling from the crystallization of the vitreous phase. These differences are due to the smaller reaction temperature and shorter time in the case of HP but also due to the sintering environments. For HP, the ceramics are tightly confined inside a graphite pressing die, while in PS the samples are in a graphite container, surrounded by a Si_3N_4 /BN powder bed

and under a N_2 atmosphere. The incorporation of TiN changes the local chemistry, since different phases are present after sintering (Fig. 1b). All the HP composites contain Si_2N_2O as a minor crystalline phase that increases its amount relatively to Si_3N_4 with increasing fraction of TiN. TiN always contains a surface oxidized layer (TiO_2) that reacts with Si_3N_4 to form TiN[5]. The amount of oxygen on the glassy phase then increases, displacing the equilibrium towards Si_2N_2O that crystallizes during cooling[9]. In the PS method, the incorporation of TiN in the composites also leads to the formation of yttrium silicates and yttrium oxynitrides, similarly to what happens with the Si_3N_4 monolithic materials, and traces of $Y_2Ti_2O_7$.

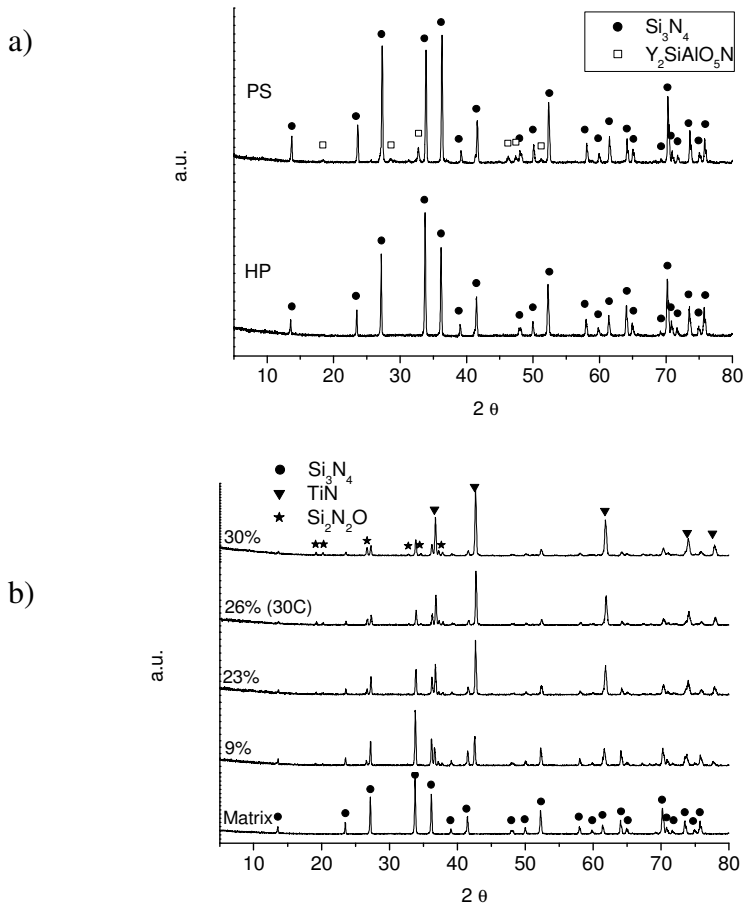

Fig. 1. XRD patterns: a) PS and HP Si_3N_4 matrices; b) HP Si_3N_4 matrix and Si_3N_4-TiN composites.

Microstructure. The two sintering methods yield quite dissimilar microstructures due to the different temperatures and sintering times used for densification. The higher the temperature, the larger is the grain size. The etched microstructures in Fig. 2a and 2b illustrate this for the unreinforced matrix. Both matrices consist of β-Si_3N_4 grains of large aspect ratio surrounded by the intergranular phase. During sintering, the glassy phase surrounds a larger area fraction of Si_3N_4 particles in the HP matrix than in the PS matrix. This contributes for the compositional differences detected by XRD, as above discussed. The larger grain size obtained by the PS method is also observed for the TiN containing composites (Figs. 2c-j). There is no appreciable difference between the grain size of the matrix and that of the corresponding composites, although TiN has been referred to as a Si_3N_4 grain growth inhibitor[3, 10, 11].

The mechanical behaviour of these materials reflects these differences. The ceramics with the smaller grain sizes (HP) are harder but less tough than those with larger grain sizes (PS), Fig. 3. When considering the effect of TiN, there is a clear trend for an increase of K_{Ic} with its volume fraction, Fig. 3b. On the contrary, the composites hardness slightly decreases due to the lower intrinsic hardness of TiN grains then those of Si_3N_4[5]. Sample 30C has the lowest hardness due to the larger volume content of sintering aids when comparing with the other composites.

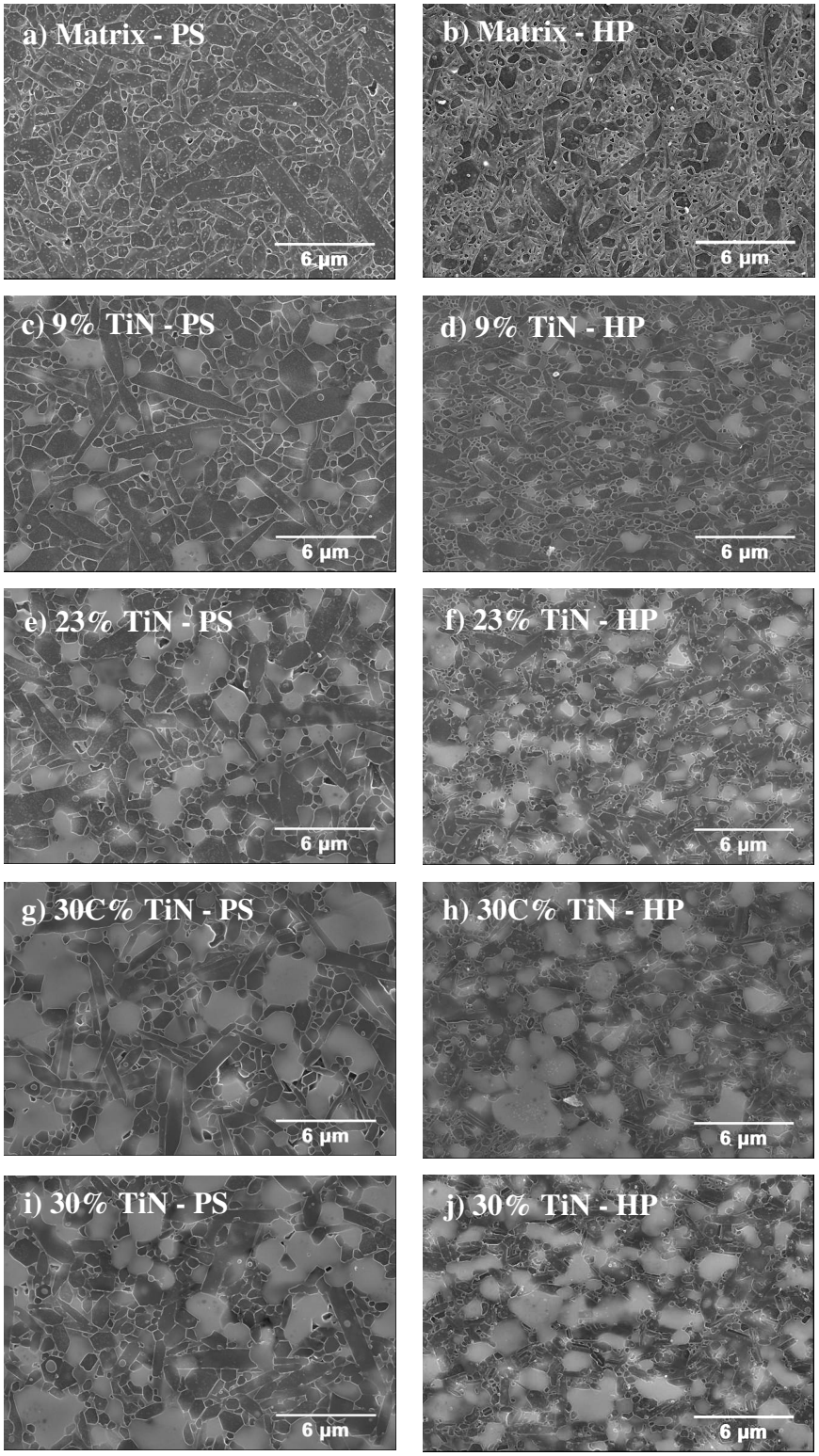

Fig.2. SEM micrographs of etched microstructures of matrix and composites produced by PS method (a, c, e, g, i) and by HP (b, d, f, h, j). Dark phase is β-Si_3N_4; bright phase is intergranular phase; light grey phase in composites is TiN.

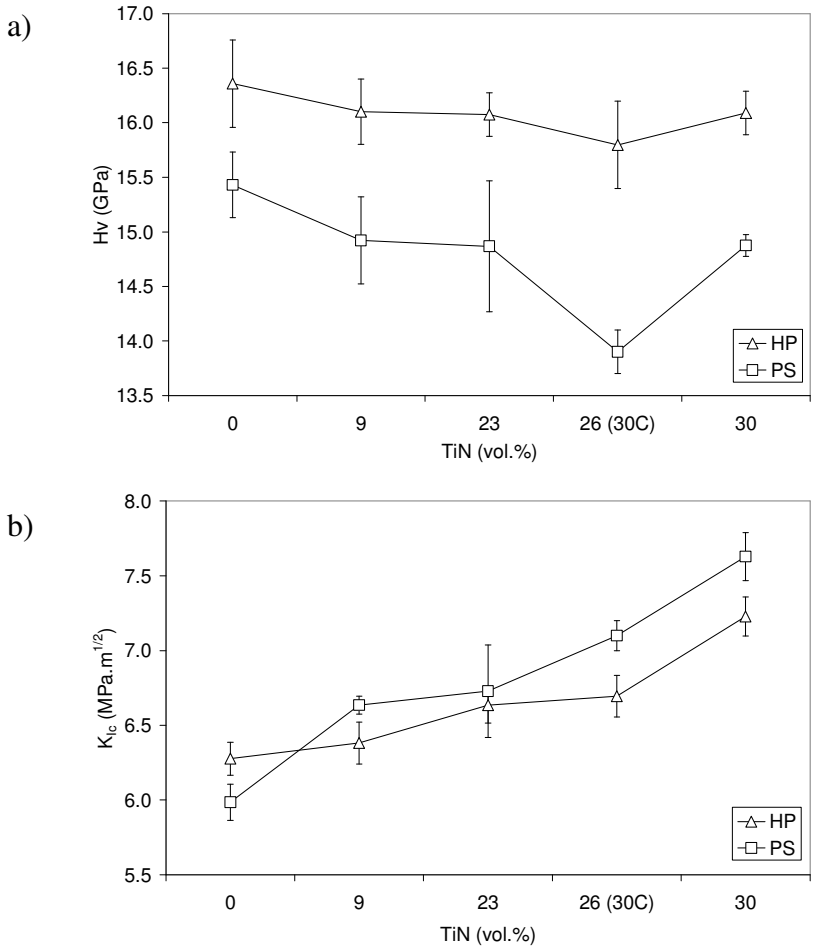

Fig. 3. Vickers hardness (a) and fracture toughness (b) of Si_3N_4-TiN composites.

Electric resistivity. The microstructures of the composites in Fig. 2 show that with the increment of the TiN content, the inter-particle contacts increase and even the TiN grains enlarge. Others[12, 13] demonstrated that in two phase materials the percolation threshold is reached for volume fractions of about 16%, and above 22% all inclusions are part of the same network in the case of spherical particles. Electrical resistivity measurements are a good indirect way of determining this percolation limit while simultaneously allows determining the ability of composites for EDM operations when conductive particles are used as reinforcement. In Fig. 4 the electrical resistivity is graphically represented as a function of TiN fraction for both sintering methods. The electrical resistivity decreases drastically from insulator ($\rho=10^{13}$-$10^{14}\Omega$.cm) to a conductive ceramic material ($\rho<10\Omega$.cm)

when the percolation concentration is reached. For the PS samples, the sharp decrease happens for the 23vol.% TiN composite, while for the HP ones it occurs for 26vol.%TiN (30C). This difference comes from the higher temperatures used in the former processing route that enhance the diffusion paths between TiN particles via the intergranular liquid phase, leading to an electroconductive network for lower TiN contents. This mechanism also explains the growth of the TiN grains by dissolution-reprecipitation mechanism observed in the PS composites. Above the percolation threshold, grain coalescence also takes place. After the sudden drop, further decreases in resistivity occur due to the improved quality of the conductive network[5] when more TiN is added.

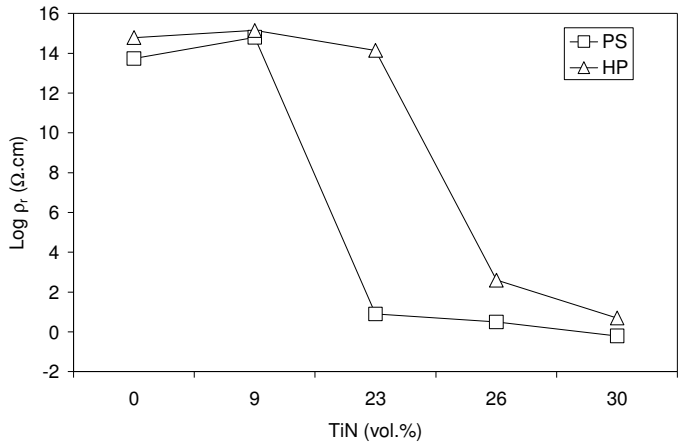

Fig. 4. Electric resistivity as a function of TiN volume fraction.

According to some authors, the measured resistivity values are low enough to allow EDM machining since they are below a required minimum of 100Ω.cm[4, 5, 14]. This was tested in a series of EDM operations, where all the PS composites containing 23vol.% or more of TiN could be cut while in the case of HP composites only the 30vol.%TiN composite is machinable. The sparks between the electrode and the sample generate high local temperatures, causing melting and evaporation of both the surface material and the wire[3, 4, 6]. The micrograph of Fig. 5, representative of the surfaces after EDM machining, shows craters, caused by the electric discharges, and re-solidified material adhered to the freshly cut surface.

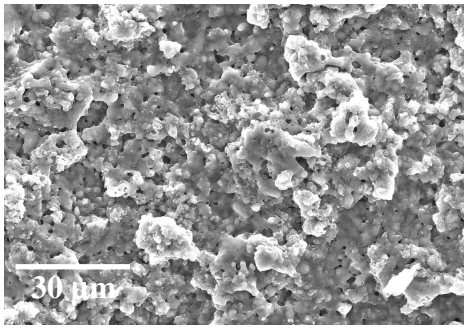

Fig. 5. Surface of the PS composite with 30% TiN cut by EDM.

4. Conclusions

Dense ceramic composites containing up to 30vol.% TiN particles were produced by pressureless sintering (PS) and by hot-pressing (HP). The higher temperature and longer times in the PS method induces a larger grain size of the β-Si_3N_4 grains with different intergranular crystallinity relatively to HP samples. Introduction of TiN in the matrix changes the equilibrium to more oxidizing conditions where oxynitrides and silicates are formed. PS composites are less hard (~15GPa) but tougher (up to 7.5MPa·$m^{1/2}$) then their corresponding HP samples.

For the PS densified composites, the TiN percolation threshold occurs with 23vol.% TiN, while for the low temperature HP route, the TiN fraction has to be increased up to 30vol.% to result in an effective electroconductive network. All samples having an electric resistivity below 7.5Ω.cm could be machined by EDM.

Acknowledgements

F.A. Almeida's work is supported by Programme Alβan, European Union Program of High Level Scholarships for Latin America, identification number E03D06378BR.

References

[1] Riley FL. Silicon nitride and related materials. J. Am. Ceram. Soc. 2000; 83: 245-265.

[2] Li K, Liao TW. Surface/subsurface damage and the fracture strength of ground ceramics. J. Mater. Proc. Techn. 1996; 57: 207-220.

[3] Liu C-C, Huang J-L. Effect of the electrical discharge machining on strength and reliability of TiN/Si_3N_4. Ceram. Int. 2003; 29: 679-687.

[4] Jianxin D, Taichiu L. Surface integrity in electro-discharge machining, ultrasonic machining, and diamond saw cutting of ceramic composites. Ceram. Int. 2000; 26: 825-830.

[5] Gogotsi YG. Particulate silicon nitride-based composites – Review. J. Mater. Sci. 1994; 29: 2541-2556.

[6] Bellosi A, Guicciardi S, Tampieri A. Development and characterization of electroconductive Si_3N_4-TiN composites. J. Eur. Ceram. Soc. 1992; 9: 83-93.

[7] Almeida FA, Oliveira FJ, Sousa M, Fernandes AJS, Sacramento J, Silva RF. Machining hardmetal with CVD diamond direct coated ceramic tools: effect of tool edge geometry. Diam. Relat. Mater. 2005; 14: 651-656.

[8] Carrapichano JM, Tallaire A, Oliveira FJ, Silva RF. Complete densification of Si_3N_4-SiC ceramic matrix composites (CMC's) by a pressureless sintering route. Mater. Sci. Forum 2004; 455-456: 225-229.

[9] Dumitrescu L, Sundman B. A thermodynamic reassessment of the Si-Al-O-N system. J. Eur. Ceram. Soc. 1995; 15: 239-247.

[10] Huang J-L, Lee M-T, Lu H-H, Lii D-F. Microstructure, fracture behavior and mechanical properties of TiN/Si_3N_4 composites. Mater. Chem. Phys. 1996; 45: 203-210.

[11] Zivkovic L, Nikolic Z, Boskovic S, Miljkovic M. Microstructural characterization and computer simulation of conductivity in Si_3N_4-TiN composites. J. Alloy Compd. 2004; 373: 231-236.

[12] Lange FF, Atteraas L, Zok F. Porter JR. Deformation consolidation of metal powders containing steel inclusions. Acta Metall. Mater. 1991; 39: 209-219.

[13] Fortulan CA, Souza DPF. Microstructural evolution of the Al_2O_3-ZrO_2 composite and its correlation with electrical conductivity. Materials Research 1999; 2: 205-210.

[14] Rak ZS, Czechowski J. Manufacture and properties of Al_2O_3-TiN paticulate composites. J. Eur. Ceram. Soc. Vol. 1998; 18: 373-380.

Chapter 3

CVD diamond: deposition parameters and film characterization

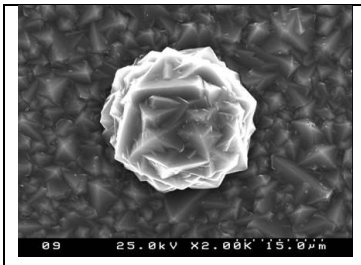

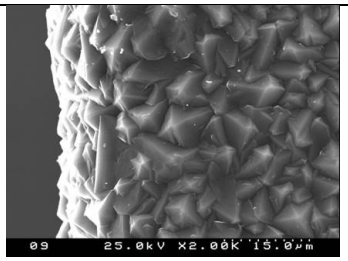

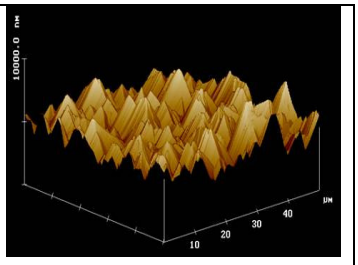

Introduction

Diamond films are among the most versatile and useful materials for advanced technological applications due to their highest hardness, chemical inertness, highest thermal conductivity, optical transparency, wide energy band gap, low dielectric constant and high carrier mobility. The crystal structure of diamond is cubic, consisting of essentially pure carbon with a hydrogen content less than 1% [1]. Each carbon atom is tetrahedrally coordinated to other four carbon atoms through sigma bonds formed from the sp^3 orbital hybridization. The lattice constant is 3.56 Å and the bond length is 1.54 Å [2].

Diamond growth at low pressures is a metastable process. Fig. 1 represents the phase diagram of carbon, where it is shown the very limited area where metastable diamond growth by chemical vapour deposition (CVD) is possible. In this region, graphite is still the thermodynamically stable phase. However, the growth of diamond at low pressures is determined by the adsorption, diffusion and linking of hydrocarbons radicals on the growth surface, as well as the reorganization of carbon atoms on the diamond lattice.

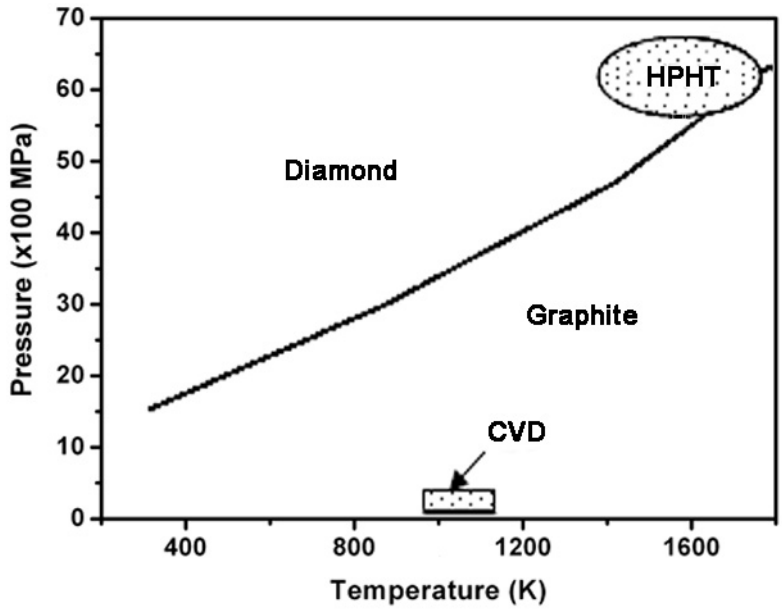

Fig 1. Phase equilibrium of diamond and graphite (adapted from [3]).

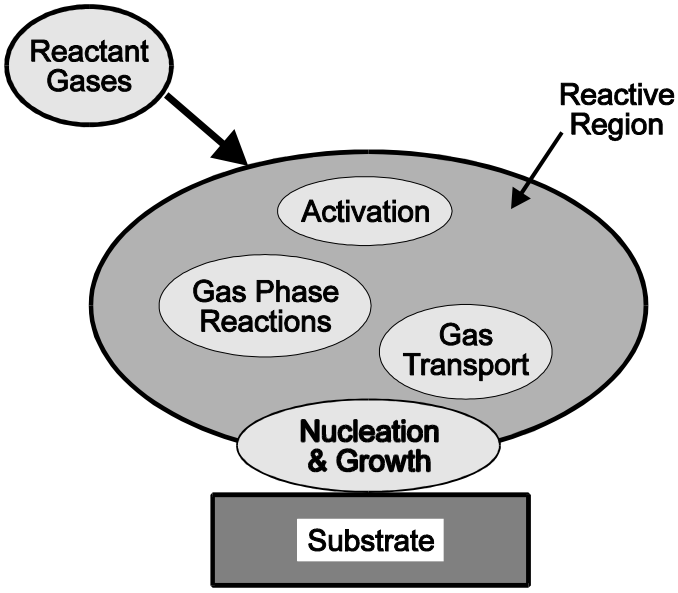

Fig. 2. Schematics of the main parts on the process of CVD diamond growth (after [4]).

CVD diamond growth process consists on the conversion of gases containing carbon species into diamond. Generally, the precursor gases are composed by hydrogen with a low percentage or hydrocarbons. The most used is methane (CH_4) in 0.1 to 5 vol.% [3,4]. The mixture of these gases flows over an activation region and react within the gas phase to produce precursor carbon species. These carbon species reach the substrate and react on its surface to promote diamond nucleation and growth. The process is schematically shown on Fig. 2.

The reason for the growth of diamond at low pressures was first theoretically advanced by Derjargin and co-workers, together with Angus [5]. They stated that the process is kinetically controlled rather than thermodynamically. The "kinetic advantage" consists on the preferential etching of graphite over diamond by hydrogen atoms. Since these two allotropic forms of carbon are formed simultaneously on the process, graphite (or graphitic phases) is removed by reaction with H faster than diamond. The sequence of events that take place on the process are shown:

1- Formation of atomic hydrogen on the activation region: In this region, supersaturation of atomic hydrogen is reached by the dissociation of molecular hydrogen at

temperatures over 2000ºC, as shown in reaction (1). Examples of energetic sources are: hot filaments, microwave plasmas, DC arcjet plasmas and combustion flames [4].

$$H_2 \Leftrightarrow H\bullet + H\bullet \quad (1)$$

2- Formation of carbon growth precursors: The kinetics of the chemical reactions occurring inside the chamber is complex, and becomes even more intricate with the increment of different reactant gases, as O_2, Ar, N_2, CF_4 [4]. The modelling of gas kinetics based on *in situ* diagnostics indicate methyl radical and acetylene (C_2H_2, produced from endothermic reaction of CH_4) as the most probable gas precursors of diamond growth because they are the most abundant species [4,6]. The formation of methyl radicals is due to the abstraction reaction of hydrogen with CH_4 molecule, as exemplified in the reaction (2):

$$CH_4 + H\bullet \Leftrightarrow CH_3\bullet + H_2 \quad (2)$$

3- Transport and adsorption of active species on the substrate surface: The hydrogen-terminated bond on the substrate surface is "attacked" by atomic hydrogen on the gas (hydrogen abstraction reaction), creating a carbon radical site on its place (Fig. 3). The acetylene molecule or methyl radical is adsorbed on this radical site (Fig. 4). After that, a recombination reaction occurs, allowing the formation of carbon-carbon bonds and thus, carbon incorporation into the diamond lattice (Fig. 4)[5]. Stabilization of the tetrahedracoordinated (sp^3 bonding) carbon species is achieved by a recombination mechanism of atomic hydrogen on the active sites, passivating the surface[5,7].

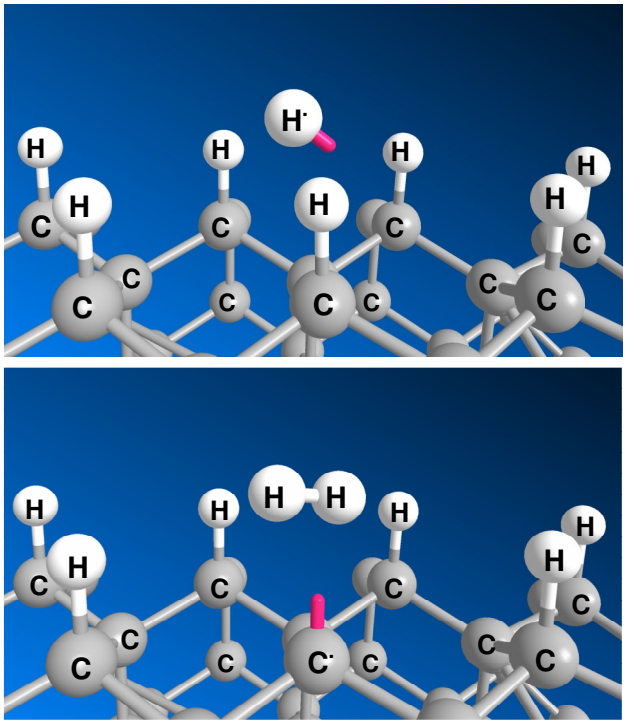

Fig 3. Scheme of diamond growth: Abstraction of atomic hydrogen and the consequent formation of activate sites on the growth surface.

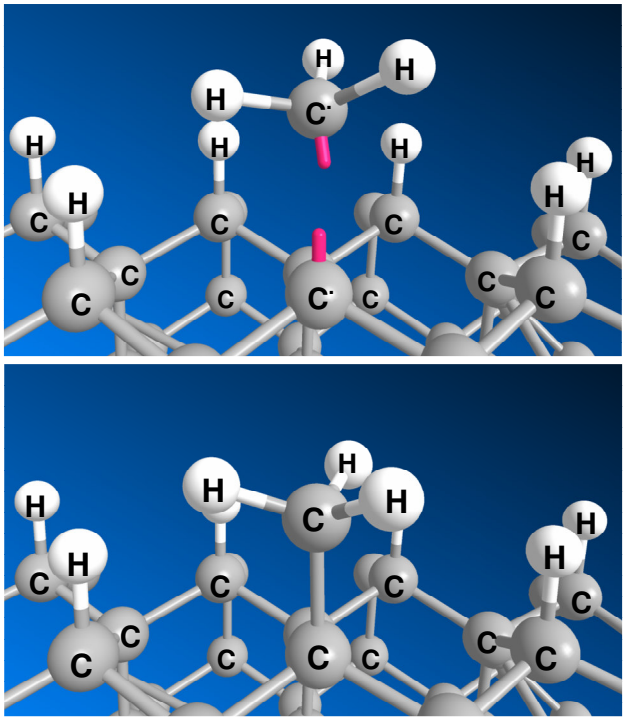

Fig 4. Scheme of diamond growth: Adsorption and recombination of methyl radicals on the growth surface (formation of sp^3 diamond bonds).

Mechanisms of diamond nucleation

The nucleation of diamond on the substrate is a very important step for high rate growth and uniformity. In the case of non-diamond substrates, the nucleation density is very low, and an efficient pre-treatment before diamond deposition is crucial. One of the most effective methods is the "scratching/seeding" one. It consists on the impregnation of the substrate with diamond powder, where very fine diamond particles are established in the irregularities of the surface. This can be done by scratching the surface with diamond powders in a dry way form [9], or by impacting it ultrasonically with a diamond suspension in an organic solvent [10]. Others abrasive powders were also used, as Al_2O_3, SiO_2, for roughening of the surfaces to create high energy sites for diamond growth. However, a much smaller nucleation density of 1.4×10^5 cm^{-2} created by Al_2O_3 against 5.7×10^9 created by diamond particles was reported [10].

A complete review on this subject is presented by Liu and Dandy [11]. They collected a number of possible explanations for diamond nucleation enhancement on scratched substrates, some of them are: (a) seeding effect, (b) minimization of interfacial energy on sharp convex surfaces, (c) breaking of a number of surface bonds, or presence of a number of dangling bonds at sharp edges, (d) strain field effects and (e) rapid carbon saturation (fast carbide formation) at sharp edges.

Although the scratching/seeding are simple and effective for diamond nucleation, it also causes surface damage and contamination. Some applications require extremely smooth and clean surfaces, as electronic devices and optical window. In such cases, alternative methods as biasing or interlayer coatings can be used with comparable to or even better results than those achieved by seeding of scratching [11-14].

Other explanations of diamond nucleation on non-diamond substrates include the formation of:

- diamond-like amorphous carbon (a-C) [11,15,16]. This mechanism proposes the formation of an a-C interlayer, providing nucleation sites to diamond. Carbon cluster are formed on the substrate surface, where the change of sp^1 to sp^2 bonds occur. The subsequent atomic hydrogen changes the bond structure to sp^3 and the competition of

sp^2/sp^3 etching occurs. The diamond structure develops due to the lower etching rate of sp^3 bonds relatively to the sp^1 and sp^2 (about 10 times). The formation of an amorphous-carbon layer was also observed by Fitzgerald and co-workers[17] using (100) silicon as diamond substrate.

- graphite [11,18]. It is proposed that graphite initially condenses on the substrate surface and that the {1100} prism planes are subsequently hydrogenated, where diamond preferentially nucleates with an almost perfect interface.

- metal carbide [11,18]. It can occur when the substrate is a carbide former, as Si, Ti, Mo, Ta and W. This mechanism proposes that initially carbon diffusion into the substrate takes place, resulting in the formation of stable metal carbide. The diamond nucleation is believed to occur only after the formation of a thin carbide layer, when the saturation of carbon on the surface reaches the limit. The formation of an interfacial SiC layer was evidenced by infrared measurements on Si substrate [19]. Another work [20], based on HRTEM analysis, reported the formation of amourphous SiC layer on Si substrates of 10 to 100 Å, followed by amourphous carbon film, where diamond nucleation occurs. Nistor and co-workers[21] related the formation of an amourphous SiC interlayer of 20-70 nm when CH_4 concentration was higher than 5% while no visible interlayer by TEM cross-section analysis was observed at lower CH_4 values [21]. Morrison and co-workers[22] performed CVD diamond growth on titanium and molybdenum. Analysis of X-Ray diffractometry showed the presence of TiC and Mo_2C. The formation of TiC interlayer was also found in an important titanium alloy, Ti_6Al_4V, used in biomedical and aerospace applications [23]. A graded interlayer of amouphous TiCN of only 8 Å was suggested by Contreras on TiN substrate, as observed by HRTEM images and EDS measurements [12]. In the case of Si_3N_4 substrate, it is believed that the SiO_2 presented on the surface reacts with carbon to produce a β-SiC interlayer [18,24]. A graded interlayer of SiCN by reaction of Si_3N_4 surface with hydrocarbons is also taken into account [18]. The formation of SiC from direct reaction of Si_3N_4 with C is reported to be possible only at temperatures above 1350 ºC [25]. Although the substrate temperature generally do not surpass 900-1000ºC, the temperature of the plasma near the surface sample can be much higher than that, and the reaction turns feasible [18]. Buchkremer-Hermanns and co-workers[26] consider the formation of a SiC interlayer between diamond and Si_3N_4, although they could not detect it by glazing incidence X-Ray

diffraction. They believed that insufficient detection sensitivity for very thin films, texture effects or presence of amorphous layers are possible reasons.

The knowledge of the exact nature of the diamond/substrate interface is not an easy task, as shared by Fitzgerald[17]. This study has also been made by cross-sectional TEM observations, and the preparation of the samples is known to have practical problems. Due to the small dimensions of the interface layers, the accurate identification of their composition and phase can not be done by electron diffraction or electron energy loss spectroscopy[17].

CVD diamond deposition techniques

The CVD techniques used to grow diamond films basically differ on the way that the gases are activated. The main ones are: microwave plasma (MPCVD), hot filament (HFCVD), arc-jet plasma (AJCVD) and combustion flame. Two techniques were used in the present thesis, the MPCVD and HFCVD, and they will be following detailed:

Microwave Plasma assisted Chemical Vapour Deposition (MPCVD): in this technique, plasma can be generated using a microwave generator of 2.45 GHz with an electron density of typically 10^{20} electrons/m^3 [2]. The gases are ionized by the high frequency electric field, and the electrons are accelerated to high energy levels, colliding with the gas molecules. Consequently, heating and dissociation of the gas molecules occurs, originating the active species to diamond deposition. Samples are placed beneath the plasma ball, being the area of deposition limited by the size of the plasma formed. Diamond growth rate is typically from < 1 $\mu m \cdot h^{-1}$ up to 10 $\mu m \cdot h^{-1}$, but it is dependent not only of the growth parameters, but is also strongly dependent of the microwave power [4]. The commercial microwave reactor, produced by Applied Science Technology Inc. (ASTEX PDS 18), was used to grow diamond on silicon nitride cutting tools. The deposition area of this reactor is 20 cm^2. Fig. 5 shows the overview of the reactor and a close-up image of the samples inside the chamber while diamond growth occurs. This reactor is located at the Physics Department of University of Aveiro.

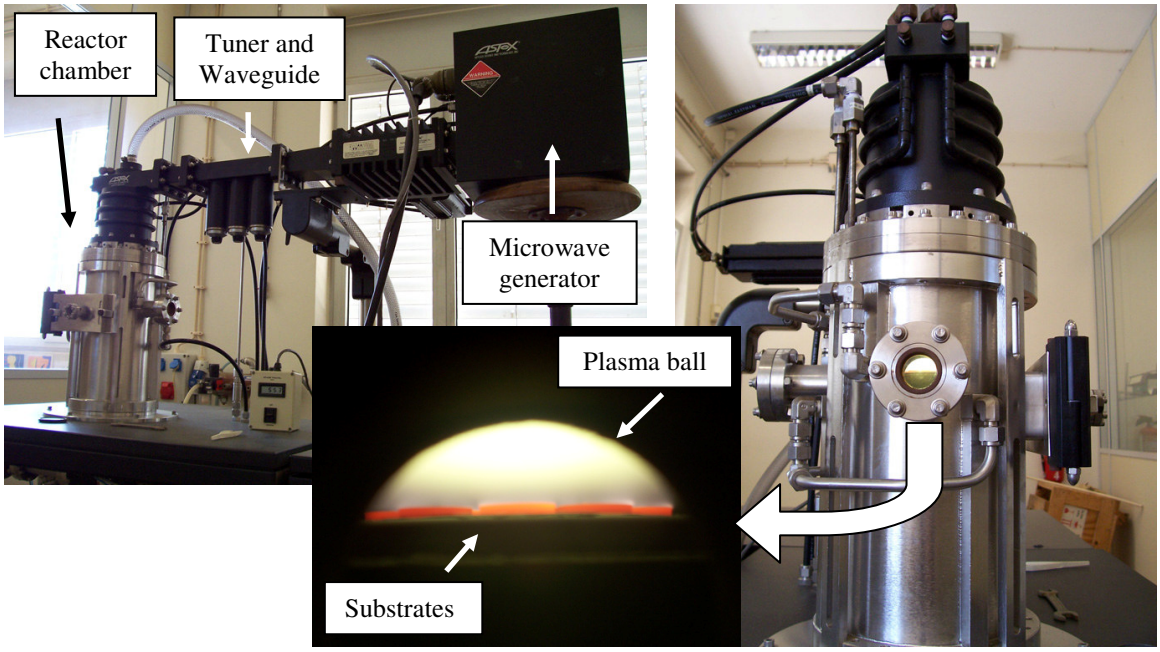

Fig. 5. General overview of the microwave plasma chemical vapour deposition system.

During MPCVD deposition, the substrate is heated only by the plasma ball and, although its temperature can not be measured accurately, it is estimated to be above 800 ºC. Growth conditions were set in earlier works of the group, taking into account requisites as: high growth rate of about 6 $\mu m \cdot h^{-1}$, good quality of the film characterized by a sharp diamond Raman peak at 1332 cm^{-1} with low graphitic contents, good adhesion to silicon nitride substrates supporting critical loads of about 1000N, as evaluated by Brale indentation method [27]. Considering this, the used deposition parameters of microcrystalline diamond were as follows: microwave power=2.25 kW; total pressure=1.2×10^4 Pa; H_2/CH_4 flow=400/25 sccm.

Hot Filament Chemical Vapour Deposition (HFCVD): in this case, the gas precursors of diamond deposition flow over hot filaments where the hydrogen is catalytically dissociated, starting the production of active species. The temperatures of the hot filaments are generally between 2000 and 2400ºC and can be made of tungsten (the most common), tantalum, rhenium or molybdenum [4]. The configuration can be coiled or linearly stretched, being the substrates placed at about 5-10 mm below the filaments. The area of deposition is restricted by the active region of an individual filament, which comprises just a small

volume around it. However, a system of multi-filaments can increase substantially the deposition area and the simplicity of such scale-up constituted a great advantage over the microwave reactors. The HFCVD growth rate range can be of the same magnitude of MPCVD, between <1-10 $\mu m \cdot h^{-1}$, depending on the deposition conditions and the required quality of the films, but is usually lower for high quality films, not exceeding 2-3 $\mu m \cdot h^{-1}$. The HFCVD reactor used in this work is a home-made steel chamber, located at the Department of Glass and Ceramics Engineering of the University of Aveiro. The overview of the reactor is presented in Fig. 6. In this system, the substrate is pre-heated by the thermal radiation of the filaments, and aided by an external power supply. The substrate temperature is measured by a K-type thermocouple placed at the back side and controlled by using a Shymaden SR24 controller while the filament temperature is measured by a two-colour pyrometer RAITEK (Marathon series MR15).

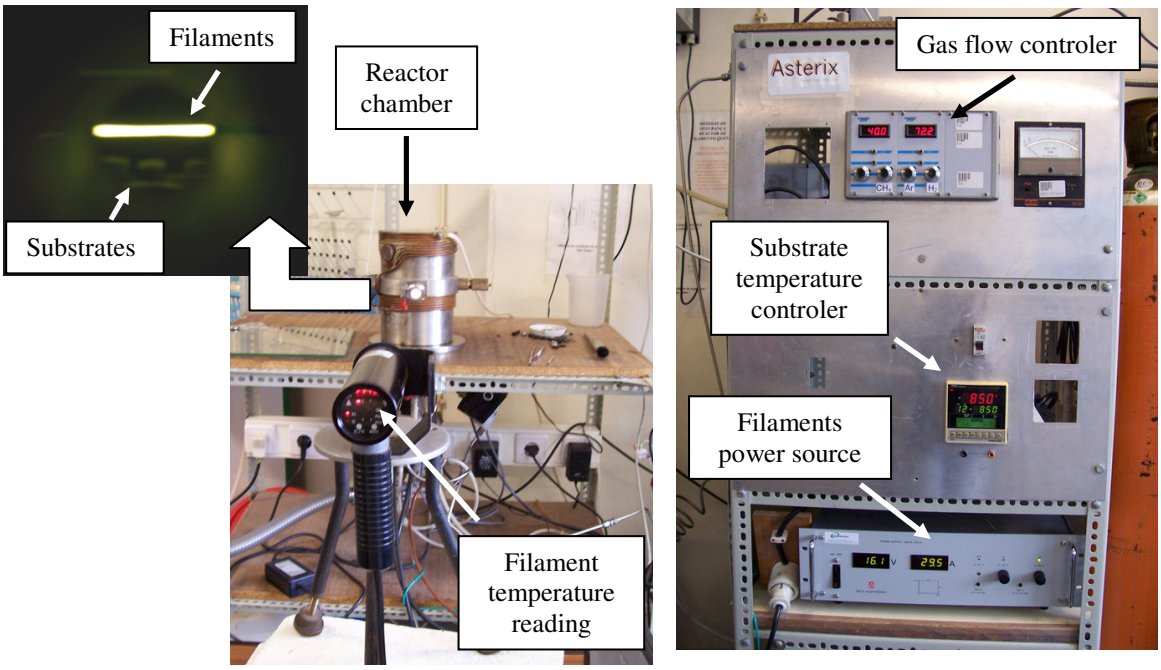

Fig. 6. General overview of the hot filament chemical vapour deposition system.

Four linear tungsten filaments wires of 250 µm diameter distanced about 5mm of each other were used as gas activator. With this configuration, a homogeneous deposition area of 6 cm^2 is possible. Before diamond deposition, a carburization step of the filaments

is necessary to avoid contamination of the samples with volatized tungsten of the wire. The carburization parameters were optimized by Tallaire[28] in his M.Sc. dissertation work. The carburization is done at the following conditions: start filament temperature = 2400ºC, CH_4/H_2 = 0.02, total pressure = 67 mbar, total flow = 100 sccm, time = 30 minutes. In this process, the formation of W_2C at the outer shell occurs, followed by a secondary conversion of W_2C/WC from the outside of the filament to the centre [29]. These structural changes increase the resistance of the filament and the temperature drops drastically. It was found that, after 30 minutes at such carburization conditions, the temperature remains constant at 2200ºC and it is ready to be used to growth step. Care has to be taken after the carburization, since the filaments are now very brittle due to the volume expansion of about 9-12% leading to crack formation on the surface of the wire [29].

Comparison between MPCVD and HFCVD techniques

Some advantages/disadvantages of both CVD apparatus can be listed:

- Higher stability of the MPCVD deposition process, which allows uninterrupted deposition, lasting for days if necessary, while in the case of HFCVD such stability depends of filament integrity (distortion, volatizing, embrittlement);
- Cleaner MPCVD environment, no film contamination from metal wires, as in the case of HFCVD;
- Growth rate is at least twice for the MPCVD diamond films than those of HFCVD for similar quality films;
- In the case of the apparatus used in this work, the deposition area of the MPCVD method is more than three times of HFCVD, at the present;
- Much easier and cost effective fabrication or up-scaling potential of HFCVD reactor, the deposition area is only dependent of number of the multi-filaments, gas distribution over them and power supply;
- Higher film thickness uniformity, less edge effect of the HFCVD films against the MPCVD ones;

- Complex sample geometry is much easier to be uniformly coated with HFCVD method than with MPCVD one;
- Both methods can use bias to enhance nucleation.

Complex geometries, edges of pointed zones disturb the electrical field, leading to a non-uniform temperature distribution, irregular grain sizes and uneven film thickness [30]. To minimize the edge effect, masks can be used to fill the empty spaces between the samples, or use the maximum number of samples keeping them as close as possible. Figure 7 presents a SEM cross-sectional view of a microcrystalline diamond film growth by the MPCVD method, were the difference of film thickness between the edge and the central part of the sample can be as high as the double (Fig. 7a and 7b, respectively). Diamond grain size is also higher on the edge than on the centre, as the respective Fig. 8 c) and d) show.

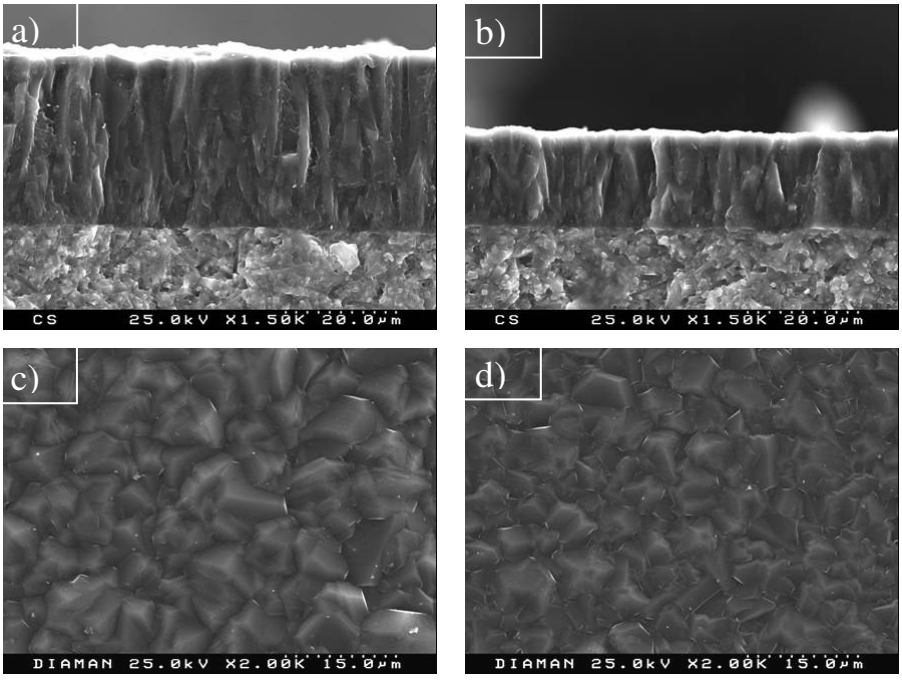

Fig. 7. Microcrystalline diamond film deposited by MPCVD method.

In the case of samples coated by HFCVD method, such difference is not so evident, although film thickness varies at about 30% from centre to the edge parts. In this case, a higher convection movement of the gases may cause such difference.

The HFCVD technique is mainly exploited for the production of nananocrystalline diamond (NCD) because a previous deposition study performed by the group successfully led to growth rates of up to 1.6 $\mu m \cdot h^{-1}$ [31]. Also, the MPCVD reactor became inoperative for a long time. The growth parameters were: filament temperature = 2300ºC; total pressure= 25-50 mbar; CH_4/H_2 = 0.02-0.04; Ar/H_2 = 0-0.1; total flow = 50-100 sccm; substrate temperature = 750-850ºC.

Micro- and nanocrystalline CVD diamond characteristics

The growth of CVD polycrystalline diamond can promote, basically, two kinds of microstructure [32]:

- Columnar: consisting of columnar grains of preferred orientation that grow from the first nucleated layer deposited on the substrate. This structure is typical of microcrystalline (MCD) diamond films.

- Equiaxed: consisting of fine and randomly oriented grains, typical of nanocrystalline (NCD) diamond.

In the case of MCD, well-faceted single crystallites are observed (Fig. 7) while in NCD deposition round-shaped crystallites grow. This change in microstructure is caused by the rate of secondary nucleation, which is low for MCD but very high for NCD diamond deposition. The most important characteristic of NCD growth is that the crystallite size does not depend on the film thickness [33,34]. Conversely, the growth of MCD films is columnar, and the crystallite size increases with thickness as a consequence of the evolutionary crystal growth mechanism [32].

The synthesis and characterization of NCD diamond film has recently received considerable attention, since it possesses several unique properties compared to the conventional MCD one [16,31-47]. The main properties can be said to have a smoother surface, lower friction coefficient against a wide range of materials, together with a wide band gap and higher electron emission efficiency [47]. These special characteristics make NCD diamond a better coating material for mechanical applications, a better candidate as an optical or electrical component and as a cold cathode material.

The control of CVD diamond film microstructure is achieved by changing the deposition parameters to growth or re-nucleation conditions of diamond. Such parameters are highly dependent on the technique used as well as geometric factors of the reactor chamber. NCD films can be produced in a microwave plasma CVD reactor from a variety of feed gas mixtures such as fullerenes/Ar, CH_4/Ar, CH_4/N_2, or CO/H_2 [36,40,41,44,46]. The diamond crystallite size typically varies from 3 to 30 nm and the surface roughness from 15 to 40 nm [42]. The hot filament CVD technique can also be used to grow such coatings either by applying a bias current that can be used to enhance growth rate and minimize grain size and surface roughness [48] or by carefully adjusting deposition conditions under $H_2/Ar/CH_4$ gas mixtures [31,40,49]. The increase of CH_4/H_2 ratio also enhances the secondary diamond nucleation, but above a given ratio, graphite may form and prevents diamond nucleation [48].

NCD is normally described as nanocrystalline diamond grains embedded in a predominant tetrahedrally coordinated amorphous carbon network [42]. However, this kind of NCD film are often termed "cauliflower" or "ballas" diamond, because of the substancial amount of sp^2-bonded nature of the grain boundaries [40,41,46]. The so-called "Ultra-Nanocrystalline" diamond (UNCD), is said to differ from NCD due to its much smaller grain sizes (3-5 nm) and have an abrupt grain boundaries with negligible sp^2-bonded carbon [40]. This material has been used to fabricate UNCD probes for nanolithography in atomic force microscopy (AFM) in non-conducting (undoped) and conducting (nitrogen-doped) states [50]. Kulisch and co-workers[32,35] classify their NCD films of "NCD/a-C films". Although their diamond grain sizes reached the UNCD domain, the μ-Raman spectra of the films showed a large contribution of the D and G band (band of the disordered (~1340 cm^{-1}) and microcrystalline (~1560 cm^{-1}) graphite, respectively), together with a suppression of the diamond peak (~ 1332 cm^{-1}). The presence of bands around 1140 and 1490 cm^{-1}, related to acetylene C-H chains, were also detected and are accepted as NCD signature [51].

Stress and adhesion of diamond film

The adhesion of the diamond film to the substrate is strongly affected by the stress that usually remains after growth. Stressed films tend to split under tension and can even peel off from the substrate under compressive strain [52]. So, the understanding of the source and nature of the residual stresses in the CVD diamond films is an important matter. Generally, the residual stress in these films is divided in two components:

- Extrinsic (thermal) stress: it appears when the sample is cooled from growth down to room temperature, caused by the difference between the thermal expansion coefficients of film and substrate. Thermal stress (σ_{th}) can be estimated as shown in Eq. 3 [53]:

$$\sigma_{th} = \frac{E}{1-\nu}\int_{T_{amb}}^{T_{dep}} (\alpha_{diam} - \alpha_{subst})dT \qquad \text{(Eq.3)}$$

where E = 1143 GPa and $\upsilon = 0.07$ are Young's modulus and Poisson's ratio for diamond, α_{diam} and α_{subst} are the temperature-dependent coefficients of thermal expansion of diamond film and substrate, respectively.

- Intrinsic stress: it develops during film growth, and is associated to the non-diamond material at the grain boundaries and also to structural defects, like impurities, micro twins, dislocations, etc.

The most common methods to determine the residual stress in diamond films are the substrate curvature technique [54], peak deviation in x-ray diffraction [55] and Raman spectra [53,56]. Particularly, Raman spectroscopy gives a simple method that evaluates the residual stress through the diamond Raman peak shifts. The diamond shift values are used to evaluate the residual stress (σ_{res}) of the coating by the expression given in Eq. 4 [53]:

$$\sigma_{res}(GPa) = -0.567\Delta\upsilon(cm^{-1}) \qquad \text{(Eq. 4)}$$

where $\Delta\nu$ is the difference between the measured and the natural stress-free (1332 cm^{-1}) diamond peak shifts. The positive shift of Raman peak from 1332 cm^{-1} is attributed to the compressive stress, while the negative shift means a tensile stress state [57].

Residual stress can be the cause of poor substrate adhesion and also contribute to the failure of the coating by its delamination. The mismatch in the thermal expansion coefficient is one of the limitating factors on the choice of the appropriate substrate of CVD diamond films for mechanical and tribological applications. In such applications, the diamond film is usually subjected to very high tensile/compressive stress, and shear forces as well as high and fluctuating temperatures. From the materials used in tooling applications, Si_3N_4 has the closest thermal expansion coefficient to diamond, together with better chemical compatibility for diamond nucleation and growth than tungsten carbide, as said before [58]. Besides the higher thermal stress, the major problem of the tungsten carbide tool inserts is the chemical interaction between the cobalt binder and diamond, catalyzing the formation of graphite and avoiding a sufficiently bonding between diamond and the carbide [4]. Efforts has been made to improve adhesion of diamond coatings to tungsten carbide tools, as using of interlayers of Si, Si_3N_4, SiC, Si(C,N), Ti-Si and CrN [58-60], introducing Si-chemical reagents to the gases during diamond growth [61] or removing the cobalt from the surface by chemical etching with H_2O_2, H_2SO_4, HNO_3 [13,62].

Adhesion is the interaction (bonding) between two adjacent surfaces (film and substrate), and can be of chemical and/or mechanical nature. The chemical bonding of the diamond film to the substrate is related to the nature and formation of an interlayer, as said before. Mechanical bonding is due to the mechanical interlocking of the surface asperities in contact [18]. As earlier referred, Si_3N_4 is chemically compatible to diamond and so, chemical bonding is assured. In order to improve the adhesion strength, the mechanical surface preparation of the substrate is a critical step to enhance the physical interlocking on the interface, at the same time that increases the surface area available for chemical bonding. The surface of the tool is usually first finished by grinding, but the strength of the mechanical bonding in this case is dependent on the direction of the force applied, parallel or normal to the feed marks [18]. More isotropic interface strength of the bonding can be reached by polishing the tool surface followed by chemical etching, e.g. HF and HNO_3 hot acids or CF_4 and H_2 plasmas, , roughening it on a microscale level. This type of interface

may provide a tough, crack deflection mechanism, redirecting the crack extension from the interface through the film or substrate [63]. Belmonte and co-workers [27] have studied the adhesion behavior of diamond coated silicon nitride by acoustic emission coupled with Brale indentation test. By this method, the interfacial cracking resistance is calculated by measuring the radial cracks produced on the vicinity of the indentation mark. They found that the adhesion can be improved with a higher roughness of the substrate.

The following papers present the characterization of the diamond films by scanning electron microscopy (SEM) with respect to their morphology, macroscopic structure and thickness, by X-ray diffraction (XRD) concerning their crystalline properties, by μ-Raman spectroscopy to access their quality and residual stress state, atomic force microscopy (AFM) to investigate the morphology and surface roughness, and Brale indentation test to evaluate the film adhesion.

References

[1] Choy KL. Chemical vapour deposition of coatings. Progress Mater. Sci. 2003; 48: 57-170.

[2] Pierson HO. Handbook of carbon, graphite, diamond and fullerenes: properties, processing and applications. New Jersey: Noyes Publications, 1993.

[3] Silva LLG. Eletrodos em diamante CVD para estudos eletroquímicos. Doctoral Thesis. Instituto Tecnológico de Aeronáutica. São José dos Campos, São Paulo, Brasil. 2001.

[4] Trava-Airoldi VJ, Corat EJ, Baranauskas V. Diamond chemical vapour deposition: emerging technology for tooling applications. Key Eng. Mater. 1998; 138-140: 195-244.

[5] Frenklach M. In: Clausing RE, Horton LL, Angus JC, Koidl P. (Eds.) Diamond and diamond-like films and coatings. New York: Plenun Press, 1991, pg. 499.

[6] Dandy DS and Coltrin ME. In: Asmussen J and Reinhard DK (Eds.) Diamond thin films handbook. New York: Marcell Dekker, 2001, cap. 4.

[7] Gupta BK and Bhushan B. Wear resistant coatings for contact recording applications. IEE Transactions of Magnetics 1995; 31: 3012-3014.

[8] Siqueira VR. Estudo da formação do hidrogênio atômico no filamento do reator HFCVD. Master Dissertation. Instituto Nacional de Pesquisas Espaciais. São José dos Campos, São Paulo, Brasil. 2006.

[9] Belmonte M, Silva VA, Fernandes AJS, Costa F, Silva R. Surface pretreatments of silicon nitride for CVD diamond deposition. J. Am. Ceram. Soc. 2003; 86: 749-754.

[10] Anger E, Gicquel A, Wang ZZ, Ravet MF. Chemical and morphological modifications of silicon wafers treated by ultrasonic impacts of powders: consequences on diamond nucleation. Diam. Relat. Mater. 1995; 4: 759-764.

[11] Liu H, Dandy DS. Studies on nucleation process in diamond CVD: an overview of recent developments. Diam. Relat. Mater. 1995; 4: 1173-1188.

[12] Contreras O, Hirata GA, Avalos-Borja M. Interface analysis of CVD diamond on TiN surfaces. Appl. Surf. Sci. 2000; 158: 236-245.

[13] Kamiya S, Yoshida N, Tamura Y, Saka M, Abé H. Quantitative measurement for the effect of enhanced nucleation on the adhesive strength of diamond coatings. Surf. Coat. Technol. 2001; 142-144: 738-742.

[14] Larijani MM, Navinrooz A, Le Normand F. The bias-assisted HF CVD nucleation of diamond: investigations on the substrate temperature and the filaments location. Thin Sol. Films 2006; 501: 206-210.

[15] Singh J. Nucleation and growth mechanism of diamond during hot-filament chemical vapour deposition. J. Mater. Sci. 1994; 29: 2761-2766.

[16] Zhou XT. Li Q, Meng FY, Bello I, Lee CS, Lee ST, Lifshitz Y. Manipulation of the equilibrium between diamond growth and renucleation to form a nanodiamond/amourphous carbon composite. Appl. Phys. Let. 2002; 80: 3307-3309.

[17] Fitzgerald AG, Fan Y, John P, Troupe CE, Wilson JIB, Tooke AO, Storey BE. Study of the interface microstructure of CVD diamond films by TEM. Mikrochim. Acta 2000; 132: 315-321.

[18] Mallika K, Komanduri R. Low pressure microwave plasma assisted chemical vapor deposition (MPCVD) of diamond coatings on silicon nitride cutting tools. Thin Sol. Films 2001; 396: 145-165.

[19] John P, Graham C, Milne DK, Jubber MG, Wilson JIB. An FTIR study of the heteroepitaxy of diamond on silicon. Diam. Relat. Mater 1996; 5: 256-260.

[20] Stoner BR, Ma GHM, Wolter, SD, Glass JT. Characterization of bias-enhanced nucleation of diamond on silicon by *in vacuo* surface analysis and transmission electron microscopy. Phys. Rev. B 1992; 45: 11067-11092.

[21] Nistor LC, Landuyt JV, Ralchenko VG, Smolin AA, Korotushenko KG, Obraztsova ED. Structural studies of diamond thin films grown from dc arc plasma. J. Mater. Res. 1997; 12: 2533-2542.

[22] Morrison NA, Drummond IC, Garth C, John P, Milne DK, Smith GP, Jubber MG, Wilson JIB. Growth of CVD diamond films over bio-medical materials. Diam. Relat. Mater. 1996: 5; 1118-1126.

[23] Azevedo AF, Corat EJ, Leite NF, Trava-Airoldi VJ. Chemical vapor deposition diamond thin films growth on Ti_6Al_4V using the Surfatron system. Diam. Relat. Mater. 2002; 11: 550-554.

[24] Lux B and Haubner R. In: Clausing RE, Horton LL, Angus JC, Koidl P. (Eds.) Diamond and diamond-like films and coatings. New York: Plenun Press, 1991, pg. 579.

[25] Rozbicki RT, Sarin VK. Nucleation and growth of combustion flame deposited diamond on silicon nitride. Int. J. Refr. Metals Hard Mater. 1998; 16: 377-388.

[26] Buchkremer-Hermanns H, Ren H, Kohlschein G, Weiβ H. Surf. Coat. Technol. 1998; 98: 1038-1046.

[27] Belmonte M, Fernandes AJS, Costa FM, Oliveira FJ, Silva RF. Adhesion behaviour assessment on diamond coated silicon nitride by acoustic emission. Diam. Relat. Mater. 2003; 12: 733-737.

[28] Tallaire A. Diamond coating of silicon nitride by hot filament chemical vapouor deposition. Master Dissertaion. Universidade de Aveiro. Aveiro, Portugal. 2002.

[29] Zeiler E, Schwarz S. Rosiwal SM, Singer RF. Structural changes of tungsten heating filaments during CVD of diamond. Mater. Sci. Eng. A 2002; 335: 236-245.

[30] Fernandes AJS, Silva VA, Carrapichano JM, Dias GR, Silva RF, Costa FM. MPCVD diamond tool cutting-edge coverage: dependence on the side wedge angle. Diam. Relat. Mater. 2001; 10: 803-808.

[31] Amaral M, Fernandes AJS, Vila M, Oliveira FJ, Silva RF. Growth rate improvements in the hot-filament CVD deposition of nanocrystalline diamond. Diam. Relat. Mater. 2006; 15: 1822-1827.

[32] Kulisch W, Popov C. On the growth mechanisms of nanocrystalline diamond films. Phys. Stat. Sol. (a) 2006; 203: 203-219.

[33] Gruen DM. Nanocrystalline diamond films. Annu. Rev. Mater. Sci. 1999; 29: 211-259.

[34] Zhou D, McCauley TG, Qin LC, Krauss, AR, Gruen DM. Synthesis of nanocrystalline diamond thin films from an Ar-CH_4 microwave plasma. J. App. Phys. 1998; 83: 540-543.

[35] Kulisch W, Popov C, Boycheva S, Jelinek M, Gibson PN, Vorlicek V. Influence of the substrate temperature on the properties of nanocrystalline diamond/amorphous carbon composite films. Surf. Coat. Technol. 2006; 200: 4731.

[36] Bruno P, Bénédic F, Tallaire A, Silva F, Oliveira FJ, Amaral M, Fernandes AJS, Cicala G, Silva RF. Deposition of nanocrystalline diamond films on silicon nitride ceramic substrates using pulsed microwave discharges in Ar/H2/CH4 gas mixture. Diam. Relat. Mater. 2005; 14: 432-436.

[37] Rabeau JR, John P, Wilson JIB, Fan Y. The role of C_2 in nanocrystalline diamond growth. J. App. Phys. 2004; 96: 6724-6732.

[38] Köpf A, Feistritzer S, Udier K. Diamond coated cutting tools for machining of non-ferrous metals and fibre reinforced polymers. Int. J. Refract. Met. Hard Mater. 2006; 24: 354-359.

[39] Abreu CS, Amaral M, Fernandes AJS, Oliveira FJ, Silva RF, Gomes JR. Friction and wear performance of HFCVD nanocrystalline diamond coated silicon nitride ceramics. Diam. Relat. Mater. 2006; 15: 739-744.

[40] May PW, Smith JA, Mankelevich YA. Deposition of NCD films using hot filament CVD and Ar/CH_4/H_2 gas mixtures. Diamond Relat. Mater. 2006; 15: 345-352.

[41] Haubner R, Lux B. Deposition of ballas diamond and nano-crystalline diamond. Int. J. Refract. Met. Hard Mater. 2002; 20: 93-100.

[42] Toprani N. Catledge SA, Vohra YK. Interfacial adhesion and toughness of nanostructured diamond coatings. J. Mater. Res. 2000; 15: 1052-1055.

[43] Gupta S, Weiner BR, Morell G. Synthesizing nanocrystalline carbon thin films by hot filament chemical vapor deposition and controlling their microstrucutre. J. Mater. Res. 2002; 17: 1820-1833.

[44] Catledge SA, Borham J, Vohra YK, Lacefield WR, Lemons JE. Nanoindentation hardness and adhesion investigations of vapour deposited nanostructured diamond films. J. Appl. Phys. 2002; 91: 5347-5352.

[45] Fries MD, Vohra Y. Properties of nanocrystalline diamond thin films grown by MPCVD for biomedical implant purposes. Diamond Relat. Mater. 2004; 13: 1740-1743.

[46] Fernandes AJS, Neto MA, Almeida FA, Silva RF, Costa, FM. Nano- and micro-crystalline diamond growth by MPCVD in extremely poor hydrogen uniform plasmas. Diamond Relat. Mater. 2007; 16: 757-761.

[47] Griffin J and Ray PC. Role of inert gas in the low-temperature nano-diamond chemical vapour deposition process. Nanotechnology 2006; 17: 1225-1229.

[48] Vojs M, Veselý M, Redhammer R, Janík J, Kadleciková M, Danis T, Marton M, Michalka M, Sutta P. Double bias HF CVD multilayer diamond films on WC-Co cutting tools. Diam. Relat. Mater. 2005 ; 14: 613-616.

[49] Zhang YF, Zhang F, Gao QJ, Peng, XF, Lin ZD. The roles of argon addition in the hot filament chemical vapor deposition system. Diam. Relat. Mater. 2001; 10: 1523-1527.

[50] Kim K-H, Moldovan N, Ke C, Espinosa HD, Xiao X, Carlisle JA, Auciello O. Novel ultrananocrystalline diamond probes for high resolution low-wear nanolitographic techniques. Small 2005; 1: 866-874.

[51] Ferrari AC, Robertson J. Origino f the 1150 cm^{-1} Raman mode in nanocrystalline diamond. Phys. Rev. B 2001; 63: 121405.

[52] Ferreira NG, Abramof E, Leite NF, Corat EJ, Trava-Airoldi VJ. Analysis of residual stress in diamond films by x-ray diffraction and micro-Raman spectroscopy. J. Appl. Phys. 2002; 91: 2466-2472.

[53] Ralckenko VG, Smolin AA, Pereverzev VG, Obraztsova ED, Korotoushenko KG, Konov VI, Lakhotkin YV, Loubnin EN. Diamond deposition on steel with CVD tungsten intermediate layer. Diam. Relat. Mater. 1995; 4: 754-758.

[54] Windischmann H, Epps GF, Cong Y. Collins RW. Intrinsic stress in diamond films prepared by microwave plasma CVD. J. Appl. Phys. 1991; 69: 2231-2237.

[55] Vila M, Amaral M, Oliveira FJ, Silva RF, Fernandes AJS, Soares MR. Residual stress minimum in nanocrystalline diamond films. App. Phys. Letters 2006; 89: 093109-1.

[56] Windischmann H and Gray KJ. Stress measurement of CVD diamond films. Diam. Relat. Mater. 1995; 4: 837-842.

[57] Pal AK. Plasma processing of super-hard coatings. Current Sci. 2002; 83: 225-236.

[58] Endler I, Leonhardt A, Scheibe H-J, Born R. Interlayers for diamond deposition on tool materials. Diam. Relat. Mater. 1996; 5: 299-303.

[59] Lin CR, Kuo, CT, Chang RM. Improvement in adhesion of diamond films on cemented WC substrate with Ti-Si interlayers. Diam. Relat. Mater. 1998; 7: 1628-1632.

[60] Polini R. Chemically vapour deposited diamond coatings on cemented tungsten carbides: substrate pretreatments, adhesion and cutting performance. Thin Sol. Films 2006; 515: 4-13.

[61] Fan F, Tang W, Liu S, Hei L, Li C, Chen G, Lu F. An effort to enhance adhesion of diamond coatings to cemented carbide substrates by introducing Si onto the interface. Surf. Coat. Technol. 2006; 200: 6727-6732.

[62] Polini R. Casadei F, D'Antonio P, Traversa E. Dry turning of alumina/aluminum composites with CVD diamond coated Co-cemented tungsten carbide tools. Surf. Coat. Technol. 2003; 166: 127-134.

[63] Cline BL and Olson JM. In: Asmussen J and Reinhard DK (Eds.) Diamond thin films handbook. New York: Marcell Dekker, 2001, cap. 10.

3.1 *Microstructural characterization and adhesion evaluation of the CVD diamond films*

NANO TO MICROMETRIC HFCVD DIAMOND ADHESION STRENGTH TO Si_3N_4

F. A. Almeida[1], M. Amaral[1], F. J. Oliveira[1], A. J. S.Fernandes[2], R. F. Silva[1]

[1] Department of Ceramics and Glass Engineering, CICECO, University of Aveiro, 3810-193 Aveiro, Portugal

[2] Department of Physics, University of Aveiro, 3810-193 Aveiro, Portugal

(Vacuum 81, 2007, 1443-1447)

Abstract

In the present study, hot filament chemical vapour deposition technique was used to grow diamond films from nanometric to microcrystalline grain sizes. Their adhesion levels to a silicon nitride ceramic were compared after Brale tip indentation testing. The best behaviour was attained by the microcrystalline diamond (MCD) grade due to its higher crystallinity and superior hardness. In contrast, nanocrystalline diamond (NCD) coatings showed the less effective chemical bonding to the ceramic substrate due to the higher degree of sp^2 content. The MCD coating supported a normal load of 1600N without spalling-off and presented an interfacial crack resistance of 12.0 $N \cdot \mu m^{-1}$, much better than that reported until the present. This behaviour may be attributed to the CF_4 plasma pre-treatment of the substrate.

Keywords: CVD diamond films; Silicon nitride; Adhesion

1. Introduction

CVD diamond coated materials possess unique properties (hardness, thermal conductivity, chemical inertness) that demand their selection as components of tribosystems working under mechanical and/or chemical severe conditions. Examples of industrial applications are cutting tools for highly abrasive materials and mechanical seals for pumping of corrosive liquids[1]. Furthermore, an interesting field of application is biomedicine, namely as coatings for articulated implants[2], where diamond's biocompatibility is an essential issue. Nevertheless, the high surface roughness of conventional microcrystalline CVD diamond is a major problem when considering such purposes, as the sliding contact of diamond asperities may increase the stress and temperature levels, leading to a wear-rate increase. To overcome this drawback, today's goal is the development of diamond crystals with nanometric size by selecting adequate CVD parameters, avoiding the typical columnar growth of microcrystalline diamond (MCD) structures. In this way, nanocrystalline diamond (NCD) coated materials are very suitable for tribological applications due to the excellent combination of high hardness and very low nominal surface roughness.

In all these tribological applications, adhesion of the film to the substrate determines the success of the component in service. In spite of the evaluation of NCD adhesion not be well characterized, namely on ceramic substrates such as silicon nitride (Si_3N_4), it represents one of the most compatible materials for CVD diamond deposition [3]. In this study, distinct grades of CVD diamond coatings of nanocrystalline, submicrometric and micrometric grain sizes were grown by hot filament technique on Si_3N_4 ceramic substrates. Their relative adhesion levels were also evaluated by Brale tip indentation.

2. Experimental Procedure

Disc-shaped Si_3N_4 substrates (Ø 10 mm × 3 mm thickness) were pressureless sintered (1750ºC-2h-0.1MPa N_2) using Y_2O_3 (7.0 wt %) and Al_2O_3 (3.7 wt %) as sintering aids. The substrates were sequentially ground with a 46 μm diamond wheel, polished with 15 μm diamond slurry in an iron/polymer plate, chemically dry etched with CF_4 plasma (1 h) and diamond seeded by a 0.5-1 μm suspension in n-hexane by ultrasound agitation (1 h).

Diamond growth was then conducted by hot filament chemical vapour deposition (HFCVD), in an in-house developed reactor. The thermal heat created by four linear and parallel tungsten wires (0.25mm diameter) were used as gas activation energy source. The distance between filaments and samples was kept at about 5 mm. Three kinds of diamond grain sizes were grown by selected deposition parameters: i) microcrystalline diamond (MCD) with flow ratio CH_4/H_2 = 0.02, chamber pressure (P) = 2.5 kPa, substrate temperature (Ts) = 850ºC, total flow (Q) = 100 sccm, deposition time (t) = 15 h; ii) submicrocrystalline diamond (SMCD) with CH_4/H_2 = 0.03, P = 2.5 kPa, Ts = 850ºC, Q = 100 sccm, t = 15 h ; iii) nanocrystalline diamond (NCD) with CH_4/H_2 = 0.04, Ar/H_2 = 0.10, P = 5.0 kPa, Ts = 750ºC, Q = 50 sccm, t = 19 h. Filament temperature was kept at about 2300ºC in all conditions. The thicknesses of the diamond films were about 30 μm, 33 μm and 39 μm for NCD, SMCD and MCD films, respectively. The diamond crystallite sizes were evaluated by X-ray diffraction as 27 nm (NCD) and 43 nm (SMCD). Although the submicrometric diamond with 43 nm of crystallite size reaches the usual nanometric assignement, this value taken from the Scherrer formula is only the lower limit of the real value[4], since SEM micrographs reveal that most of diamond grains fall in the range of 100-200 nm. The MCD grain size was estimated from SEM to be 12 μm.

The identification of diamond and graphitic phases were done by Raman spectroscopy at room temperature with an Ar ion laser (λ=488 nm). Adhesion was evaluated using diamond Brale indenters (cone angle of 120º and tip radius of 0.2 mm) adapted to an universal testing machine at discrete loads from 50 to 1700 N with a crosshead speed of 0.5 $mm \cdot min^{-1}$. During the experiments, the diamond indenter was carefully observed using a stereoscope and replaced when damaged. At least three

indentations per load were performed for each diamond grade. Circumferential (lateral) cracks of all the indentation imprints were measured using optical and scanning electron microscopy.

3. Results and Discussion

Highly faceted diamond grains and the columnar growth, typical of conventional microcrystalline diamond, can be seen in Fig. 1a for the MCD samples. The SMCD grade was obtained after increasing the methane concentration by 1vol.% relatively to the MCD growth, which lead to a much smaller diamond grain size and a very smooth surface, as can be seen in Fig. 1b. Finally, NCD films were grown by partial substitution of hydrogen by Argon and further methane increase, promoting the renucleation of diamond [5], resulting in tiny diamond grains with an intrinsic ultra-smooth film surface (Fig. 1c). These morphological differences are further evidenced by their physical properties, as can be seen by the corresponding Raman signatures (Fig. 1d-f). One important feature is the suppressing of the diamond peak (1332 cm^{-1}) and the raising of the graphitic D-band (~ 1360 cm^{-1}), as the diamond crystallite size decreases. Also, the intensity of the G-band of graphite (~1560 cm^{-1}) notably increases in both the SMCD and NCD coatings. In addition, the Raman spectra deconvolution evidences the presence of peaks near 1140 and 1480 cm^{-1}, assigned to C-H chain structures as trans-polyacetylene [trans-$(CH)_n$] and widely accepted as typical of nanocrystalline diamond. The increase in the sp^2 character of the films can be explained by the high hydrocarbon supersaturation and decrease of atomic H density in SMCD and NCD samples, which is responsible for etching the non-diamond carbon phases[5, 6].

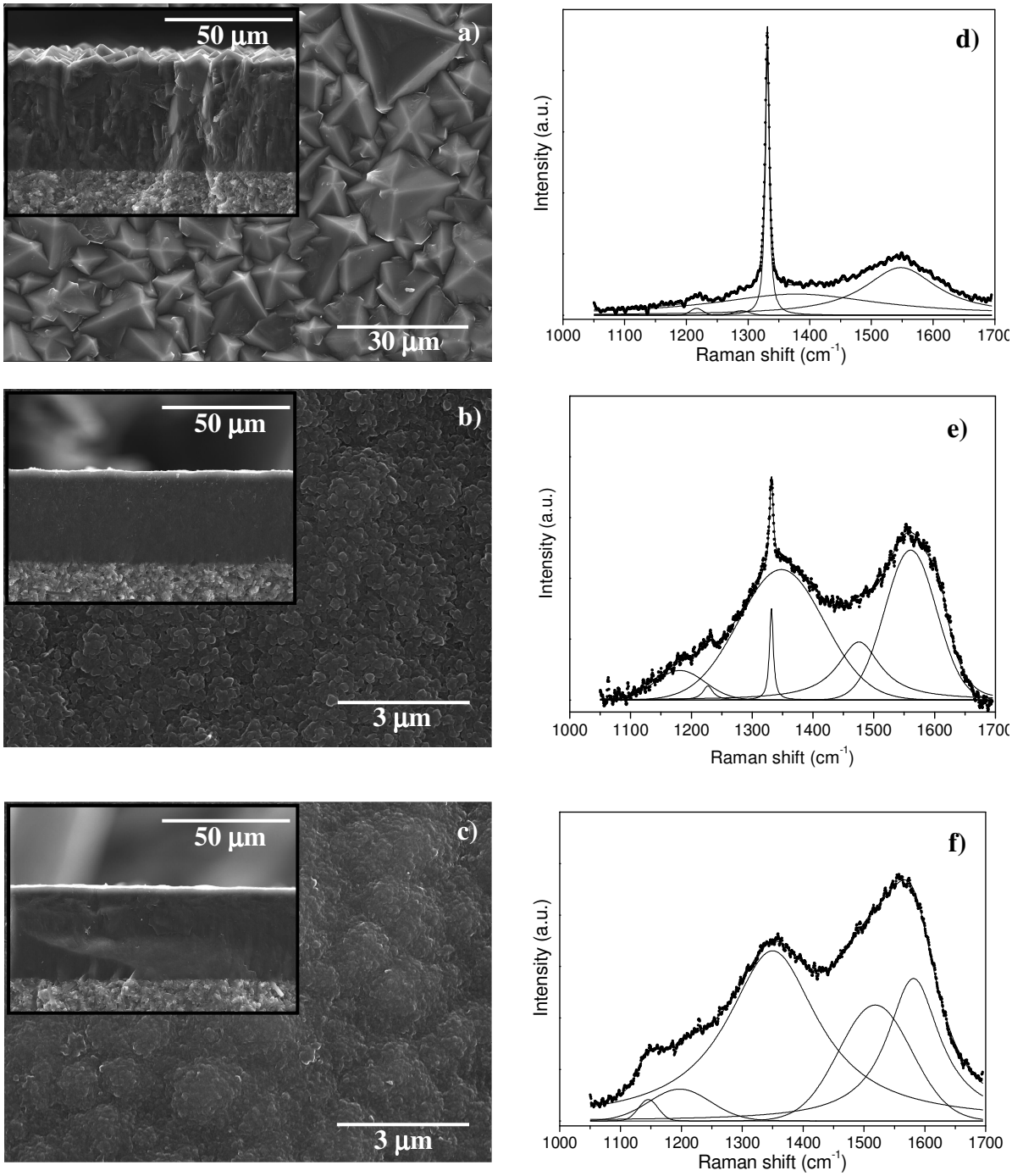

Fig. 1. SEM micrographs and cross-section insets of: a) MCD; b) SMCD and c) NCD; d) to f) are the respective Raman spectra.

Despite the very low difference in the thermal expansion coefficient between diamond and silicon nitride ceramic when compared to other substrates such as hardmetal[7], intrinsic and thermal stresses may develop during film growth and cooling down step, respectively. Stress effects elastically deform the diamond crystals and cause the displacement of the Raman diamond shift from the value of natural diamond (1332 cm^{-1}). The peak fitting of the Raman spectra resulted in diamond shift values at 1331.3 cm^{-1} for MCD, 1331.6 cm^{-1} for SMCD samples, which corresponds to very low tensile stresses (σ) of 0.40 and 0.23 GPa, respectively, using the expression $\sigma(GPa) = -0.567\Delta\nu(cm^{-1})$, where $\Delta\nu$ is the difference between the measured and the natural stress-free diamond peak shifts [8]. The slight diminution of the tensile stress of SMCD relatively to MCD one can be a result of the higher graphitic phase content at the diamond grain boundaries of the former diamond grade, which contribute with compressive stresses[9].

SEM micrographs of the Brale imprints at selected loads on the three different diamond grades are depicted in Fig. 2. The left hand column groups the crack patterns for loads just below film spalling-off (1600 N, 1000N and 400 N for MCD, SMCD and NCD, respectively), while in the right hand side the corresponding indent features at the spalling-off loads (1700 N, 1100N and 500 N for MCD, SMCD and NCD, respectively) are shown. As the indenter penetrates through the film and leaves the sample, a sequence of events takes place: i) in the silicon nitride substrate: elastic and quasi-plastic deformation, lateral and radial/median vents nucleation at the elastic/plastic transition and their growth towards the film/substrate interface; ii) at the film/substrate interface: propagation of the radial and lateral (circumferential) cracks due to the combination of a set of factors - residual stresses, mechanical properties of both the film and the substrate and interfacial fracture resistance [10]; iii) propagation of the former vents along the film and its spalling-off when both crack systems meet. It must be emphasized that, due to the brittle nature of the substrate, cracking phenomena initiate in the substrate, as it was illustrated by Belmonte et al[11] showing that the crack pattern of the diamond coated silicon nitride is the same for the bare one, although amplified in that case.

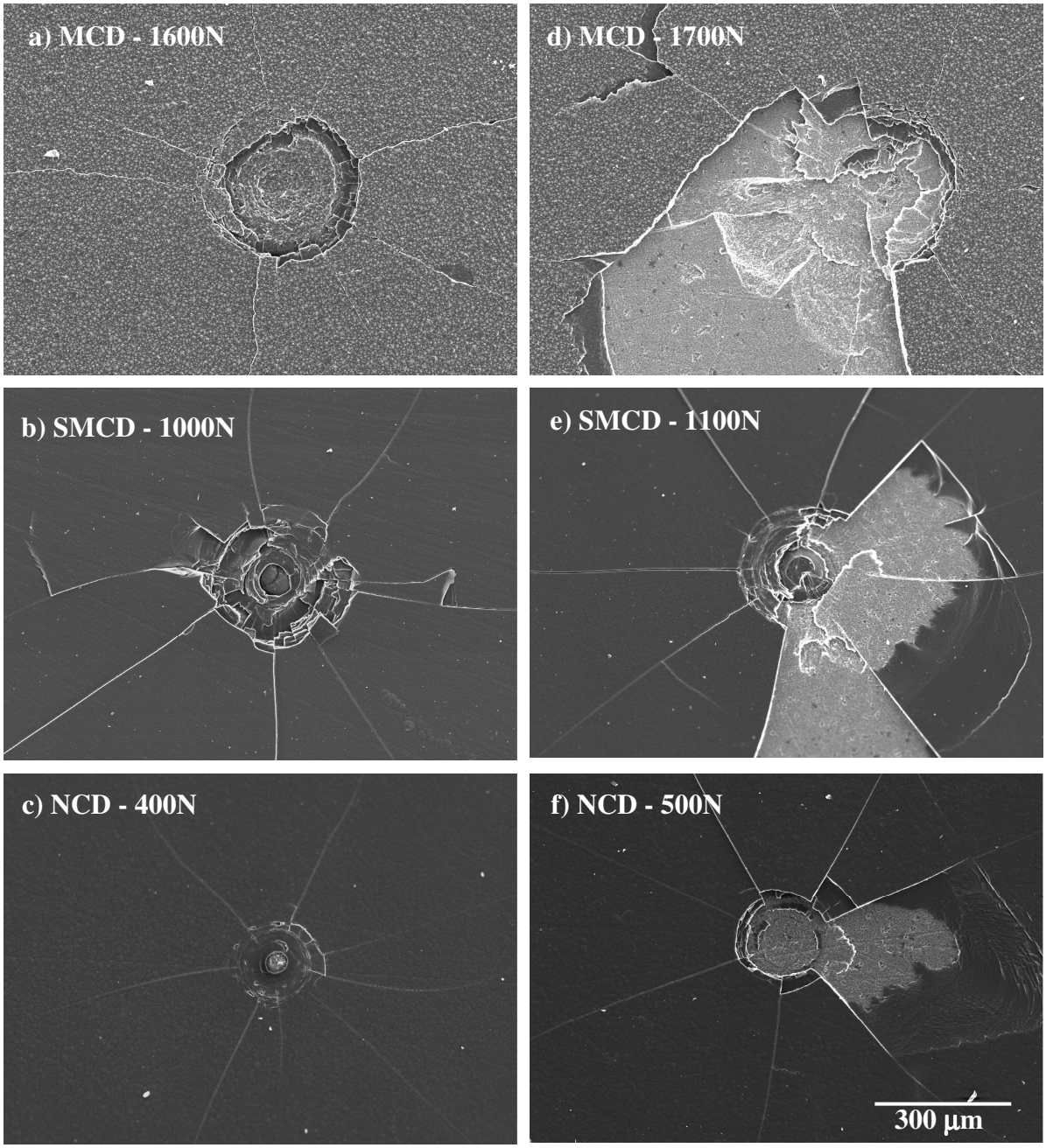

Fig. 2. SEM micrographs of the Brale imprints at selected loads on the three different diamond grades; left column: crack patterns for loads just below film spalling-off; right side: the corresponding indent features at the spalling-off loads.

Measurements of the circumferential (lateral) crack radii are plotted as a function of the indentation load in Fig. 3. As can be seen in Fig. 2 and 3, the MCD samples supported the largest load before spalling-off and presented the lowest values of circumferential crack dimensions for all the applied loads. From the above estimation on the Raman diamond peak deviation, the MCD samples undertook higher residual stress values than the SMCD ones, which suggest that the stress alone is not governing the film adhesion. As stated with respect to the crack propagation sequence, diamond film features (crystallinity, hardness and thickness) and interfacial characteristics (bonding strength and nature) also contribute to the response under the indentation testing. First of all, the MCD crystalline purity, and thus hardness, is higher when compared to the other grades. In fact, the MCD sample has the smallest non-diamond phase content, as could be seen on the Raman spectra (Fig. 1d-f), and consequently the highest hardness. Also, the thickness of MCD film is slightly higher than those of the SMCD and NCD coatings. The combination of a harder and thicker coating upholds the applied load and reduces the plastic deformation volume in the substrate[12]. Moreover, the lower is the graphite content at the interface the higher is the bonding strength to the substrate[13]. As a result of all these contributions, adhesion of the diamond coating to the substrate is much improved in the MCD grade relatively to SMCD and NCD.

The same trend is emphasized when comparing SMCD and NCD samples (Fig. 2 and 3). Adhesion is much lower for the NCD grade and this may be attributed to the higher degree of sp^2 content, as proved by Raman spectra (Figures 1e-f), together with a distinct surface chemistry and deposition temperature. The SMCD deposition process was carried out with methane supersaturation which is considered to promote the formation of a SiC or a SiC_xN_y interlayer on the Si_3N_4 surface, enhancing the adhesion to this ceramic[13]. In the case of NCD, Argon is the renucleation agent and so the surface carburization step prior to diamond growth is probably not so effective. In addition, the deposition temperature of the NCD process (750ºC) was lower than for the SMCD growth (850ºC) which dictates a less thermally activated process, lowering the species interdiffusion at the substrate surface.

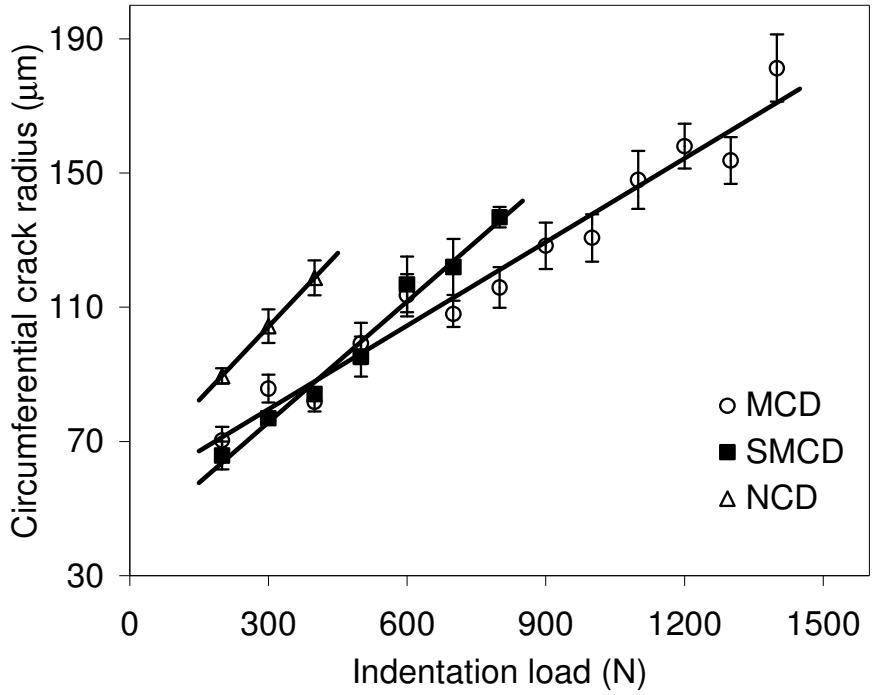

Fig. 3. Circumferential crack radius *versus* indentation load measured for the three CVD diamond coated silicon nitride substrates.

From the reciprocal of slopes in Fig. 3 it is possible to estimate the interfacial crack resistance parameter before film spalling-off for the three diamond grades: 12.0 $N \cdot \mu m^{-1}$, 8.3 $N \cdot \mu m^{-1}$ and 6.8 $N \cdot \mu m^{-1}$, corresponding to the intervals 200-1400 N, 200-800 N, 200-400N, respectively, for MCD, SMCD and NCD. In the literature, a value of app. 5.0 $N \cdot \mu m^{-1}$ is reported for microcrystalline diamond deposition assisted by microwave plasma using the same kind of ceramic substrate[13]. In the same work, the coating delaminated at 600N of applied load close to that observed for NCD, while in the present work the MCD film survived until 1600N. Despite the distinct CVD technique and deposition parameters, the better adhesion found in the present work may be attributed to a much improved mechanical interlocking provided by CF_4 plasma etching of the ceramic. Besides, this treatment activates the Si_3N_4 grains by surface fluorination, roughening the surface at the silicon nitride grain scale.

4. Conclusions

CVD diamond coatings with nanometric (NCD, 27 nm), submicrometric (SMCD, 43 nm) and microcrystalline (MCD, 12 μm) average grain sizes were grown on ceramic silicon nitride substrates with high adhesion levels, suitable for tribological purposes. Optical and SEM observations of Brale indentation imprints in the range 50-1700N, and measurements of the corresponding circumferential crack radii, allow the ranking of the different diamond grades as NCD→SMCD→MCD, from the lowest to the highest adhesion resistance. The lowest graphitic phase content and the highest hardness explain the best behaviour of the MCD grade. On the contrary, the deposition conditions for the NCD coating, cause a less effective chemical bonding to the ceramic substrate.

The MCD coating supported a normal load of 1600N without spalling-off and presented an interfacial crack resistance of 12.0 $N \cdot \mu m^{-1}$, much higher than the values reported in the literature with Si_3N_4 ceramic substrates. The SMCD presents a value of interfacial crack resistance of 8.3 $N \cdot \mu m^{-1}$ and NCD of 6.8 $N \cdot \mu m^{-1}$. These values are calculated in the load intervals of 200-1400 N, 200-800 N and 200-400 N for the MCD, SMCD and NCD, respectively. This enhanced adhesion level comes from the more effective mechanical interlocking provided by CF_4 plasma etching of the substrate prior to the deposition.

Acknowledgements

F.A. Almeida's work is supported by Programme Alβan, European Union Program of High Level Scholarships for Latin America, identification number E03D06378BR. M. Amaral acknowledges FCT for the grant SFRH/BD/9272/2002. Funding from FCT project POCI/CTM/59449/2004-"NANODIAM" is gratefully acknowledged.

References

[1] Tome MA, Fernandes AJS, Oliveira FJ, Silva RF, Carrapichano JM. High performance sealing with CVD diamond self-mated rings. Diam. Relat. Mater. 2005; 14: 617-621.

[2] Papo MJ, Catledge SA, Vohra YK. Mechanical wear behavior of nanocrystalline and multilayer diamond coatings on temporomandibular joint implants. J.Mater. Sci. Mater. Med. 2004; 15: 773-777.

[3] Amaral M, Oliveira FJ, Belmonte M, Fernandes AJS, Costa FM, Silva RF. Tailored Si_3N_4 ceramic substrate for CVD diamond coating. Surf Eng 2003;19:410-416.

[4] Brühne K, Kumar KVK, Fecht HJ, Gluche P, Flöter A. Nanocrystalline HF-CVD grown diamond and its industrial applications. Rev. Adv. Mater. Sci. 2005; 10: 224-228.

[5] Haubner R, Lux B. Deposition of ballas diamond and nano-crystalline diamond. Refract. Metals Hard. Mater. 2002; 20: 93-100.

[6] Zhang YF, Zhang F, Gao QJ, Peng, XF, Lin ZD. The roles of argon addition in the hot filament chemical vapor deposition system. Diam. Relat. Mater. 2001; 10: 1523-1527.

[7] Takeuchi S, Kojima M, Takano S, Kanda K, Murakawa M. Adhesion strength of multi-layered diamond films on WC-Co alloy substrate. Thin Solid Films 2004; 469-470: 190-193.

[8] Ralckenko VG, Smolin AA, Pereverzev VG, Obraztsova ED, Korotoushenko KG, Konov VI, Lakhotkin YV, Loubnin EN. Diamond deposition on steel with CVD tungsten intermediate layer. Diam. Relat. Mater. 1995; 4: 754-758.

[9] Bergman L, Nemanich R. Raman and photoluminescence analysis of stress state and impurity distribution in diamond thin films. J. Appl. Phys. 1995; 78: 6709-6719.

[10] Marshall DB, Evans AG. Measurement of adherence of residually stressed thin films by indention. I. Mechanisms of interface delamination. J. Appl. Phys. 1984; 56: 2632-2638.

[11] Belmonte M, Fernandes AJS, Costa FM, Oliveira FJ, Silva RF. Adhesion behaviour assessment on diamond coated silicon nitride by acoustic emission. Diam. Relat. Mater. 2003; 12: 733-737.

[12] Nesládek M, Vandierendonck K, Quaeyhaegens C, Kerkhofs M, Stals LM. Adhesion of diamond coatings on cemented carbides. Thin Solid Films 1995; 270: 184-188.

[13] Mallika K, Komanduri R. Low pressure microwave plasma assisted chemical vapor deposition (MPCVD) of diamond coatings on silicon nitride cutting tools. Thin Solid Films 2001; 396: 145-165.

3.2 *Deposition of CVD diamond films on Si_3N_4-TiN ceramic composites*

MPCVD diamond coating of Si_3N_4-TiN electroconductive composite substrates

F. A. Almeida[1], M. Belmonte[2], A.J.S. Fernandes[3], F. J. Oliveira[1], R. F. Silva[1]

[1] Department of Ceramics and Glass Engineering, CICECO, University of Aveiro, 3810-193 Aveiro, Portugal

[2] Institute of Ceramics and Glass, CSIC, Campus de Cantoblanco, c/Kelsen s/n, 28049 Madrid, Spain

[3] Department of Physics, University of Aveiro, 3810-193 Aveiro, Portugal

(Diamond and Related Materials 16, 2007, 978-982)

Abstract

A study of microwave plasma (MPCVD) diamond deposition on Si_3N_4–TiN composites with different TiN amounts (0–30 vol.% TiN) is performed. These ceramic composites are requested in order to obtain a suitable material to be cut by electrodischarge machining (EDM), aiming their use as substrates for cutting tools and tribological components. TiN is an electrical conductor, contrarily to Si_3N_4, but it is characterized by a higher thermal expansion coefficient value than Si_3N_4 and diamond. The estimated thermal stresses are found to be low and tensile (0.90 GPa) when using the monolithic Si_3N_4 substrate, but compressive for the Si_3N_4–TiN composites, and even relatively high in magnitude (−1.9 GPa) for the Si_3N_4–30 vol.% TiN composite. Brale indentation assessed the adhesion strength of diamond on the different substrate grades. Optimal behaviour (very low residual stress; no film delamination under 1000 N) is observed for the Si_3N_4–9 vol.% TiN substrate, corresponding to the lowest thermal mismatch and minimal residual stress magnitude.

Keywords: *CVD diamond; Silicon nitride, Titanium nitride, Ceramic matrix composites (CMC's).*

1. Introduction

Silicon nitride (Si_3N_4) ceramics have been successfully coated with micro and nanocrystalline CVD diamond for mechanical application purposes, such as cutting tools for machining of hard and abrasive alloys[1,2], and tribological components such as mechanical seals[3]. Shaping of Si_3N_4 parts is usually done by time-consuming mechanical cutting and grinding methods with abrasive diamond tools. In the case of the cutting inserts, the edges have to be accurately sharpened, together with the limitation of the geometries for simple shapes. A gainful alternative is electrical discharge machining (EDM) but, in order to do so, the Si_3N_4-based materials must be electroconductive which can be accomplished by the incorporation of conductive phases, namely titanium nitride (TiN) [4]. So, the EDM technique can be used on the substrates before the deposition of CVD diamond films.

Like Si_3N_4, TiN is used for tribological applications, but in coating configuration, due to its high thermal conductivity, low friction coefficient against a wide range of materials, chemical inertness and wear resistance. Titanium nitride is commonly used as a thin film buffer layer for CVD diamond deposition in metal substrates, e.g. iron and steel[5]. It acts as a barrier diffusion for C and Fe, preventing soot formation on the surface by hindering the catalytic effect of the Fe substrate and also the diffusion of C into the bulk Fe. Moreover, TiN relaxes the stress state caused by the high thermal coefficient mismatch (8.0×10^{-6} K^{-1} [4] for TiN and 12×10^{-6} K^{-1} [6] for high speed steel.

In the present work, Si_3N_4–TiN composites with a TiN content varying from 0 to 30 vol.% were coated with CVD microcrystalline diamond in a microwave reactor. In addition to the electrical conductivity advantage, the use of TiN as second phase on the Si_3N_4 matrix affords higher fracture toughness values to the substrate material[7]. The resulting CVD diamond microstructure and film adhesion were correlated with the different substrate properties, namely the thermal conductivity and thermal expansion coefficient.

2. Experimental Procedure

Si_3N_4–TiN substrates were manufactured by powder processing technology and pressureless sintering as detailed elsewhere[7]. The Si_3N_4 matrix (with 3.7 wt.% Al_2O_3 and 7.0 wt.% Y_2O_3 sintering aids), hereinafter termed SN, was replaced by TiN powder in volume percentages of 9, 23 and 30%, so the composites are named as 9TiN, 23TiN and 30TiN, respectively.

The thermal diffusivity (α) of the ceramic composites was measured by the laser flash method. Tests were carried out from room temperature up to 1273 K in argon atmosphere. The thermal conductivity (κ) was calculated by $\kappa = \rho \cdot \alpha \cdot Cp$, where ρ is the density of the material, α is the thermal diffusivity and Cp is the specific heat, which was estimated by the Si_3N_4 and TiN weight fractions and the corresponding specific heat data from de Pablos et al. calculations[8] and JANAF tables[9], respectively. The coefficients of thermal expansion (CTE) were measured by dilatometry technique, in air, in the range 473–1073 K.

All the substrate grades were ground with 46 μm diamond grit wheel, polished with 15 μm diamond slurry in an iron/polymer plate, diamond (0.5–1.0 μm) seeded in n-hexane suspension by ultrasonic agitation (1 h), and rinsed in ethanol for 10 min to remove loose diamond particles. Diamond depositions were performed in a microwave plasma CVD reactor with the following growth parameters: microwave power=2.25 kW; total pressure=1.2×10^4 Pa; H_2/CH_4 flow=400/25 sccm; deposition time=4 h.

The characterization of the coatings was performed by: SEM, to observe the diamond film microstructure and cross section; AFM with scan field sizes of 50×50 μm^2 in intermittent contact mode, to evaluate the diamond surface roughness (RMS); and micro-Raman spectroscopy (λ=488 nm) to access the diamond quality.

Adhesion was evaluated by the indentation technique at discrete loads from 200 to 1000 N. A Brale diamond indenter with a cone angle of 120° and a tip radius of 0.2 mm, adapted to a universal testing machine, was employed to carry out the experiments at a crosshead speed of 0.5 $mm \cdot min^{-1}$.

3. Results and Discussion

The thermal conductivity of the different materials is plotted in Fig. 1. At room temperature the addition of TiN significantly increases the thermal conductivity of the composites (~30 $W \cdot m^{-1} \cdot K^{-1}$), compared to the reference SN material (~25 $W \cdot m^{-1} \cdot K^{-1}$), despite the reported k value of bulk TiN (~29 $W \cdot m^{-1} \cdot K^{-1}$ [10]), which is relatively close to the reference SN. Moreover, the augment in thermal conductivity is independent of the amount of TiN of the composite. This could be explained considering that TiN additions affect the amount and location of glassy phases at the grain boundaries, the glassy phase crystallization and even result in the occurrence of solid solutions, influencing in a different way the thermal conductivity.

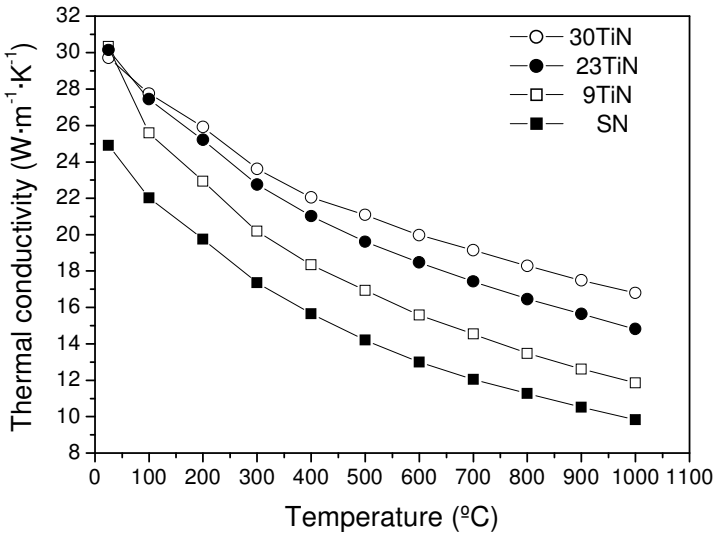

Fig. 1. Thermal conductivity as a function of temperature for the Si_3N_4–TiN composites.

On the other hand, the thermal behaviour as a function of temperature mainly depends on the TiN content. In this way, the thermal conductivity variation with temperature is less steep for 30TiN than that for lower TiN content materials (Fig. 1). The evolution of the thermal conductivity with temperature depends on the carriers of heat. While in insulating Si_3N_4 ceramics the thermal conduction carriers are phonons[8,11], the heat

in the electrical conductor TiN is carried by conduction phonons and mostly by conduction electrons, which leads to a different temperature dependence[12]. In fact, the conduction by electrons increases the thermal conductivity with temperature, whereas the conduction by phonons produces the reversed effect.

At 800 °C, the common temperature reached during the diamond deposition process, the thermal conductivity of the specimens increases with the TiN content, from 11.3 $W \cdot m^{-1} \cdot K^{-1}$ for SN to 18.3 $W \cdot m^{-1} \cdot K^{-1}$ for 30TiN. Accordingly, during the diamond deposition, the SN surface attains a higher temperature than 30TiN, which leads to a larger nucleation density and growth rate and, therefore, to a thicker diamond film[13]. Such relationship between the film thickness and the thermal conductivity of the ceramic substrates was confirmed in the present work (Table 1). Diamond grain sizes and surface roughness have no clear dependence on the TiN content (Table 1), although the richer TiN grade (30TiN samples) presents the smallest grain size (5.5 μm) and surface roughness (437 nm), related to the lowest film thickness (22 μm), as would be expected.

Table 1. Diamond grain size, film thickness, surface roughness (RMS), coefficient of thermal expansion (CTE), thermal stress and residual stress of the diamond coated Si_3N_4–TiN composites.

Grade	Film thickness (μm)	Diamond grain size (μm)	RMS (nm)	CTE ($10^{-6}K^{-1}$)	Thermal stress (GPa)	Residual stress (GPa)
SN	29	6.5	494	7.8×10^{-1} $+2.3\times10^{-3}T$	0.90	0.45
9TiN	30	8.2	495	3.9	-0.57	0.28
23TiN	25	7.0	473	4.3	-0.95	-1.76
30TiN	22	5.5	437	5.3	-1.90	-2.21

The dependence of the CTE values on temperature is presented in Table 1. It can be observed an increasing relationship between CTE and TiN content. For room temperature, the monolithic SN sample presents a CTE value of 1.5×10^{-6} K^{-1}, while in the literature, a value of 8.0×10^{-6} K^{-1} is reported for monolithic TiN[4]. This corroborates the trend for the

CTE increment in the composite materials. The CTE dependence on temperature for CVD diamond is CTE (10^{-6} K^{-1}) = $-1.4 + 9.7 \times 10^{-3}$ T $- 3.7 \times 10^{-6}$ T^2, as estimated from the values reported by others[14], which means an average value of 3.3×10^{-6} K^{-1} in the range 298–1073 K. During cooling from diamond growth temperature to room temperature, thermal stresses at the interface arise due to the CTE mismatch between the diamond film and the substrate. Using the CTE variation with temperature for the different substrate grades and diamond, it is possible to calculate the thermal stress values presented in Table 1, from the well known equation reported by Ralckenko et al.[15]. It can be seen that these extrinsic stresses are fairly low and tensile when using the SN substrate, but change to a compressive nature when the Si_3N_4–TiN substrates are coated. The lowest value is reported for the sample 9TiN, corresponding to the minimal CTE mismatch relative to diamond among all the composites (Table 1). The composites with TiN content above 23 vol.% present quite large compressive values, although much lower than those found for metal substrates, e.g. steel (−7.2 GPa[15]) and Ti_6Al_4V (−6.0 GPa[16]).

The residual stress of the diamond coatings can be assessed by Raman spectroscopy, since it is related with the displacement of the Raman diamond shift from the value of natural diamond (1332 cm^{-1}). The Raman shifts of the diamond films tend to displace for higher values with the increment of TiN on the Si_3N_4 composite (Fig. 2). The peak fitting of the Raman spectra resulted in diamond shift values that were used to evaluate the residual stress of the coating by the expression σ (GPa)= $-0.567\Delta\nu$ (cm^{-1}), where $\Delta\nu$ is the difference between the measured and the natural stress-free diamond peak shifts[15]. The complete set of results for the different grades is presented in Table 1. Similar to the thermal stresses, the trend is the change from slight tensile to compressive stresses with increasing TiN content, denoting that the thermal mismatch plays an important role in the residual stress state.

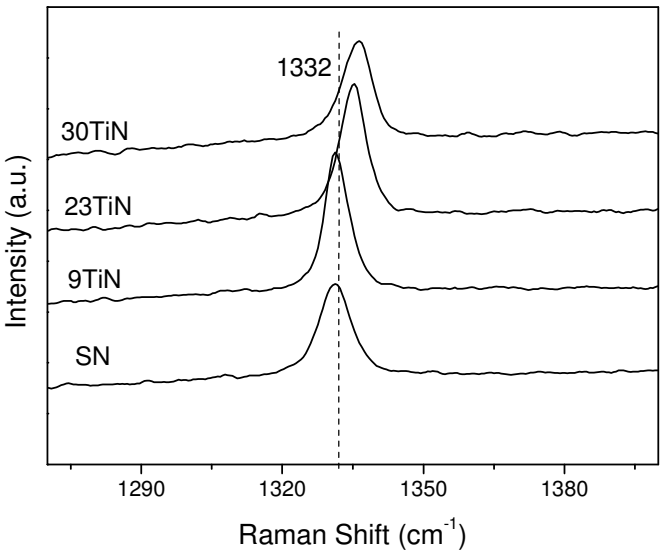

Fig. 2. Raman spectra of the diamond coated Si_3N_4–TiN composites.

SEM micrographs of the Brale imprints at selected loads on the SN, 9TiN, 23TiN and 30TiN samples are depicted in Fig. 3. The left column groups the indentation marks at a load of 600 N, while in the right hand side the corresponding indent features at maximum applied load of 1000 N (for SN, 9TiN, 23TiN) and 800 N (for 30TiN) are shown. Radial (star-shaped) and lateral (circumferential-shaped) cracks are visible in some cases. It is reported[17] that lateral and radial/median vents nucleate on the Si_3N_4 substrate, and they grow towards the film/substrate interface. At the interface, radial and lateral cracks propagate due to the combination of factors, namely residual stress, mechanical properties of both the film and the substrate, and interfacial fracture resistance. It is worth noting that the radial cracks decrease in number and length when TiN is added to SN (Fig. 3, left column). This is related to the higher fracture toughness values of the composites, since the cracking phenomena initiate in the substrate[17]. The mechanical properties of these ceramics were evaluated in a previous work[7]. It was found that the hardness of the composites slightly decreases from a value of about 15.5 to 15.0 GPa for the SN and 30TiN samples, due to the lower intrinsic hardness of TiN grains. But, the fracture toughness is improved with the addition of TiN, which values range from ~6.0 to 7.5 $MPa \cdot m^{1/2}$ for SN and 30TiN samples, respectively.

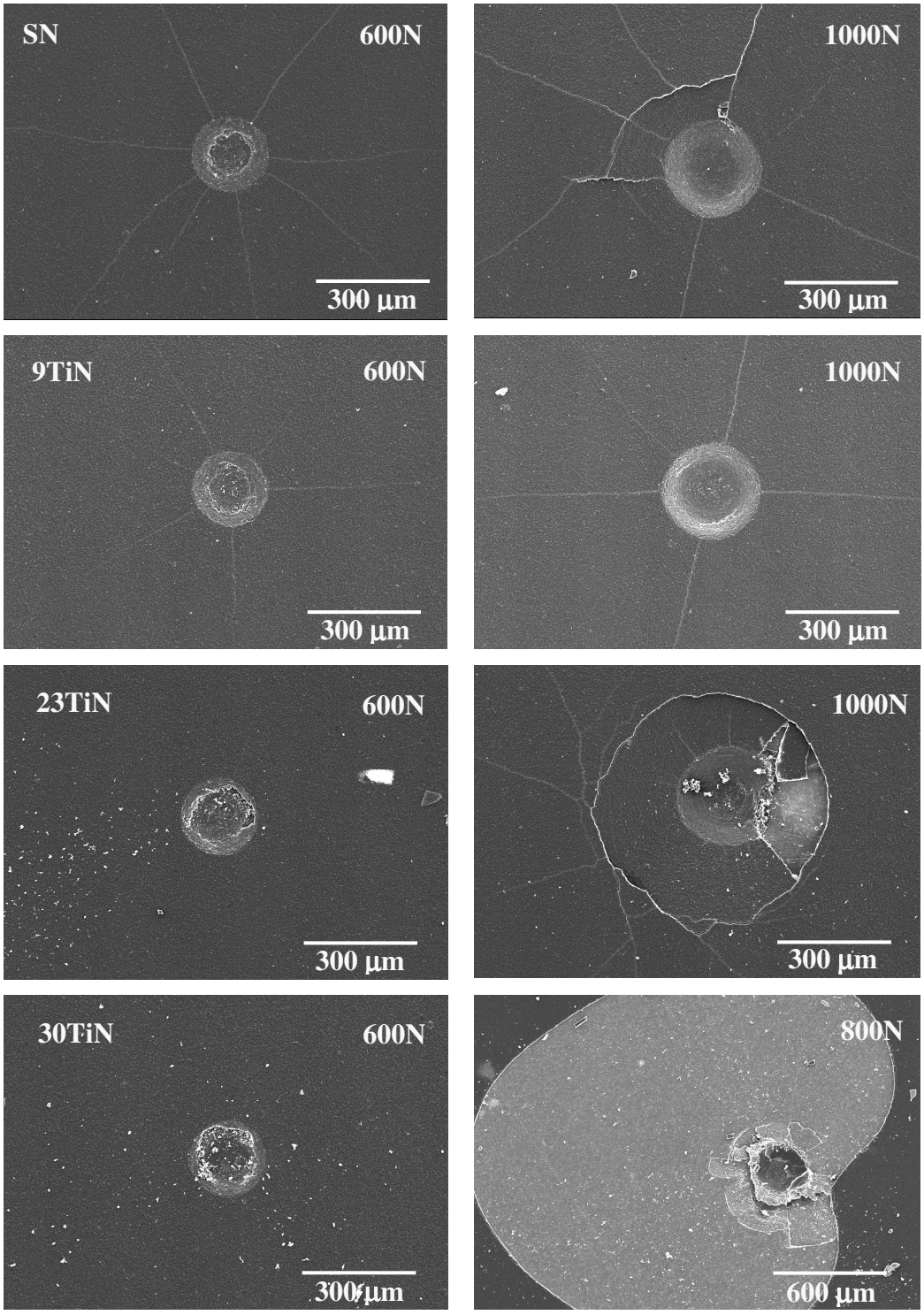

Fig. 3. SEM micrographs of the Brale imprints at selected loads on the different CVD diamond/substrates grades; left column: indentation marks at a load of 600 N; right column: the corresponding indent features at a maximum load of 1000 N (for SN, 9TiN, and 23TiN) and 800 N (for 30TiN), respectively.

However, at 600 N of applied load no film delamination takes place in all cases. On the contrary, under 1000 N, partial circumferential cracking is observed in the SN coated sample and full circumferential cracking develops in the 23TiN grade. In the case of the richest TiN composite (30TiN), extensive delamination takes place at 800 N denoting a lack of adhesion. The best behaviour is observed for the 9TiN grade, where only the subsurface radial cracks arise, even with 1000 N of indentation load. This optimal condition is linked to the minimal residual stress magnitude (Table 1). For comparison, critical loads of about 600 N were reported for Si_3N_4 CVD diamond coated materials[18]. Although the 23TiN and 30TiN undergo a compressive state, its absolute value is relatively high for the present ceramic/diamond system and 1000 N, in the first case, or 800 N, in the second, represents critical delamination loads. A further explanation of this behaviour can be found regarding the detrimental effect of TiN content on diamond nucleation adhesion. The TiN chemical interlocking with diamond is probably weak as no formation of either TiC or TiCN at the substrate/film interface is reported, but only of a-C thin film[5]. However, this is not a closed issue as other authors[19] describe the formation of a very thin (8 Å) carbon nitride layer. So, it is not conclusive if TiN has a positive effect on diamond adhesion comparatively to Si_3N_4. For the latter, it is thought to happen as a reaction of carbon and hydrogen with the SiO_2 coating that invariably covers the Si_3N_4 surface, resulting in the formation of a SiC layer with a great affinity to diamond[18].

4. Conclusions

CVD diamond deposition on Si_3N_4–TiN composites with different TiN contents was performed. The addition of TiN to the Si_3N_4 matrix enhances the thermal conductivity of the bulk leading to a decreasing surface temperature during diamond growth and, therefore, to thinner, finer grained, smoother diamond films.

TiN has a higher coefficient of thermal expansion (CTE) than Si_3N_4, consequently, the CTE values increase with the increment of the TiN content, and so the thermal expansionmismatch between the substrate and the diamond film. The estimated thermal stresses were found to be low and tensile (0.90 GPa) for the monolithic Si_3N_4 substrate,

changing to a compressive nature for the Si_3N_4–TiN composite substrates (−1.90 GPa for Si_3N_4–30 vol.% TiN). The residual stress values calculated from the deviation of the Raman diamond shift corroborate this trend, denoting the influence of the thermal mismatch.

Brale imprints demonstrate that the subsurface radial cracks decrease in number and length when TiN is added to Si_3N_4, this behaviour being related to increasing fracture toughness of the substrate. No CVD diamond film delamination takes place at 600 N for every kind of substrate, but at 1000 N partial or full circumferential cracking is observed for the monolithic Si_3N_4 sample or the high content TiN grades. The optimal behaviour (no film delamination under 1000 N), which corresponds to the minimal residual stress magnitude, is observed for the Si_3N_4–9 vol.% TiN substrate.

Acknowledgements

F.A. Almeida's work is supported by Programme Alβan, European Union Program of High Level Scholarships for Latin America, identification number E03D06378BR. Funding from FCT project POCI/CTM/59449/2004—"NANODIAM" is gratefully acknowledged.

References

[1] Almeida FA, Oliveira FJ, Sousa M, Fernandes AJS, Sacramento J, Silva R.F. Machining hardmetal with CVD diamond direct coated ceramic tools: effect of tool edge geometry. Diam. Relat. Mater. 2005; 14: 651-656.

[2] Almeida FA, Fernandes AJS, Silva RF, Oliveira FJ. Re-sharpenable thick CVD diamond-coated Si_3N_4 tools for harmetal turning. Surf. Coat. Technol. 2006; 201: 1776-1782.

[3] Tome MA, Fernandes AJS, Oliveira FJ, Silva RF, Carrapichano JM. High performance sealing with CVD diamond self-mated rings. Diam. Relat. Mater. 2005; 14: 617-621.

[4] Gogotsi YG. Particulate silicon nitride-based composites – Review. J. Mater. Sci. 1994; 29: 2541-2556.

[5] Weiser PS, Prawer S, Hoffman A, Paterson PJK, Manory RR. Chemically vapor deposited diamond films grown on titanium nitride coated and uncoated iron substrates. J. Appl. Phys. 1994; 76: 2164-2168.

[6] Narayan RJ. Adhesion properties of functionally gradient diamond composite films on medical and tool alloys. J. Adhes. Sci. Technol. 2004; 18: 1339-1365.

[7] Almeida FA, Bóia H, Santos C, Monteiro J, Oliveira FJ, Silva RF. Electroconductive ceramic composites for cutting tools. Mater. Sci. Forum 2006; 514–516: 638-642.

[8] de Pablos A, Osendi MI, Miranzo P. Effect of microstructure on the thermal conductivity of hot-pressed silicon nitride materials. J. Am. Ceram. Soc. 2002; 85: 200-206.

[9] Chase MW. NIST-JANAF Termochem. Tables, 4th Ed. J. Phys. Chem. Ref. Data, 1996, Monograph 9.

[10] Shackelford JF, Alexander W, Park JS (Eds.). CRC Materials Science and Engineering Handbook. 1994; 2nd ed., CRC Press.

[11] Bruls RJ, Hintzen HT, Metselaar R. A new estimation method for the intrinsic thermal conductivity of nonmetallic compounds: a case study for $MgSiN_2$, AlN and β-Si_3N_4 ceramics. J. Eur. Ceram. Soc. 2005; 25: 767-779.

[12] Williams WS. High-temperature thermal conductivity of transition metal carbides and nitrides. J. Am. Ceram. Soc. 1966; 49: 156-159.

[13] Belmonte M. Diamond coating on coloured Si_3N_4 ceramics. Diam. Relat. Mater. 2005; 14: 54-59.

[14] Slack GA, Bartram SF. Thermal espansion of some diamondlike crystals. J. Appl. Phys. 1975; 46: 89-98.

[15] Ralckenko VG, Smolin AA, Pereverzev VG, Obraztsova ED, Korotoushenko KG, Konov VI, Lakhotkin YV, Loubnin EN. Diamond deposition on steel with CVD tungsten intermediate layer. Diam. Relat. Mater. 1995; 4: 754-758.

[16] Azevedo AF, Corat EJ, Ferreira NG, Trava-Airoldi VJ. Wettability and corrosion tests of diamond films grown on Ti_6Al_4V alloy. Surf. Coat. Technol. 2005; 194: 271-275.

[17] Belmonte M, Fernandes AJS, Costa FM, Oliveira FJ, Silva RF. Adhesion behaviour assessment on diamond coated silicon nitride by acoustic emission. Diam. Relat. Mater. 2003; 12: 733-737.

[18] Mallika K, Komanduri R. Low pressure microwave plasma assisted chemical vapor deposition (MPCVD) of diamond coatings on silicon nitride cutting tools. Thin Solid Films 2001; 396: 145-165.

[19] Contreras O, Hirata GA, Avalos-Borja M. Interface analysis of CVD diamond on TiN surfaces. Appl. Surf. Sci. 2000; 158: 236-245.

Chapter 4

Cutting tool behaviour and wear mechanisms in turning of sintered WC-Co and EDM graphite

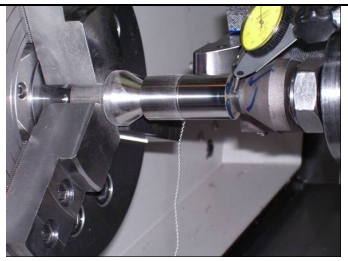

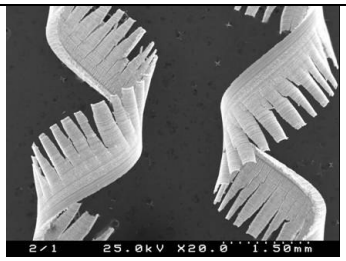

Introduction

The produced CVD diamond direct coated cutting tools were tested in turning operations using two kinds of hard and abrasive workpieces: hardmetal and EDM graphite. The machining capabilities of the first material are of great general industrial interest, in particular for Durit, a Portuguese hardmetal producer. Their products are developed to attend a wide branch of industry, including chemical, medical, automotive, packaging, textiles, mining, oil and gas, siderurgy, and for shaping and drawing technologies.

The machining of hardmetal using superhard cutting inserts is a recent technology, due to the high hardness and abrasive nature of hardmetal. The option for turning process instead of grinding ones brings several advantages as: better surface quality, reduction of production steps, reduction of product time delivery, shortening the manufacture cycles, higher geometry flexibility (corners, radius and grooves) and finally less energy consumption. A tenfold decrease on the machining time compared with the conventional diamond wheel grinding method was achieved by thick CVD diamond brazed tools in facing WC-27wt%Co [1]. In such applications, polycrystalline diamond (PCD) and polycrystalline cubic boron nitride (PCBN) are the most established market options, together with thick CVD diamond brazed films. Just a few works are devoted to this issue [1-6], despite some of them are about micro-machining, where the depth-of-cut is only of a few micrometers (3 μm) [4,5]. There is a technical guide on the use of PCD or PCBN tools associated to the binder phase content, typically cobalt, of the hardmetal workpiece [3]. Accordingly, PCD is used when the binder content is below 18wt%, due to its superior abrasion resistance. However, PCBN should be used when the binder content is above this value, regarding its higher thermal and chemical stability. This is due to the chemical affinity between carbon and cobalt, and so, binder contents higher than 18wt% increases considerably the carbon solubility, leading to detrimental effects in its wear resistance properties [3]. Chemical vapour deposited (CVD) diamond can be an excellent alternative for both PCBN and PCD tools, considering that its higher hardness and absence of cobalt binder allows its use for machining a wider range of hardmetal's cobalt content without need to have several types of cutting tools. Previous works [1,2] of our group had already

proved the adequacy of using a thick CVD diamond brazed tool in hardmetal turning and, comparatively to PCD and PCBN ones, it presented higher wear resistance [1].

Another workpiece material used in this thesis is graphite for electrodischarge machining (EDM) electrodes. This material was supplied by the company Moldit (Loureiro), specialized in manufacturing moulds for plastic injection. EDM graphite is not so difficult-to-machine like hardmetal, but its polycrystalline nature and, above all, its strong anisotropy, confers abrasiveness, quickly wearing conventional cutting tools. In turning operations, an improvement in tool life of almost three-fold was achieved by PCD tools comparatively to hardmetal [7]. In milling operations a tool life gain of more than 10 times was reported using CVD diamond coated hardmetal tools in comparison with the uncoated ones [8,9]. Coatings of TiAlN and TiN on hardmetal tools are also used in milling and turning operations of EDM graphite [10,11], but the diamond coated hardmetal tools still presented an improved life time of more than 25 times compared to TiN-coated ones, accordingly to a EDM graphite producer [11]. A recent work reports the advantage of using a CVD diamond film coated hardmetal with a controllable diamond grain size in graphite turning in comparison to conventional diamond coatings and PCD, although delamination of the film occurred after about 1480 m of cutting length, which was attributed to the high blasting velocity of the graphite powder against the insert rake face, combined with the compressive residual stress in the diamond film [12].

The sintered ceramic parts produced in this thesis were ground to standard normalized geometries of round or triangle shaped indexable inserts, accordingly to ISO 5608 [13] insert identification system. An example, the designation TNMN160308FN means:

Position 1 - insert shape: “T” letter is used for triangle shaped inserts and “R” for round shaped ones;

Position 2 – clearance angle: “N” letter is used to inserts with right angled side (0º);

Position 3 – dimension tolerances: “M” letter is used to tolerances range from 0.08 to 0.18 mm;

Position 4 – chip breaker/central hole: “N” letter is used to inserts without chipbreaker and without central hole;

Position 5 – cutting edge length: “16” number is side length of the insert, in millimeters;

Position 6 – insert thickness: “03” number is the thickness of 3.18 mm;

Position 7 – corner radius: “08” number means 0.8 mm;

Position 8 - cutting edge geometry: “F” letter means a sharp edge, while “E” and “T” is used to honed (rounded) an chamfered (negative land) edges, respectively;

Position 9 – hand of the tool: “N” letter means that the tool can either be right (R) or left (L) hand cutting.

The turning tests were done in Durit using a CNC lathe (Mori Seiki) with a maximum spindle speed of 3500 rpm. A three-axis piezoelectric dynamometer platform (Kistler 9257BA) was coupled into the lathe, where the tool holder is fixed. In this way, the signals were amplified in a Kistler 5011 apparatus and connected to a PC by coaxial cables and an acquisition board (PCMCIA, Keithley). The workpiece surface quality was determined using a portable profilometer (Mahr). Fig. 1a shows the overall apparatus and while in Fig 1b is possible to see some equipment details in a turning operation. The resultant wear modes were measured accordingly with the ISO 3685 standard [14] using optical (Nikon) and scanning electron microscopes (Hitachi).

Fig. 1. a) overall apparatus for turning tests; b) turning of WC-Co.

The following papers present the cutting tool behaviour in real turning of hardmetal and graphite workpieces. Aspects related to tool wear, workpiece surface finish, effect of tool edge geometry, effect of diamond grain size and film thickness effect are here presented.

References

[1] Belmonte M, Ferrro P, Fernandes AJS, Costa FM, Sacramento J, Silva RF. Wear resistant CVD diamond tools for turning of sintered hardmetals. Diam. Relat. Mater. 2003; 12: 738-743.

[2] Belmonte M, Oliveira FJ, Sacramento J, Fernandes AJS, Silva RF. Cutting forces evolution with tool wear in sintered hardmetal turning with CVD diamond. Diam. Relat. Mater. 2004; 13: 843- 847.

[3] Collier M, Cheynet J. PM2002 Hard Materials and Diamond Tooling Congress and Exhibition. 7–9th October 2002, Lausanne, Switzerland, 2002.

[4] Liu K, Li XP, Rahman M. Characteristics of high speed micro-cutting of tungsten carbide. J. Mater. Process. Technol. 2003; 140: 352-357.

[5] Liu K. Li XP, Rahman M, Liu X.D. CBN tool wear in ductile cutting of tungsten carbide. Wear 2003; 255: 1344-1351.

[6] Miyamoto T, Heo SJ, Hanasaki S, Fujiwara J. Cutting of wear and impact resistant cemented carbides. Proceedings of the 7th International Conference on Progress of Machining Technology, Aviation Industry Press, Suzhou (P.R. China). 2004, 44-48.

[7] Cook MW. A guide to machining carbon and graphite with syndite PCD. Ind. Diam. Review 1994; 54: 174-178.

[8] Kanda K, Takehana S, Kanda K, Takehana S, Yoshida S, Watanabe R, Takano S, Ando H, Shimakura F. Application of diamond-coated cutting tools. Surf. Coat. Technol. 1995; 73: 115-120.

[9] Myers D. Machining graphite using diamond-coated tools - Part 3: Machine tool considerations and application results. MoldMaking Technology Online. http://www.moldmakingtechnology.com/articles/129905.html

[10] Schroeter RB, Kratochvil R, Gomes JO. High-speed finishing milling of industrial graphite electrodes. J. Mater. Proc. Technol. 2006; 179: 128-132.

[11] Mucha T. Machining graphite. EDM Today November/December 2003. http://us.gfac.com/intech/newsroom/documents/graphite1.pdf

[12] Cabral G, Reis P, Polini R, Titus E, Ali N, Davim JP, Grácio J. Cutting performance of time-modulated chemical vapour deposited diamond coated tool inserts during machining graphite. Diam. Relat. Mater. 2006; 15: 1753-1758.

[13] International Standard ISO 5608 (1995). Turning and copying tool holders and cartridges for indexable inserts – designation.

[14] International Standard ISO 3685 (1993). Tool life testing with single-point turning tools.

4.1 *Effect of tool edge geometry*

Machining hardmetal with CVD diamond direct coated ceramic tools: effect of tool edge geometry

F. A. Almeida[1], F. J. Oliveira[1], M. Sousa[1], A. J. S. Fernandes[2], J. Sacramento[3], R. F. Silva[1]

[1] Department of Ceramics and Glass Engineering, CICECO, University of Aveiro, 3810-193 Aveiro, Portugal

[2] Department of Physics, University of Aveiro, 3810-193 Aveiro, Portugal

[3]High School of Technology and Management, Águeda, Portugal

(Diamond and Related Materials 14, 2005, 651-656)

Abstract

A new challenge for chemical vapour deposited (CVD) diamond tools is the machining of hardmetal, one of the most difficult tasks a tool has to accomplish due to the extreme hardness of the workpiece. The development of cutting tool inserts made via direct diamond deposition on silicon nitride ceramic substrates for machining WC–Co materials was recently pointed as an alternative to the conventional brazed CVD diamond tips. In the present work, silicon nitride round inserts having different edge geometry, namely sharp, honed and chamfered edges, were produced by pressureless sintering. Turning of hardmetal containing 25 wt.% Co was conducted in a numerically controlled lathe with ~15 μm thick CVD diamond coatings. The effects of depth of cut (0.1 to 0.3 mm), feed rate (0.03 to 0.3 mm rev^{-1}) and wear on the cutting forces were monitored online using a dynamometer and were related to the surface finishing of the workpiece. Honed tools were more prone to diamond film delamination from the cutting edge than the chamfer or sharp edge ones. Adequate finishing quality ($Ra<0.2$ μm) can be achieved with the sharp edge tools while machining tolerances are respected.

Keywords: *CVD diamond, Silicon nitride, Machining, Hardmetal.*

1. Introduction

A recent issue on precision hard turning is the use of polycrystalline diamond (PCD), polycrystalline cubic boron nitride (PCBN) tools and of chemical vapour deposited (CVD) diamond ones in machining of hardmetals (WC–Co)[1,2]. A successful solution to this challenge will allow diminishing the costs associated to the conventional time consuming methods (grinding and polishing) used for hardmetal shaping. Also, dry machining has been an important environmental matter since it does not require the use of polluting coolants.

There exists actual industrial knowledge on the machining of certain grades of hardmetal with diamond and PCBN tools[3] but efforts have to be made regarding the study of directly diamond coated tools before they can be advantageously used. Preliminary work has shown that for extreme conditions delamination of diamond from the flank face of a sharp diamond coated tool may occur[4], depending on the cutting conditions. Edge geometries such as sharp, chamfer (or T-land) and hone (or round) are commercially employed with the purpose of strengthening the cutting edge of conventional tools[5]. Although complex substrate preparation could enhance the wear resistance of diamond films[6,7], the use of these tools on aggressive machining operations is still restricted due to insufficient adhesion[6, 8, 9]. The good thermal and chemical compatibility of silicon nitride ceramics makes them suitable substrates for enhanced adhesion of diamond and allows using them as cutting tools[6, 10 ,11]. In this work, Si_3N_4 round tools coated with a diamond film were used for dry turning WC–25wt.%Co cylindrical bars at different feed (f), depth-of-cut (d) and edge geometries conditions. The cutting forces were monitored during the tests by a dynamometer and the final tool damage was evaluated using scanning electron microscopy while workpiece finish was assessed by surface roughness measurements.

2. Experimental

Disc-shaped Si_3N_4 substrates with a relative density over 99% were obtained by pressureless sintering in a graphite furnace at 1750 ºC for 2 h under an N_2 atmosphere. All the substrates were ground to three distinct normalized insert geometries concerning cutting edge shape (RNMN1003FR; RNMN1003TR; RNMN1003ER), as illustrated by the sketches in Fig. 1. After edge preparation, the substrates were polished with 15 μm diamond paste followed by scratching with 0.5–1 μm sized diamond powder. This last procedure is required for diamond seeding and specific surface area improvement purposes before the diamond coating step.

Diamond depositions were performed in a microwave plasma CVD reactor (ASTeX PDS 18) with the following growth parameters: microwave power=2.7 kW; total pressure= 1.2×10^4 Pa; H_2/CH_4 flow=400/22 sccm; deposition time=2.5 h. The samples were fitted into graphite holders in order to avoid the "edge effect" caused by higher plasma concentration and locally increased temperature.

The workpiece material for dry turning experiments was sintered WC–25 wt.% Co with an average hardness of 8.5 GPa. The tests were carried out in a CNC lathe (Mori Seiko) under the following conditions: fixed cutting speed (v) of 15 $m \cdot min^{-1}$; depth of cut (d) varying in the range 0.1–0.3 mm; and feed rate (f) within 0.03–0.30 $mm \cdot rev^{-1}$.

The orthogonal components of the cutting force, namely Fc (main cutting force), Fd (depth-of-cut force), and Ff (feed force), were assessed at real time by a dynamometer (Kistler). Scanning electron microscopy (SEM, Hitachi) was used to evaluate tool wear, namely rake face wear (KM) and maximum flank wear (VBmax). The workpiece surface quality was determined using a portable profilometer (Mahr).

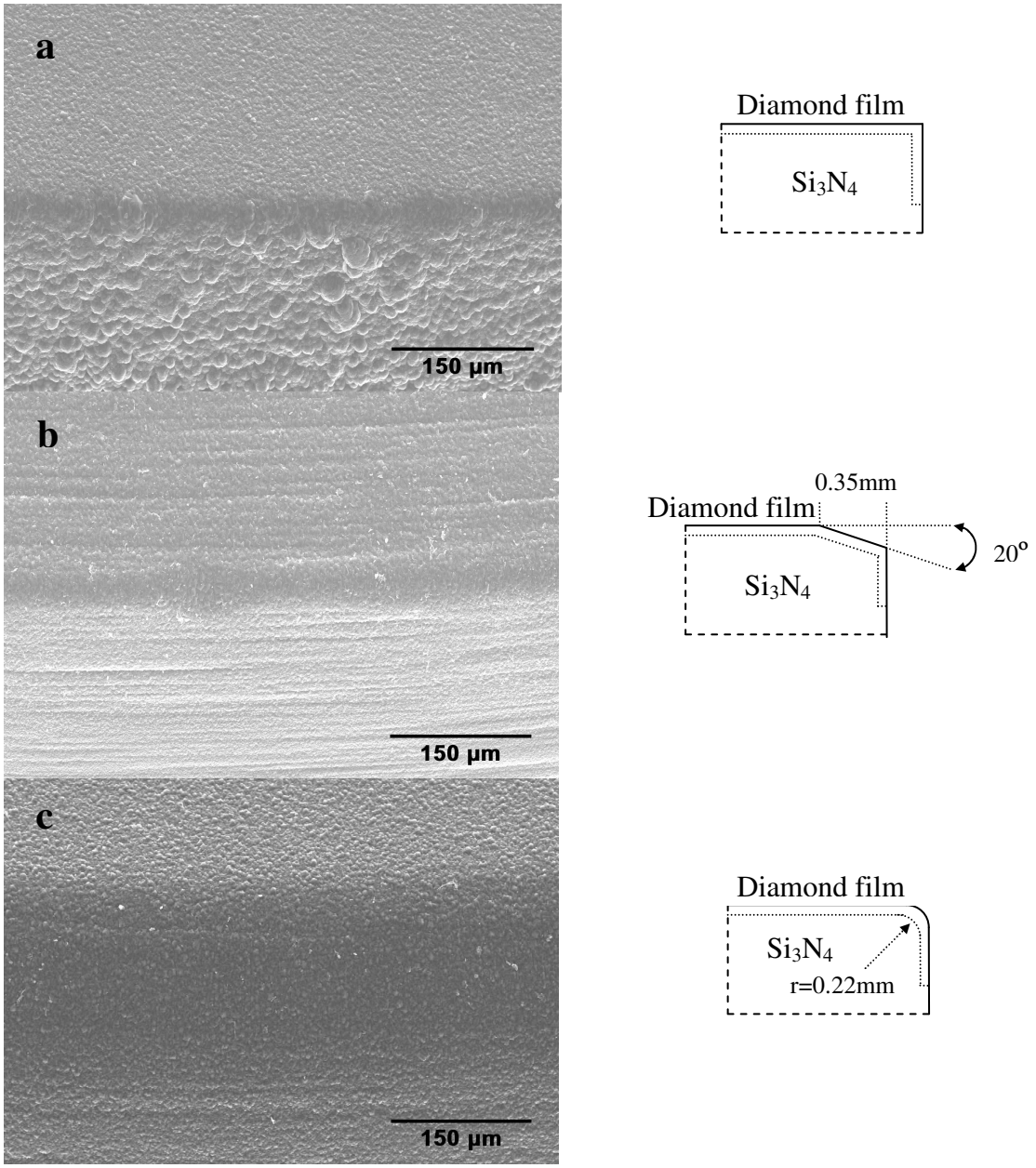

Fig. 1. SEM micrographs and sketches of the diamond coating of the three different edge geometries: (a) sharp; (b) chamfer; (c) hone.

3. Results and discussion

Low magnification SEM micrographs of the diamond coatings on the three distinct tools before the cutting tests are shown in Fig. 1a–c. Besides edge geometry, another

difference is put in evidence: the formation of a few "igloo-shaped" aggregates of submicrometric diamond crystallites on the sharp tool flank face (Fig. 1a). These hemispherical structures display a broad, low-intensity, Raman peak at ~1332 cm^{-1}, resulting from an insufficient process temperature for the growth of good quality diamond[12]. On the contrary, the chamfered and honed inserts present more homogeneous diamond morphology along the transition from the rake to the tool flank face.

The hard turning experiments on the cemented carbide workpiece showed notable differences among the distinct edge geometries. Firstly, the force components increase with the edge bluntness, the lower values being found for the sharp tool and the higher for the honed insert, as illustrated in Fig. 2. This behaviour is related to the wider contact area between the workpiece and the tool leading to larger forces for material shearing. According to Yen et al[5], experiments and FEM calculations on cutting forces as a function of the edge hone radius showed that the force components and the specific cutting energy increase with the edge radius. The same is reported by Thiele and Melkote[13] in the machining AISI 52100 steel with CBN inserts.

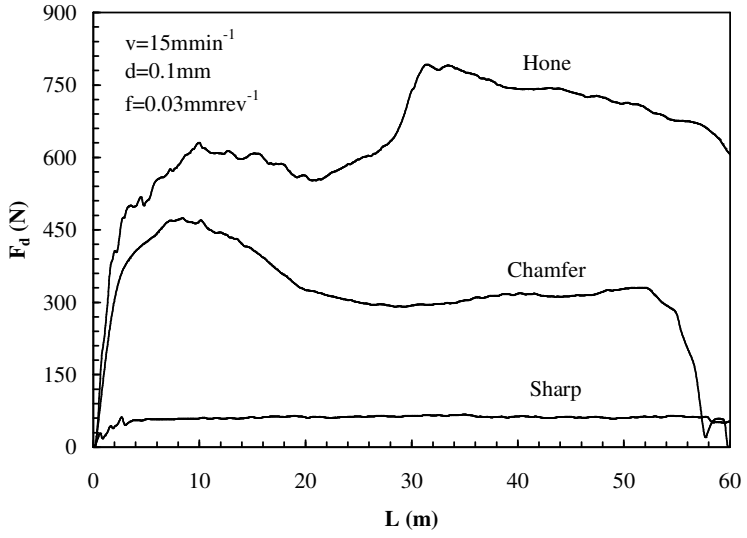

Fig. 2. Real time evolution of F_d force as a function of the cutting length (L) for the three different cutting edges at v=15 m·min^{-1}; d=0.1 mm and f=0.03 mm·rev^{-1}.

The evolution of the machining force, as illustrated in Fig. 2 for F_d, depicts the type of events occurring during the cutting process. For the sharp edge inserts, after an initial peak, the force is nearly constant throughout the machining operation. The transient higher forces result from early film delamination on the flank face, as shown in Fig. 3a. Here, diamond/substrate interfacial failure is favoured under the specific stress state imposed by the right angle geometry. The exposed ceramic substrate suffers from the hardmetal abrasive action, leading to measurable flank wear (VB) (Fig. 3a and Table 1) while the diamond on the rake face withstands the chip flow and allows the tool to continue the cutting action. For the chamfered tool (Fig. 3b), the diamond coating did not delaminate at the flank face, but it progressively worn out in this zone, also exposing the silicon nitride substrate. In spite of much larger cutting forces on the cutting edge, this geometry, unlike that of sharp edge tools, prevents the film delamination at low feeds. This is evidenced in the SEM micrograph of Fig. 3b, where the wear land on the flank face is surrounded by adherent diamond. Although with a less steep variation, the depth-of-cut cutting force follows a similar trend to that of the sharp edge tool, with initial high values that decrease with the cutting length (Fig. 2). Diamond film and substrate wear recess the edge and cause a slight loss in the machined tolerances that account for the decrease in the cutting force. Finally, for all the tests with honed edge inserts, the tools failed catastrophically in the early stages of machining, by film delamination on both flank and rake faces and substrate rupture. This corroborates the above-mentioned effect of this particular tool geometry on causing a severe mechanical solicitation. The excessive abrasive wear and chipping of the uncoated ceramic edge (Fig. 3c) provoke changes in the tool geometry further increasing the cutting force (F_d) to nearly 10 times those of the sharp edge inserts (Fig. 2).

The ratio of the depth-of-cut and feed forces to the main cutting force, F_d /F_c and F_f/F_c, respectively, can be used to better understand the effect of edge geometries on the orthogonal components of the cutting force. Data in Table 1 show that both ratios are larger for the chamfered tools than for the sharp ones. Generally, F_d is the force component with the larger modulus and F_f is the one with smaller values for all geometries and cutting conditions. F_d values are represented as a function of cutting length in Fig. 4a varying the feed rate in the range 0.03 to 0.30 mm·rev^{-1}, for turning tests performed with sharp tools at d=0.1 mm. Interestingly, in spite of the increase of the cutting force with the feed rate as portrayed in Fig. 4a, the F_d/F_c ratio decreases reaching a nearly constant value of 0.9

(Table 1). In the case of chamfer tools, the F_d/F_c ratio has a similar trend, decreasing with increasing feed ratio at depth of cut of 0.1 mm (Table 1). For the tested round-shaped inserts, higher feed rates result in larger chip/rake face contact area which mainly affects the F_c value comparatively to F_d, this one being more dependant on the depth-of-cut parameter.

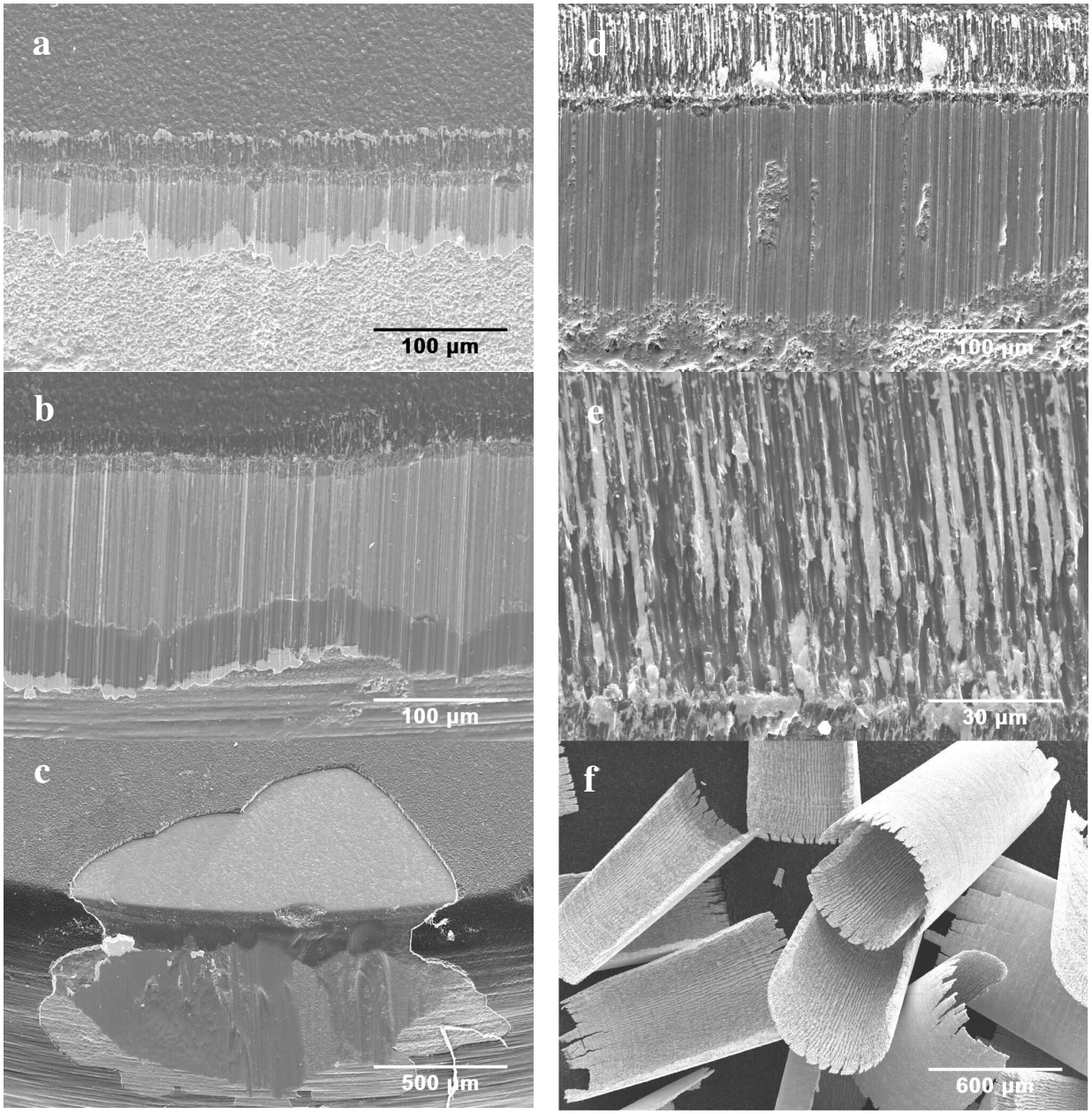

Fig 3. SEM micrographs of the tools cutting edges after turning tests at v= 15m·min^{-1}; d=0.2mm; f=0.03mm·rev^{-1}: a) sharp; b) chamfered; c) honed tool. d) Flank wear, cratering on the rake face and hardmetal deposition on the sharp cutting edge at v= 15m·min^{-1}; d=0.3mm; f=0.09mm·rev^{-1}. e) High magnification of the cratering on the rake face for sharp tool at v=15m·min^{-1}; d=0.1mm; f=0.24mm·rev^{-1}. f) Hardmetal chips produced during turning tests at v= 15m·min^{-1}; d=0.1mm; f=0.15mm·rev^{-1}.

Table 1. F_d/F_c and F_f/F_c ratios, KM and VBmax wear values as a function of edge geometry and cutting parameters.

		Sharp edge				Chamfer edge			
d (mm)	f (mm rev^{-1})	F_d/F_c	F_f/F_c	KM (μm)	VB_{max} (μm)	F_d/F_c	F_f/F_c	KM (μm)	VB_{max} (μm)
0.1	0.03	1.5	0.2	46	89	3.5	0.4	31	227
	0.06	1.2	0.2	14	75	3.2	0.3	31	293
	0.09	1.1	0.2	64	112	2.3	0.2	49	287
	0.12	1	0.1	64	87	2.8		66	229
	0.15	0.9	0.1	86	100	-	-	-	-
	0.18	0.9	0.1	76	152	-	-	-	-
	0.21	0.9	0.1	91	162	-	-	-	-
	0.24	0.9	0.1	95	179	-	-	-	-
	0.3	0.8	0.1	- *	- *	-	-	-	-
0.2	0.03	1.1	0.2	36	74	3.6	0.2	-	-
	0.09	1.0	0.2	75	135	-	-	- *	- *
0.3	0.09	0.9	0.2	84	223	-	-	-	-

Fig. 4a also shows that the cutting force steeply increases for feed rates larger than 0.15 mm·rev^{-1}. For the highest feed rate, tool failure even occurs during cutting. Evaluation of tool integrity can thus be done by monitoring the real time evolution of forces which allows stopping the operation before damage could occur to both tool and workpiece. This type of evolution has been related to wear of the cutting tip and the associated geometry change[14] and in the present case yields the upper limit of the feed rate (0.15 mm·rev^{-1}) for a depth of cut of 0.1 mm when using these diamond coated sharp tools. Data graphically presented in Fig. 4b illustrates the result of both effects on the cutting force. Although affecting the cutting force, the depth-of-cut condition is less stringent than the feed rate.

Measurements of wear on the rake and flank faces of sharp tools showed that KM and VB increase with the feed rate (Table 1) while for the chamfered ones KM increases and VB is approximately constant. Even considering that for large feed rates the machining distances are shorter, the effects of the force increase exceed those and the edges wear more rapidly. The chamfered tools always present larger VB values than the sharp tools and comparable values of KM for the same machining conditions. The chamfer of the tool insert results in larger Fd forces and thus in an increased flank wear. A comparison can be made between Fig. 3a and d to illustrate the effect of cutting conditions on the damage extension of a sharp tool.

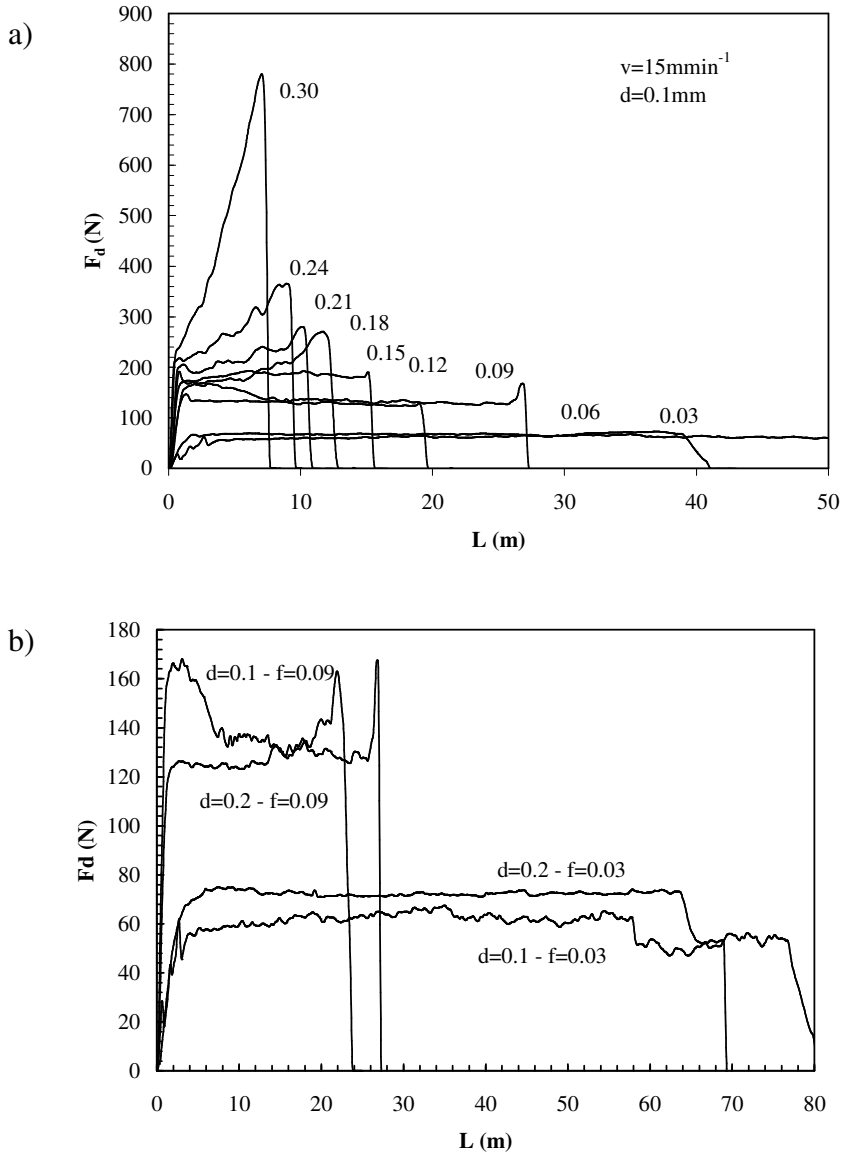

Fig. 4. a) Effect of feed rate and machining length (L) on F_d for sharp edge tools at v=15m·min^{-1} and d=0.1mm; b) effect of depth of cut and feed rate on F_d for sharp edge tools at v=15m·min^{-1}.

Fig. 3e is a detailed micrograph of the wear land on the rake face provoked by the sliding action of the discontinuous chips (Fig. 3f). The trailing edge of the crater contains bright agglomerates of debris from the workpiece material that also spread along the worn land. The chips are intrinsically abrasive not only due to the WC content, but also by the

diamond debris transport and as such, intensive scratching of both the debris layer and the diamond film takes place.

Within the established working conditions of sharp and chamfered tools, namely feed rate below 0.15 mm·rev^{-1} for a depth of cut up to 0.2 mm, the surface roughness of workpiece is given in Fig. 5. Smaller Ra values were measured in the workpieces machined with the chamfered tools where the forces are larger than for the sharp tools for identical machining conditions. This can be due to temperature raise, and thus workpiece plasticity enhancement, coupled to the higher cutting energy required for chip formation[5]. A similar behaviour takes place for the sharp tools, since for larger depths of cut and feed rates, and thus larger forces, the roughness lowers or becomes nearly constant (Fig. 5). For the sharp tools, Ra increases with the feed rate but decreases with the cut depth. The finishing condition of Ra<0.2 μm is attained only for feed rates smaller than 0.06 mm·rev^{-1} when machining with the chamfered tool and for feed rates of ≈ 0.03 mm·rev^{-1} when turning with sharp tools. Productivity increases together with good finishing can be achieved with these tools if only the last pass of the tool is made at these conditions.

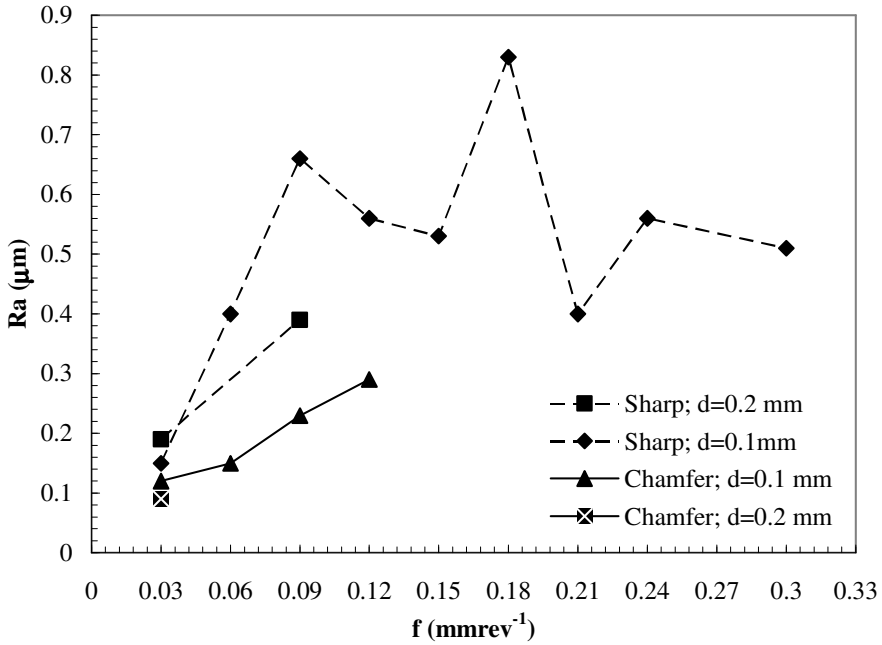

Fig. 5. Workpiece surface roughness as a function of the different cutting edges and cutting conditions.

4. Conclusions

The cutting forces developed in hardmetal turning with CVD diamond tools increase with the bluntness of the cutting edge in the following order: sharp<chamfer<hone. Chamfer tools preserve the diamond film integrity on the edge at feed rates below 0.06 mm·rev^{-1} whereas for sharp edge tools film delaminates from the flank face during the machining test although without affecting the tool performance. Flank wear is always larger for the chamfered tools than for sharp ones while rake face wear is similar for the same machining conditions. Although wear of the cutting edges increases by aggravating the machining conditions, sharp edge tool integrity can be kept for a machining speed of 15 m min^{-1}, depth of cut of 0.1 mm for feed rates up to 0.15 mm·rev^{-1}. A good workpiece finishing is obtained for the same cutting speed and depth of cut but for the lowest feed rate of 0.03 mm·rev^{-1}. Film delamination and edge fracture occurred for honed edge tools at all tested conditions. The absence of diamond film delamination from the rake face at high feed rates suggests that thicker films could be used for long time machining of hardmetal under near production requirements.

References

[1] Belmonte M, Ferrro P, Fernandes AJS, Costa FM, Sacramento J, Silva RF. Wear resistant CVD diamond tools for turning of sintered hardmetals. Diam. Relat. Mater. 2003; 12: 738-743.

[2] Belmonte M, Oliveira FJ, Sacramento J, Fernandes AJS, Silva RF. Cutting forces evolution with tool wear in sintered hardmetal turning with CVD diamond. Diam. Relat. Mater. 2004; 13: 843- 847.

[3] Collier M, Cheynet J. PM2002 Hard Materials and Diamond Tooling Congress and Exhibition. 7–9th October 2002, Lausanne, Switzerland, 2002.

[4] Almeida FA, Belmonte M, Oliveira FJ, Sacramento J, Fernandes AJS, Silva RF. The use of CVD diamond coated Si_3N_4 tools for machining sintered hardmetal. 4th Int. Conf. THE Coatings April 2004, Erlangen, Germany, 2004.

[5] Yen YC, Jain A, Altan T. A finite element analysis of orthogonal machining using different tool edge geometries. J. Mater. Process. Technol. 2004; 146: 72-81.

[6] Uhlmann E, Lachmund U, Brücher M. Wear behavior of HFCVD-diamond coated carbide and ceramic tools. Surf. Coat. Technol. 2000; 131: 395-399.

[7] Deuerler F, Lemmer O, Frank M, Pohl M, Heβing C. Diamond films for wear protection of hardmetal tools. Refract. Met. Hard Mater. 2002; 20: 115-120.

[8] D'Errico GE, Calzavarini R. Turning of metal matrix composites. J. Mater. Process. Technol. 2001; 119: 257-260.

[9] Yoshikawa H, Nishiyama A. CVD diamond coated insert for machining high silicon aluminum alloys. Diam. Relat. Mater. 1999; 8: 1527-1530.

[10] Itoh H, Shimura S, Sugiyama K, Iwahara H. Improvement of cutting performance of silicon nitride tool by adherent coating of thick diamond film. J. Am. Ceram. Soc. 1997; 80: 189-196.

[11] Belmonte M, Silva VA, Fernandes AJS, Costa FM, Silva RF. Surface pretreatments of silicon nitride for CVD diamond deposition. J. Am. Ceram. Soc. 2003; 86: 749-754.

[12] Fernandes AJS, Silva VA, Carrapichano JM, Dias GR, Silva RF, Costa FM. MPCVD diamond cutting-edge coverage: dependence on the side wedge angle. Diam. Relat. Mater. 2001; 10: 803-808.

[13] Thiele JD, Melkote SN. Effect of edge geometry and workpiece hardness on surface generation in the finish hard turning of AISI 52100 steel. J. Mater. Process. Technol. 1999; 94: 216-226.

[14] Belmonte M, Oliveira FJ, Lanna MA, Silva CM, Corat EJ, Silva RF. Turning of CFRC composites using Si_3N_4 and thin CVD diamond coated Si_3N_4 tools. Mater. Sci. Forum 2004; 455–456: 609-613.

Acknowledgements

F.A. Almeida's work is supported by Programme Alβan, European Union Program of High Level Scholarships for Latin America, identification number E03D06378BR.

4.2 *The use of thick CVD diamond direct coated Si_3N_4*

Re-sharpenable thick CVD diamond-coated Si_3N_4 tools for hardmetal turning

F. A. Almeida[1], A. J. S. Fernandes[2], R. F. Silva[1], F. J. Oliveira[1]

[1] Department of Ceramics and Glass Engineering, CICECO, University of Aveiro, 3810-193 Aveiro, Portugal

[2] Department of Physics, University of Aveiro, 3810-193 Aveiro, Portugal

(Surface & Coatings Technology 201, 2006, 1776-1782)

Abstract

Sharpening and re-sharpening ability of CVD diamond-coated ceramic tools for turning operations is addressed in this work. Thick CVD diamond films (150 μm) were deposited by MPCVD on pressure-less sintered silicon nitride ceramics. These disc-shaped tools could be sharpened to the desired geometry using grinding wheels without film detachment. The tools were tested in the dry turning of three types of hardmetal differing in WC grain size (2–6 μm) and Co content (18–27 wt.%). The lower Co content hardmetal grade (GD40) is more aggressive than GD50 or GD60 to the cutting edge, always resulting in faster wear and larger cutting forces for the same machining parameters. The depth of cut was fixed at 0.2 mm for the three hardmetal grades while the speed and feed were reduced from 30 m·min^{-1} and 0.15 mm·rev^{-1} (GD50 and GD60) to 20 m·min^{-1} and 0.1 mm·rev^{-1} for GD40. Wear changes the cutting edge geometry and increases the cutting force to values above which the tool fails (F_d~700 N). Wear of the tool occurs by microchipping of the CVD diamond, resulting in abrasion of the rake and flank faces by diamond debris. Up to 2000 m dry machining length per tool could be achieved before the re-sharpening operation has to be performed. When a cutting fluid is used, increased tool life is easily achieved due to reduction of Co adhesion and enhancement of diamond debris removal from the cutting edge.

Keywords: *Machining, Sharpening, Hardmetal, Thick CVD diamond film, Direct coating, Silicon nitride.*

1. Introduction

Tungsten carbide-based cermets (hardmetals) are well known hard and tough materials that are usually machined by conventional grinding and polishing or by EDM (electrodischarge machining). Recent reports have shown the feasibility of turning using superhard cutting tools such as PCBN[1–4] and PCD[3, 5, 6] and thick brazed CVD diamond[4, 6, 7]. Even more recently, a silicon nitride tool coated with a thin diamond film was used in the machining of hardmetal[8].

CVD diamond cutting tools are commercially available as thick film brazed CVD diamond tips and thin film CVD diamond coatings. Several steps are involved in the production of brazed tools. After thick film diamond (150 to 1000 μm) growth on Si wafers, the diamond sheet becomes free-standing by chemically etching the silicon. It is then laser cut in small tips and brazed onto hardmetal inserts. The final geometry is achieved by grinding and polishing techniques. An alternative approach is the thin film CVD diamond coating by depositing a layer directly on hardmetals or non-oxide ceramic inserts. The thickness is generally in the range of 5 to 50 μm[6, 9]. There are problems inherent to the use of hardmetal as substrate, since the Co binder induces the formation of sp^2 bonded carbon (graphitization). Adhesion is poor due to the weak mechanical properties at the interface and to the high-thermal expansion mismatch between diamond and hardmetal. A number of techniques have been adopted to overcome this problem[10, 11] but the use of chemically and thermally compatible ceramic substrates such as SiAlON, SiC, and Si_3N_4 is another approach that guarantees a suitable adhesion[6, 12, 13]. These ceramics have been used as substrates for diamond direct coating and tested as cutting tools in the machining of different materials such as Al–Si alloys, C–C composites and hardmetal[14–16].

Previous results with thin CVD diamond (~15 μm) coated Si_3N_4 tools in the turning of WC–25 wt.% Co showed satisfactory results using tools with sharp edge geometry[16]. In that work, all the tests with sharp edge tools resulted in delamination of the diamond film from the flank face at the very beginning of cutting, although without affecting the tool performance. Good workpiece finishing, tolerances and stable cutting forces were achieved for finishing conditions. The absence of diamond film detachment from the rake face even

at high feeds demonstrated a sufficient diamond coating adhesion to silicon nitride substrates. A drawback of those tools is that, as a consequence of the small thickness of the diamond coating, the recession of the cutting edge due to wear results in flank wear that rapidly reaches the silicon nitride substrate.

In the present work, a third kind of CVD diamond tool, falling between the thick brazed and thin coated ones, is proposed: thick film direct coating with sharpening and resharpening capabilities. These new tools should possess as advantages a smaller number of fabrication steps, increased tool geometry flexibility and cost reductions compared to the other thick film techniques[17]. The new tools, produced by sharpening much in the same way of PCD, PCBN, and CVD thick diamond brazed ones, are tested in the turning of three hardmetals differing in Co content and WC grain size. The cutting forces and wear of the tools are investigated as a function of the workpiece material and cutting parameters.

2. Experimental

2.1. Tools fabrication

Disc shaped silicon nitride tools were made by pressure-less sintering (1750 °C–2 h–N_2) using aluminium and yttrium oxides as sintering aids[16]. The dense substrates (>99% theoretical density) were machined to the normalized geometry RBMN1003M0FN and the tool rake face was flat lapped with 15 μm diamond slurry. Before diamond deposition, the tools were scratched for seeding purposes with 0.5–1.0 μm size diamond powder and then ultrasonically cleaned using ethanol. The ceramic tools were diamond coated in a microwave plasma assisted CVD (MPCVD) reactor (ASTeX PDS 18) using the following parameters: microwave power= 2.7 kW; total pressure=1.2×10^4 Pa; H_2/CH_4 flow=400/25 sccm; deposition time=18 h. After diamond deposition, the cutting edge was dry sharpened by diamond wheels to achieve the final radius of 5.6 mm and a tool flank angle of 5°. The average thickness of the diamond film near the cutting edge of the tools was ~ 150 μm.

2.2. Workpiece materials

Three hardmetal grades with Co content in the range 18– 27 wt.% were used in this work. The main properties of these materials are summarized in Table 1. The microstructure differences are evidenced in Fig. 1, namely the bi-modal grain size of GD60 (and GD50, whose only difference to GD60 is the Co content) and the smaller grain size of GD40.

Table 1. Characteristics of the three hardmetal workpieces.

Grade	Co (wt.%)	WC grain size (μm)	HV30 (GPa)
GD40	18	2.5	10.2±0.1
GD50	25	2 - 6	7.9±0.1
GD60	27	2 - 6	7.5±0.1

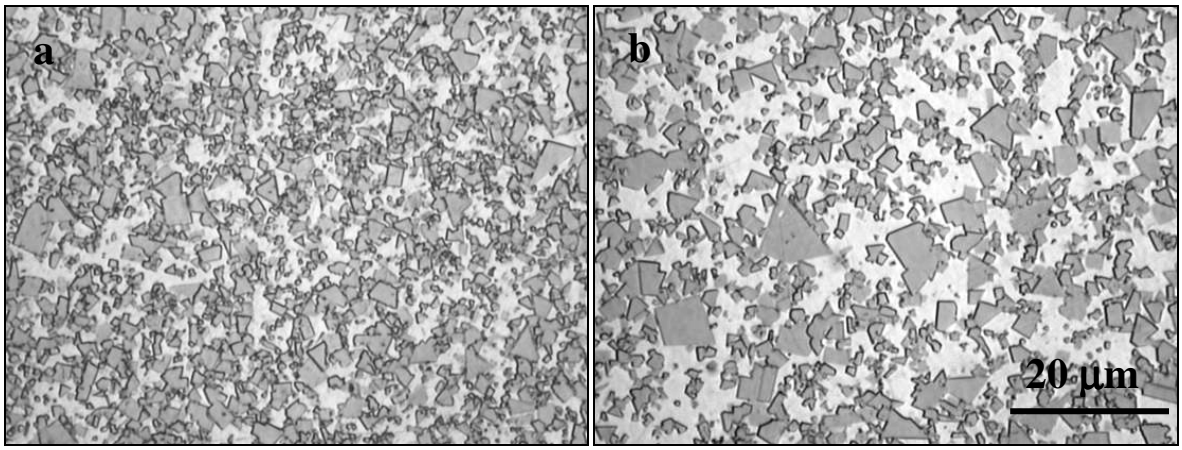

Fig. 1. Optical micrographs illustrating the microstructures of: a) GD40 and b) GD60.

2.3. Machining tests

Unlubricated tests were carried out at 20–30 $m \cdot min^{-1}$ of cutting speed (S), depth-of-cut (d) of 0.2–0.4 mm and feed (f) of 0.1–0.15 $mm \cdot rev^{-1}$. The three orthogonal components of the cutting force, namely F_c (main cutting force), F_d (depth-of-cut force), and F_f (feed force) were assessed in real time by a dynamometer (KISTLER, Switzerland) while the workpiece quality was evaluated by a portable roughness profilometer (Mahr, Germany). The final tool damage was evaluated by optical (OM) and scanning electron microscopy (SEM S-4100, Hitachi, Japan) observations.

3. Results and discussion

3.1. Tool preparation

The use of cutting tools with directly coated thick (>50 μm) diamond films is not a straightforward issue. During diamond deposition in a MPCVD reactor, and due to geometric constraints on the electric field distribution and thus on the plasma shape, the temperature at the edges of the substrates is increased relatively to more central areas. In the case of silicon nitride ceramic substrates, it was demonstrated that the grain size of diamond at the edges is larger than at the centre of 60° and 75° edged samples[18]. For very long deposition times, this effect may become more pronounced even for 90° edged substrates where the heat removal is easier than for the 60° and 75° ones. The photomicrograph in Fig. 2a illustrates this, where excessive diamond growth leads to a blunt edge. It has already been shown that this type of geometry is clearly unfavourable for machining hardmetal[16]. The diamond in the flank face is not fully uniform due to the deposition process. A columnar structure develops during growth, the diamond grain size being much larger at the free surface than at the interface with the substrate.

In Fig. 2b, the same edge appears after being sharpened with resin-bonded diamond wheels. Due to the referred grain structure of microcrystalline diamond films, small vertical scratches are visible near the free surface while small pullouts appear at the tool flank, as can be observed in Fig. 2b. The system Si_3N_4 ceramic/thick diamond film has thus

proven to have adhesion high enough to withstand the very aggressive dry grinding needed for producing sharp cutting edges. After this operation, the cutting edge and rake face roughness are determined by the grain size of the diamond. The removal of diamond deposited on the flank face is not an issue since on one hand the diamond film is thick and on the other hand, previous tests have shown that it would spontaneously delaminate during the turning operation[16].

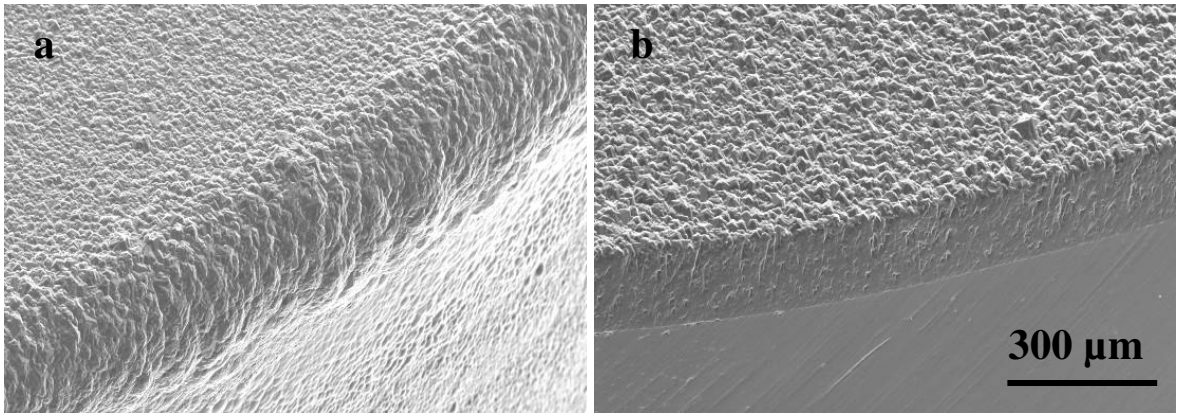

Fig. 2. General aspect of the edge of the diamond coated silicon nitride tool seen under SEM at 45º tilt: a) after MPCVD growth; b) after sharpening.

3.2. Machining performance

Part of the present work aims at determining the best machining parameters for the three hardmetal grades. Their inherent differences in WC grain size, Co content and hardness suggest that the depth-of-cut, feed and speed can not be the same for the three grades if the tool life is to be kept at comparable levels. Also, the machining must be performed under conditions such that their use may fit industrial productivity needs. Bearing these limits in mind along with the conclusions of previous works[4, 7, 8, 16], the cutting speed was fixed at 20–30 $m \cdot min^{-1}$, the depth of cut at 0.2–0.4 mm and the feed at 0.1–0.15 $mm \cdot rev^{-1}$. They correspond to what may be termed as "rough machining" opposed to "finishing" in hardmetal turning. The effect of these cutting parameters on the cutting force is depicted in Fig. 3, where a comparison is made for the evolution of the three orthogonal components of the cutting force with cutting length, for GD50 and GD60.

For the present tool geometry (RBMN1003M0FN) the larger component of the cutting force is the depth-of-cut force (F_d), followed by the main cutting force (F_c) and finally by the smaller one (feed force – F_f). Considering that small differences exist between the WC–Co materials GD50 and GD60, Table 1, their effect on the cutting force is nevertheless evident. It has been previously shown that wear of the cutting edge in diamond tools induces larger values of the cutting force, mainly of F_d, due to increased contact area and to diminished cutting efficiency[16]. The comparison of data in Fig. 3a and b clearly indicates that, for the same machining conditions, GD50 is more aggressive to the cutting edge than GD60, as the larger starting cutting forces and their steeper increase with machining distance shows. This may indicate that the turning parameters are near the limit of the tool for GD50 machining.

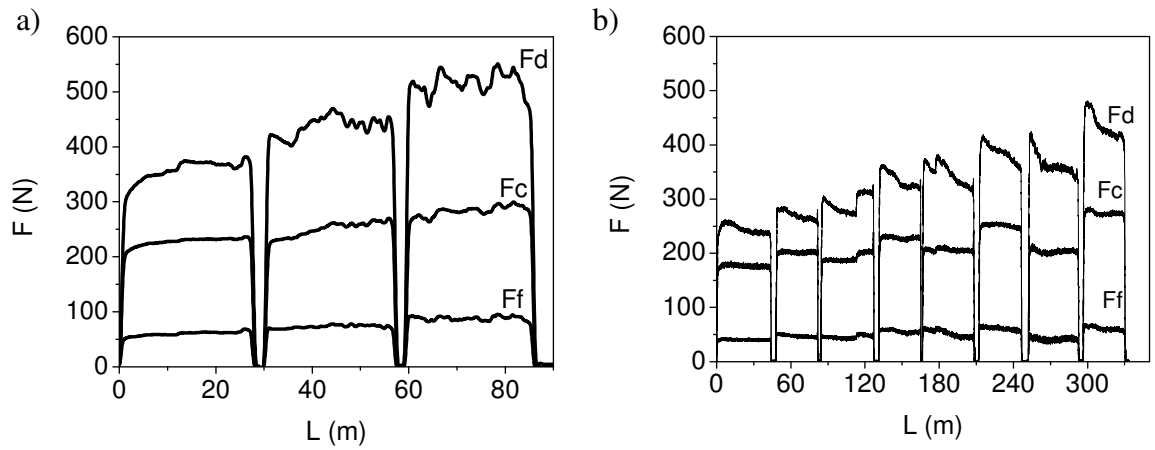

Fig. 3. Evolution of the cutting force with distance at a cutting speed of 30 m·min^{-1}, depth of cut of 0.2 mm and feed of 0.15 mm·rev^{-1} in the machining of: a) GD50; b) GD60.

In spite of the lower starting cutting forces relative to GD50, the turning of GD60 also results in wear of the cutting edge, as the continuously increased values of the cutting force indicate. However, instead of a steady increase up to the usable limit of the cutting tool, it is clear that additional features are at stake during machining, since force leaps occur during and between successive passes of the same cutting test (Fig. 3b). The result of a first pass of these newly developed tools in the machining of rods of the three hardmetals can be seen in the micrographs of Fig. 4. The top view micrographs show the cutting edge

and the rake face of the tools. It becomes clear that the larger the content of Co binder, the larger is the tendency for formation of built-up-edge (BUE). This is eased by the considerable high roughness due the diamond grains on the tool rake face that favour anchoring of the Co binder. The jumps in the machining force observed during unlubricated dry turning of GD60 are most likely related to sudden removal of Co built up at the edge and formation of new BUE (Fig. 3b). This effect should become even more pronounced for larger depths of cut as the BUE shown in the micrograph of Fig. 4d indicates.

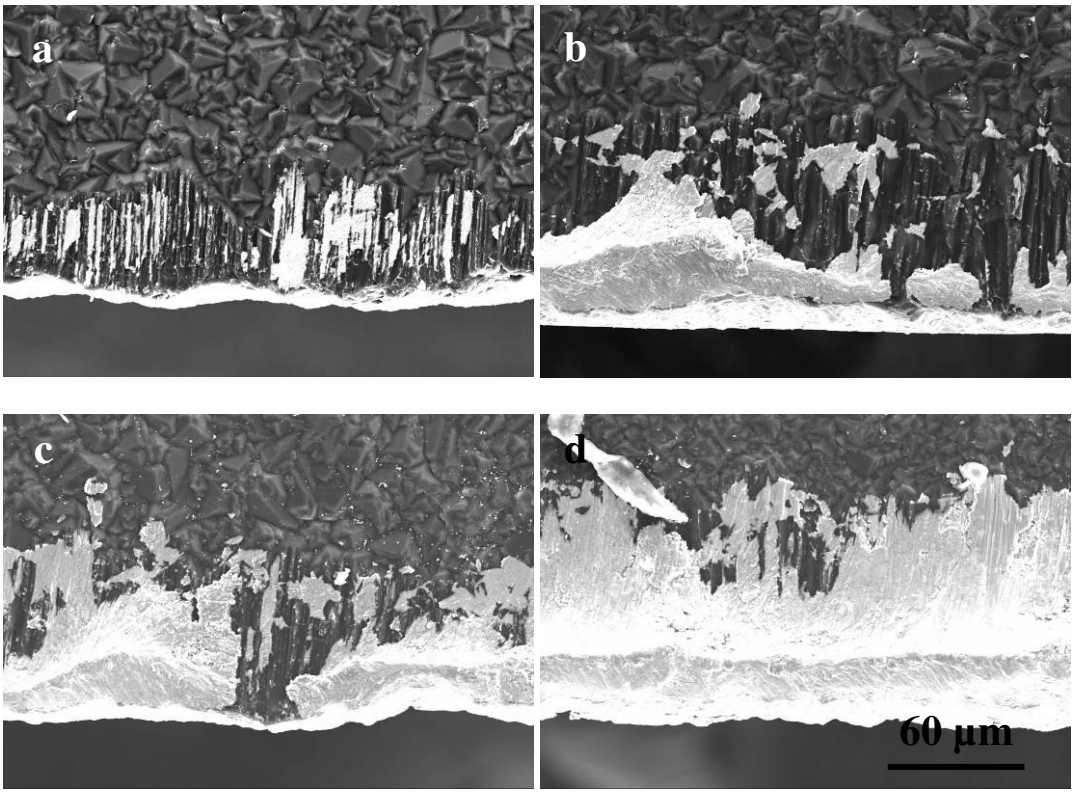

Fig. 4. Top views of the rake face and cutting edge of the coated and sharpened CVD diamond tool after one pass in the machining of three hardmetal rods: a) GD40 (S = 20 m·min^{-1}, d = 0.2 mm, f = 0.10 mm·rev^{-1}); b)GD50 (S = 30 m·min^{-1}, d = 0.2 mm, f = 0.15 mm·rev^{-1}); c) GD60 at (S = 30 m·min^{-1}, d = 0.2 mm, f = 0.15 mm·rev^{-1}); d) GD60 (S = 30 m·min^{-1}, d = 0.4 mm, f = 0.15 mm·rev^{-1}).

The machining conditions of GD40 had to be adjusted after a first set of experiments. Tool failure occurred when the same cutting conditions used for machining GD50 and GD60 were tested. According to the knowledge on the relationships between cutting parameters, cutting force and tool wear in the machining of hardmetal[7, 8, 16], the cutting speed and feed were slightly lowered (to 20 $m \cdot min^{-1}$ and 0.1 $mm \cdot rev^{-1}$, respectively) for turning GD40 hardmetal. This allowed successful machining of GD40 with cutting forces and tool wear comparable to that obtained for GD50 and GD60 turning. The micrographs of Fig. 5a and b allow comparing the effect of the machining length on the cutting edge and flank face, evidencing the recession of the cutting edge after 300 m (Fig. 5b) that allows the flank wear scars to reach the silicon nitride substrate. The same effect occurs for GD50 and GD60 (Fig. 5c) machining, although here Co appears extensively smeared at the flank and rake faces.

During machining, the cutting forces increase (Fig. 3a and b), but even when the substrate is reached, the diamond edge keeps cutting the hardmetal workpieces, although at larger stress levels. For the depth of cut component of the cutting force, Fd, if a value of about 700 N is surpassed due to wear on the flank face, the tools fail by fracture of the edge and/or delamination of the diamond film. This value corresponds to the working limit of these sharpened cutting tools and may used as a trigger to stop the machining operation when real-time force acquisition is used. It is worth noting that the flank wear land (VB) does not reach the standard tool life criterion of 0.3 mm[19] after the 300 m test. However, considering the coating thickness of the present cutting tools, a maximum VB value of 0.15 mm should be assumed. Although a crater is visible on the rake face, its depth, KT, is of the order of only a few micrometers for all tested conditions.

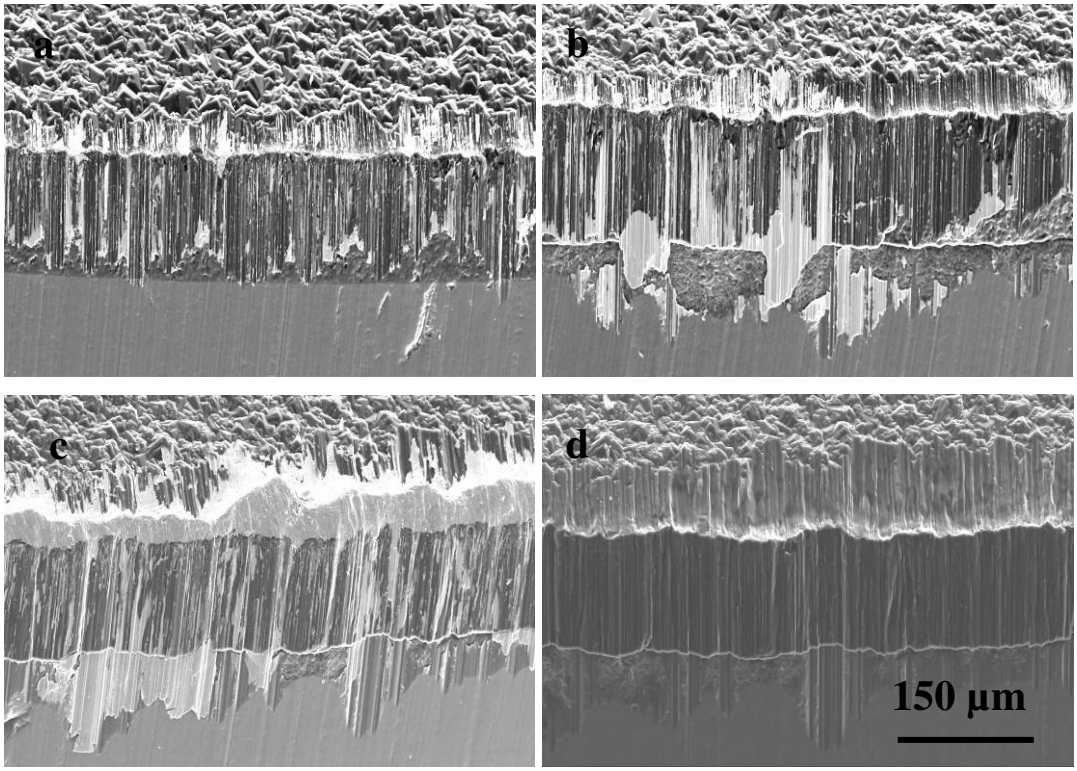

Fig. 5. Details of the wear observed after different machining: (a,b) GD40 (S = 20 m·min^{-1}, d = 0.2 mm, f = 0.10 mm·rev^{-1}) turned for one pass and 300 m, respectively. (c,d) GD60 turned for 300 m at S = 30 m·min^{-1}, d = 0.2 mm, f = 0.15 mm·rev^{-1} before and after cobalt removal, respectively. All micrographs taken with 45º tilt under SEM.

3.3. Tool wear mechanisms

The wear of the diamond tools when machining hardmetals is characterised by scars on both the rake and flank faces, denoting a prevailing abrasion mechanism[3]. The main visual difference after machining of low Co content GD40 grade and the two other grades is the presence of adhered Co in the case of the latter (Fig. 5c). However, after Co leaching (20 min HF/HNO_3 1:1), the wear features are the same, regardless the workpiece material, as the micrographs in Fig. 5c and d show.

Other failure mechanisms contribute to the wear of the diamond tools in the machining of WC–Co, their relative importance being a function of the machining parameters. While for high speed machining diffusion plays a determinant role, for the low

and medium ranges of optimised cutting conditions used in the present work, Co adhesion leads to microweldings and to the formation of the BUE. The cutting edge is thus periodically loaded with localised extreme stresses for a short time, Fig. 3b. This may result in diamond chipping near the cutting edge (Fig. 6a), leading to uneven edge break-out (Fig. 6b). Loose diamond debris from both microchipping and transgranular fracture are the abrasive agents contributing to the general abrasion of the rake and flank faces, together with the action of the WC hard particles. Notching due to the depth-of-cut and to the escape of the small WC–Co chips is another observed wear mechanism.

Although most of the work done has been carried out under dry cutting conditions, some tests were also conducted using a coolant/lubricant fluid to allow determining its effect on the wear of the tools. Another reason is that in multi-pass turning of cylinders, as is the case of the present experimental tests, they heat excessively, rendering nearly impossible to obtain reproducible machining tolerances. Fig. 6c and d illustrate the differences in wear of the cutting edge without and with coolant, respectively, when machining GD60 at 0.4 mm of cutting depth. The differences are remarkable, since when using a cutting fluid the wear is much decreased and nearly no Co adhered to the cutting edge. Without cooling and for this depth of cut value, the cutting edge wears rapidly, rendering the tool unusable for further machining, Fig. 6c, and forcing the tool re-sharpening. Debris removing and cooling/lubrication actions have thus a large effect on the weight of the mentioned wear mechanisms of both diamond abrasion and Co adhesion to the tool. A balance between the tool life and productivity on one side and environmental issues[14] and machine protection from WC–Co debris on the other side has to be solved to define the best turning conditions.

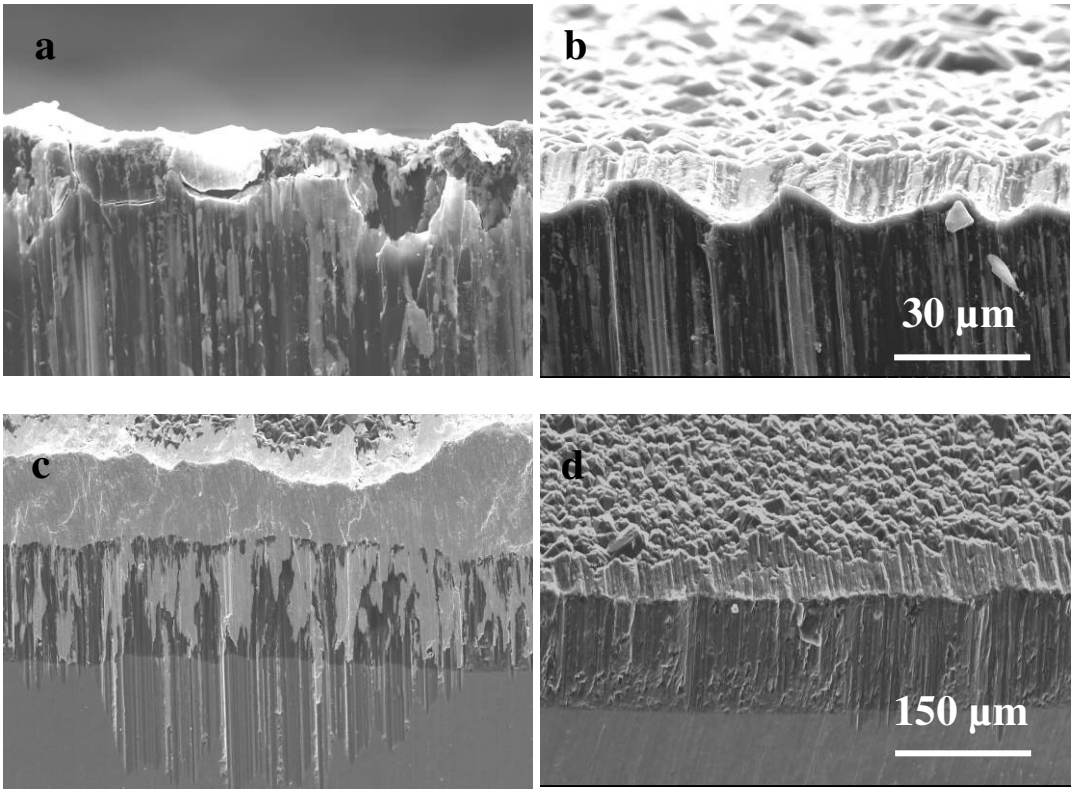

Fig. 6. Aspects of the cutting edge after machining: a) micro-chipping (GD50, S = 20 m·min^{-1}, d = 0.2 mm, f = 0.15 mm·rev^{-1}); b) uneven wear (GD40, S = 30 m·min^{-1}, d = 0.2 mm, f = 0.10 mm·rev^{-1}). Morphology of wear in the machining of GD60 at S = 30 m·min^{-1}, d = 0.4 mm, f = 0.15 mm·rev^{-1} with (c) and without (d) lubrication observed with 45º tilt.

3.4. Re-sharpening

On what matters the re-sharpening of these new tool materials, one must bear in mind that after long term machining (about 300 m in the present work), the flank wear reaches the substrate surpassing the adopted tool life criterion of VB≈coating thickness. Issues related to tool construction and tool life assessment are here at stake. When comparing the recession of the cutting edge due to wear (e.g. Fig. 4a) with the amount of diamond that was machined to form the first cutting edge (Fig. 2), it becomes clear that re-sharpening is a much easier operation than the initial sharpening one. The resultant tool has the same morphology of the sharpened tool shown in Fig. 2b. To retain here is the fact that if tool integrity is kept after sharpening, resharpening will not pose any problems since

diamond adhesion is guaranteed during machining by selecting the right parameters for each workpiece material. For the particular geometry of these tools, a machining length of 2000 m is possible before resharpening by successively exposing unused edge, what permits dry machining lengths of up to 10000 m (considering up to 4 resharpening operations) with a single disc-shaped thick film diamond coated silicon nitride tool.

5. Conclusions

Thick film CVD diamond (~150 μm) was directly deposited by the microwave plasma technique on silicon nitride tools and sharpened using grinding processes without loss of adhesion or film detachment from the substrate.

Machining parameters were adjusted to suit different hardmetal grades, the speed and feed being respectively reduced to 20 $m \cdot min^{-1}$ and 0.1 $mm \cdot rev^{-1}$ for the lowest Co binder grade (18 wt.%), while for the coarser WC grades containing larger amounts of Co, the speed and feed were kept at 30 $m \cdot min^{-1}$ and 0.15 $mm \cdot rev^{-1}$, keeping the depth of cut at 0.2 mm. For the selected tool geometry (RBMN1003M0FN), the larger component of the cutting force is the one due to the depth-of-cut. The lower Co content hardmetal grade, GD40, yields the larger cutting force and wear when using the same machining parameters for GD50 and GD60. The higher Co content grade induces easy formation of built up edge resulting in discontinuities in the cutting force.

Due to the wear, the cutting edge recession occurs and flank wear increases. This change of the cutting edge geometry increases the cutting force and reaches a threshold value corresponding to Fd~700 N above which the tool fails. Wear of the CVD diamond tool occurs due to abrasion of the rake and flank faces mainly by diamond debris. Diamond microchipping, enhanced by the adherent Co built-up-edge (BUE), and transgranular fracture are the source of the loose diamond particles.

A tool life criterion of VB≈diamond thickness was considered allowing cutting lengths of 2000 m per tool under optimised dry turning conditions. Up to four re-sharpening operations are expected before the tool has to be rejected. When a cutting fluid

is used, increased tool life is easily achieved due to reduction of Co adhesion and enhancement of diamond debris removal from the cutting edge.

References

[1] Liu K, Li XP, Rahman M. Characteristics of high speed micro-cutting of tungsten carbide. J. Mater. Process. Technol. 2003; 140: 352-357.

[2] Liu K. Li XP, Rahman M, Liu X.D. CBN tool wear in ductile cutting of tungsten carbide. Wear 2003; 255: 1344-1351.

[3] Miyamoto T, Heo SJ, Hanasaki S, Fujiwara J. Cutting of wear and impact resistant cemented carbides. Proceedings of the 7th International Conference on Progress of Machining Technology, Aviation Industry Press, Suzhou (P.R. China). 2004, 44-48.

[4] Belmonte M, Ferrro P, Fernandes AJS, Costa FM, Sacramento J, Silva RF. Wear resistant CVD diamond tools for turning of sintered hardmetals. Diam. Relat. Mater. 2003; 12: 738-743.

[5] Collier M, Cheynet J. PM2002 Hard Materials and Diamond Tooling Congress and Exhibition. 7–9th October 2002, Lausanne, Switzerland, 2002.

[6] Cline BL, Olson JM. CVD diamond solutions for machining and other mechanical applications. In: Asmussen J and Reinhard DK, editors. Diamond Films Handbook. New York: Marcell Dekker, 2001.

[7] Belmonte M, Oliveira FJ, Sacramento J, Fernandes AJS, Silva RF. Cutting forces evolution with tool wear in sintered hardmetal turning with CVD diamond. Diam. Relat. Mater. 2004; 13: 843- 847.

[8] Almeida FA, Belmonte M, Oliveira FJ, Sacramento J, Fernandes AJS, Silva RF. The use of CVD diamond coated Si_3N_4 tools for machining sintered hardmetal. 4th Int. Conf. THE Coatings April 2004, Erlangen, Germany, 2004.

[9] D'Errico GE, Calzavarini R. Turning of metal matrix composites. J. Mater. Process. Technol. 2001; 119: 257-260.

[10] Polini R, Bravi F, Casadei F, D'Antonio P, Traversa E. Effect of substrate grain size and surface treatments on the cutting properties of diamond coated Co-cemented tungsten carbide tools. Diam. Relat. Mater. 2002; 11: 726-730.

[11] Deuerler F, Gruner H, Pohl M, Tikana L. Wear mechanisms of diamond-coated tools. Surf. Coat. Technol. 2001; 142–144: 674-680.

[12] Belmonte M, Fernandes AJS, Costa FM, Oliveira FJ, Silva RF. Adhesion behaviour assessment on diamond coated silicon nitride by acoustic emission. Diam. Relat. Mater. 2003; 12: 733-737.

[13] Amaral M, Oliveira FJ, Belmonte M, Fernandes AJS, Costa FM, Silva RF. Tailored Si_3N_4 ceramic substrate for CVD diamond coating. Surf Eng 2003;19:410-416.

[14] Uhlmann E, Lachmund U, Brücher M. Wear behavior of HFCVD-diamond coated carbide and ceramic tools. Surf. Coat. Technol. 2000; 131: 395-399.

[15] Belmonte M, Oliveira FJ, Lanna MA, Silva CM, Corat EJ, Silva RF. Turning of CFRC composites using Si_3N_4 and thin CVD diamond coated Si_3N_4 tools. Mater. Sci. Forum 2004; 455–456: 609-613.

[16] Almeida FA, Oliveira FJ, Sousa M, Fernandes AJS, Sacramento J, Silva RF. Machining hardmetal with CVD diamond direct coated ceramic tools: effect of tool edge geometry. Diam. Relat. Mater. 2005; 14: 651-656.

[17] Knotek O, Löffler F, Krämer G. Applications to cutting tools. Chapter 7. In: Bunshah RF (Ed.). Handbook of Hard Coatings. New York: William Andrew Publishing, 2001.

[18] Fernandes AJS, Silva VA, Carrapichano JM, Dias GR, Silva RF, Costa FM. MPCVD diamond cutting-edge coverage: dependence on the side wedge angle. Diam. Relat. Mater. 2001; 10: 803-808.

[19] International Standard ISO 3685 (1993). Tool life testing with single-point turning tools.

Acknowledgements

F. A. Almeida's work is supported by Programme Alßan, European Union Program of High Level Scholarships for Latin America, identification number E03D06378BR. Funding from FCT project POCI/CTM/59449/2004–"NANODIAM" is gratefully acknowledged.

4.3 *The effect of different grain sizes of CVD diamond direct coated Si_3N_4 on the machining behaviour*

Machining behaviour of silicon nitride tools coated with micro-, submicro and nanometric HFCVD diamond crystallite sizes

F. A. Almeida, M. Amaral, F. J. Oliveira, R. F. Silva

Department of Ceramics and Glass Engineering, CICECO, University of Aveiro, 3810-193 Aveiro, Portugal

(Diamond and Related Materials 15, 2006, 2029-2034)

Abstract

Very smooth CVD diamond films are used as direct coatings on Si_3N_4 tool substrates. By adjusting deposition parameters, namely Ar/H_2 and CH_4/H_2 gas ratios, and substrate temperature, nano- (27 nm) and submicrometric (43 nm) crystallite sized grades were produced in a hot filament reactor. Also, a conventional 5 and 12 μm micrometric grain size types were produced for comparison. Normalized coated inserts were tested for dry turning of WC–25 wt.% Co hardmetal. All the CVD diamond grades endured the hardmetal turning showing slight cratering, having the flank wear as the main wear mode. Their turning performance was distinct, as a consequence of morphology and surface roughness characteristics. Among all the tested tools, the more even surface and the submicrometric grade presented the best behaviour regarding cutting forces, tool wear and workpiece surface finishing. For this coating, the depth-of-cut force attained the lowest value, 150 N, the best combination of wear types (KM=30 μm, KT=2 μm and VB=110 μm) and workpiece surface finishing (Ra=0.2 μm).

Keywords: *Cutting tools, Diamond film, Hot filament CVD, Nanocrystalline.*

1. Introduction

CVD diamond coated materials possess outstanding tribological properties due to diamond extreme hardness, high thermal conductivity and low friction coefficient against a wide range of materials. A widespread application is the case of cutting tools, where CVD diamond coatings are used for machining abrasive and hard materials, such as MMC's, aluminum–silicon alloys and tungsten carbide[1–3]. However, the relatively high surface roughness of conventional microcrystalline CVD diamond can be detrimental for wear resistance. To overcome this drawback a solution is the development of diamond crystals with submicrometric or even nanometric size. These diamond grades can be produced in a microwave plasma CVD reactor from a variety of feed gas mixtures such as fullerenes/Ar, CH_4/Ar, CH_4/N_2, or just using higher ratios of CH_4/H_2[4–8]. This way, the columnar structure that forms during the microcrystalline diamond growth, which is responsible for a high roughness of the free surface, is avoided. The hot filament CVD technique is a less referred method to grow such coatings. Here, a bias current can be applied to enhance the growth rate and minimize the grain size and surface roughness[9] or carefully adjusted deposition conditions under $H_2/Ar/CH_4$ gas mixtures can be used[5, 10].

Machining of hardmetal parts by chip removal is a challenge for a cutting tool but microcrystalline CVD diamond has already proved its adequacy[3, 11]. However, there are no published works concerning the use of smoother CVD diamond in this application, although it has been reported for machining of Al–Si alloys and GFRP[12]. In the present work, diamond films with two distinct crystallite sizes are investigated as direct coatings on Si_3N_4 tool substrates: i) submicrometric diamond (43 nm) and ii) nanocrystalline diamond (27 nm). These diamond films were grown by hot filament CVD technique, and also as conventional micrometric (5–12 μm) sized ones, for comparative purposes. The cutting performance of normalized coated inserts is evaluated in turning of WC–25 wt.% Co hardmetal workpieces.

2. Experimental

Fully dense Si_3N_4 ceramic discs were made by pressureless sintering[11]. The ceramic parts were grinded to achieve final tool insert geometry of RNMN1003M0FN. Surface treatments before CVD diamond deposition included: flank face grinding with diamond wheel, rake face polishing with 15 μm diamond slurry, etching by CF_4 plasma (1 h), and scratching/seeding in a diamond suspension in n-hexane by ultrasonification (1 h).

Diamond growth was conducted by hot filament chemical vapour deposition (HFCVD). The selected growth parameters resulted in three types of diamond films found that are labelled in Table 1 as: MCD, for microcrystalline diamond; SMCD, for submicrocrystalline diamond; and NCD, for nanocrystalline diamond. For each diamond grade, short (labelled 1) and long time (labelled 2) deposition runs were conducted. Filament and substrate temperature were measured with a two colour pyrometer and a K-type thermocouple placed at the back side of the substrate, respectively. The samples were heated by thermal radiation to a temperature of about 550 °C. Further substrate temperature increment was given by an external power supply. The surface roughness of the different diamond films was determined using AFM microscopy from 50 μm×50 μm scan areas. Diamond crystallite sizes were estimated by the broadening of the XRD diffraction peak at 2θ~44°, corresponding to the diamond (111) plane.

The turning tests were conducted in a CNC lathe under dry cutting conditions. The workpiece material was a WC–25 wt.% Co cylinder (Ø=32 mm, length=60 mm). The cutting performance of the three types of diamond coated tools was evaluated at fixed conditions: speed=15 m min−1, depth-of-cut=0.1 mm and feed=0.1 mm rev−1. The three components of the cutting force, namely F_d (depth-of-cut force), F_c (main cutting force) and F_f (feed force), were acquired for all tests using a dynamometer. The workpiece surface finishing was determined by profilometry. Tool damage was evaluated using SEM and optical microscopy.

3. Results and discussion

3.1. Coatings morphology and surface roughness characterization

SEM cross-sections at the cutting edges of the CVD diamond distinct grades are shown on Fig. 1a, b and c. The respective insets were taken from the rake face of the inserts. The different morphologies are further evidenced in Fig. 1d, e and f where 3D AFM scans are shown. The MCD film has a columnar structure, originating large diamond grains at the free surface (Fig. 1.a). These are responsible for the high values of roughness well visualized by AFM 3D scanning (Fig. 1.d). SMCD and NCD films have a very distinct kind of structure, as grain growth is suppressed by decreasing the atomic H density with the increment of CH_4, in the former case, or partial substitution by Ar, in the latter, thus increasing the renucleation of diamond[4]. Therefore, very small crystallites develop along all the thickness (Fig. 1.b and c) and the surface roughness is very low when compared with the MCD ones (Fig. 1.e and 1.f). RMS roughness of the films can be found in Table 1. The nominal RMS value of the silicon nitride substrate is about 0.4 μm. Both MCD films had rougher surface values than the substrate, as is expected by the columnar grain growth and sustained by the larger value of the thicker film. For the smoother films, SMCD and NCD, their RMS values were lower than the substrate, surpassing the high differences between peaks and valleys, by lateral growth of the surfaces[13].

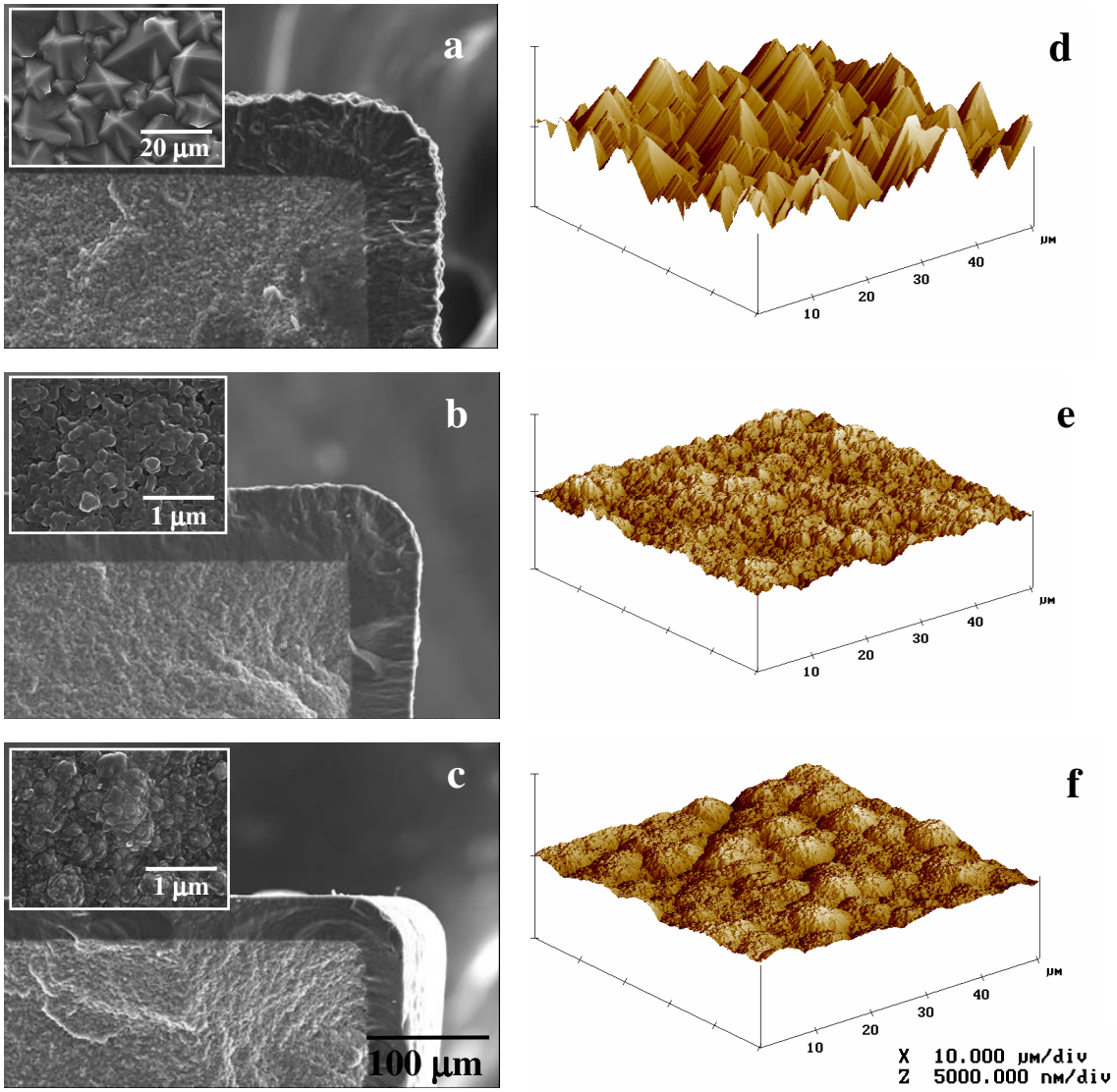

Fig. 1. SEM cross-sections and top view insets of: a) MCD-2; b) SMCD-2 and c) NCD-2. Pictures d) to f) are the respective AFM scans.

Table 1. Hot filament deposition parameters and characteristics of different CVD diamond coating.

Tool type	CH_4 /H_2	Ar/ H_2	Gas flow (sccm)	Total pressure (mbar)	Filament temperature (ºC)	Substrate temperature (ºC)	Growth rate ($\mu m \cdot h^{-1}$)	Thickness (µm)	RMS (µm)	Crystallite size (nm)
MCD-1	0.02	-	100	25	2300	850	2.7	20	0.55	-
MCD-2								42	0.78	
SMCD-1	0.03						3.1	23	0.18	43
SMCD-2								50	0.23	
NCD-1	0.04	0.1 0	50	50		750	1.3	13	0.18	27
NCD-2								23	0.26	

The crystallite size estimated from the broadening of the XRD diamond peak is 43 and 27 nm for SMCD and NCD films, respectively. Although the submicrometric diamond with 43 nm of crystallite size reaches the usual nanometric assignment, the crystallite size taken from the Scherrer formula is only a lower limit of the real value, as it involves peak broadening only caused by the finite crystallite size, ignoring broadening by mechanical stress in the layer[14]. Besides, the crystallite size is only equivalent to the grain size if the individual grains are defect-free single crystals[15]. Supporting this, SEM micrographs of the submicrometric grade reveal a grain size of about 100–200 nm (see inset of Fig. 1b).Differently, the NCD morphology appears to be formed by agglomerates of very tiny grains (inset of Fig. 1c). Raman spectroscopy in the centre and near the insert edges revealed the diamond characteristic peak at ~1332 cm^{-1} and the features usually associated to the graphitic phases D and G bands (at 1350 cm^{-1} and 1580 cm^{-1}, respectively) and transpolyacetylene (at 1140 and 1480 cm^{-1}), typical of NCD films[16]. In the case of MCD films, the grain size at the free surface was calculated by image analysis from a SEM micrograph of the films, since the broadening of the DRX peak is negligible when the crystallite size is larger than 200 nm[15]. The mean grain size values found were about 5 and 12 μm for MCD-1 and MCD-2, respectively.

An important feature of the HFCVD method is the accentuated attenuation of the "edge effect" characteristic of the MPCVD process. In the latter process, plasma discharges concentrate at sharp edges locally rising the temperature and the growth rate, leading to a heterogeneous distribution of grain size and bumped edges. Thus, the roundness of the cutting edges of the HFCVD diamond inserts is mainly related to the film thickness and curvature radius.

3.2. Cutting performance of distinct crystallite size diamond films

The differences between the coatings characteristics are somehow reflected in the force analysis performed during the hardmetal cutting. The values of the depth-of-cut, main and feed component of the cutting force, F_d, F_c and F_f, respectively, are shown in Fig. 2. The effect of film thickness is only evident for MCD, where further rounding of the tool due to the increase in thickness is complemented by the increment of the edge roughness (Table 1). When the tool surface is very rough, the friction between tool and workpiece is

excessive and high forces are generated during the cutting operation. SMCD tools, although being thicker than the NCD ones and having quite the same value of surface roughness, present an even surface, while the NCD coatings are formed by ball-shaped agglomerates (Fig. 1e and f). As a result of this, the SMCD tools present the smallest cutting forces, followed by NCD and MCD tools (Fig. 2a). In all grades, F_d has the highest value, a characteristic feature of circular shaped insert geometries, due to the high contact area with the workpiece.

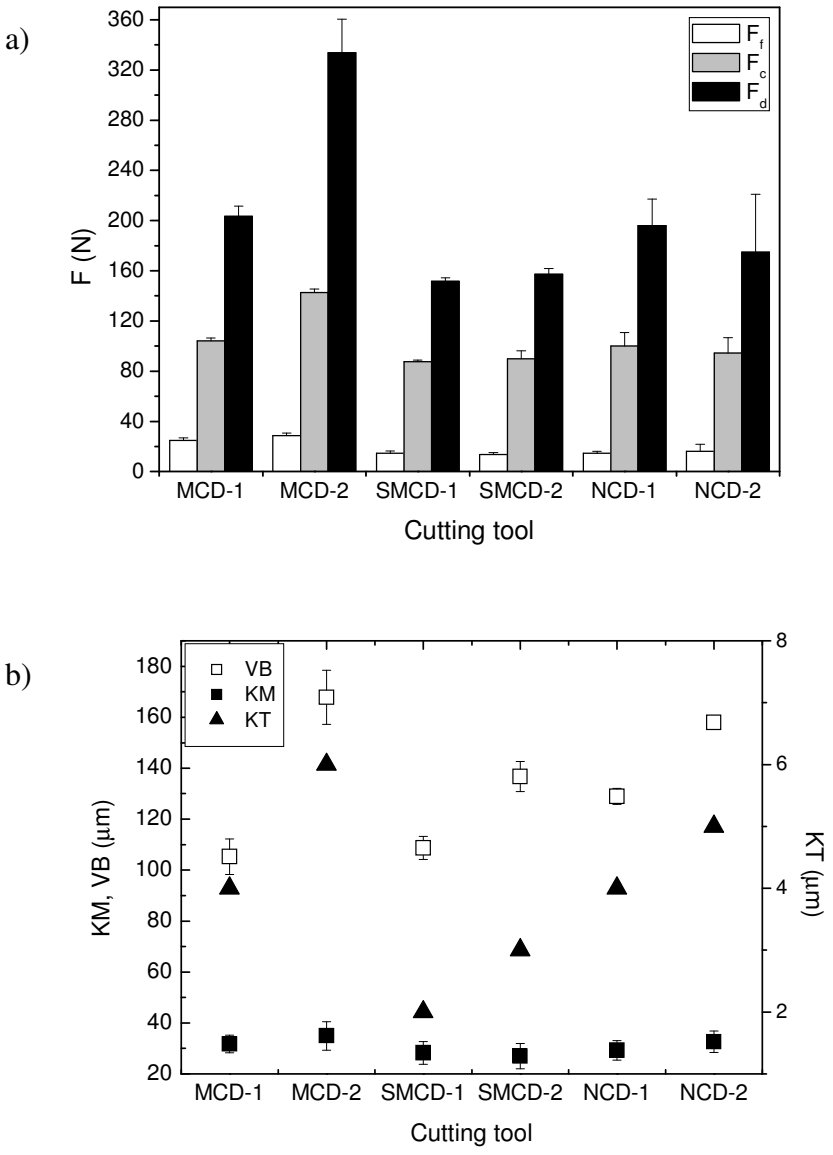

Fig. 2. Cutting forces (a) and wear parameters at rake and flank faces (b) of the distinct diamond grades and film thickness after one turning pass (~60 m cutting length, 4 min of cutting time).

The evolution of the cutting forces is closely linked with the tool wear. SEM micrographs of the cutting edge feature after one pass (~60 m cutting length, which corresponds to 4 min of cutting time) are visualized in Fig. 3.a–c and e–g. Fig. 2.b summarizes the set of values of the crater centre distance (KM), average flank wear width (VB) and crater depth (KT). KT was estimated by focus/de-focus procedure in an optical microscope, while KM and VB were measured from SEM micrographs. KT values have a very low magnitude, from 2 to 6 μm, the lowest values occurring for the SMCD grade and the largest ones for the MCD tools. This is likely to be a consequence of the increasing surface roughness and higher probability of diamond microchipping and transgranular fracture. The dominant wear mechanism is abrasion caused by loose diamond debris and WC hard particles from the sliding action of the chip and workpiece rubbing on the rake and flank faces, respectively[11]. KM has a lower magnitude than VB, presenting a value of about 30 μm for all tool types. Flank wear is the predominant kind of tool wear. Comparing left and right columns of Fig. 3, it is worth noting that the VB width increases with the diamond thickness, for all the three types of diamond tools. This is a consequence of the simultaneous increment of the cutting forces due to the edge curvature radius and film surface roughness, with film thickness. For the thickest coatings among all the diamond grades, there is a relationship between the magnitude of the forces and the width of the wear scars. This is patent in the VB wear type as SMCD-2 performance is superior both in terms of cutting forces and tool wear (Fig. 2.a and b).

According to the ISO Standard 3685, a VB value of 0.3 mm is adopted for tool life criterion. This value of VB limit was not achieved after 4 min of cutting time by any of the tools. The MCD-2 tool was tested for longer times, reaching the VB limit after 12 min (Fig. 3.d and h). For this cutting edge, wear values were about 13 μm (KT), 40 μm (KM) and 310 μm (VB).

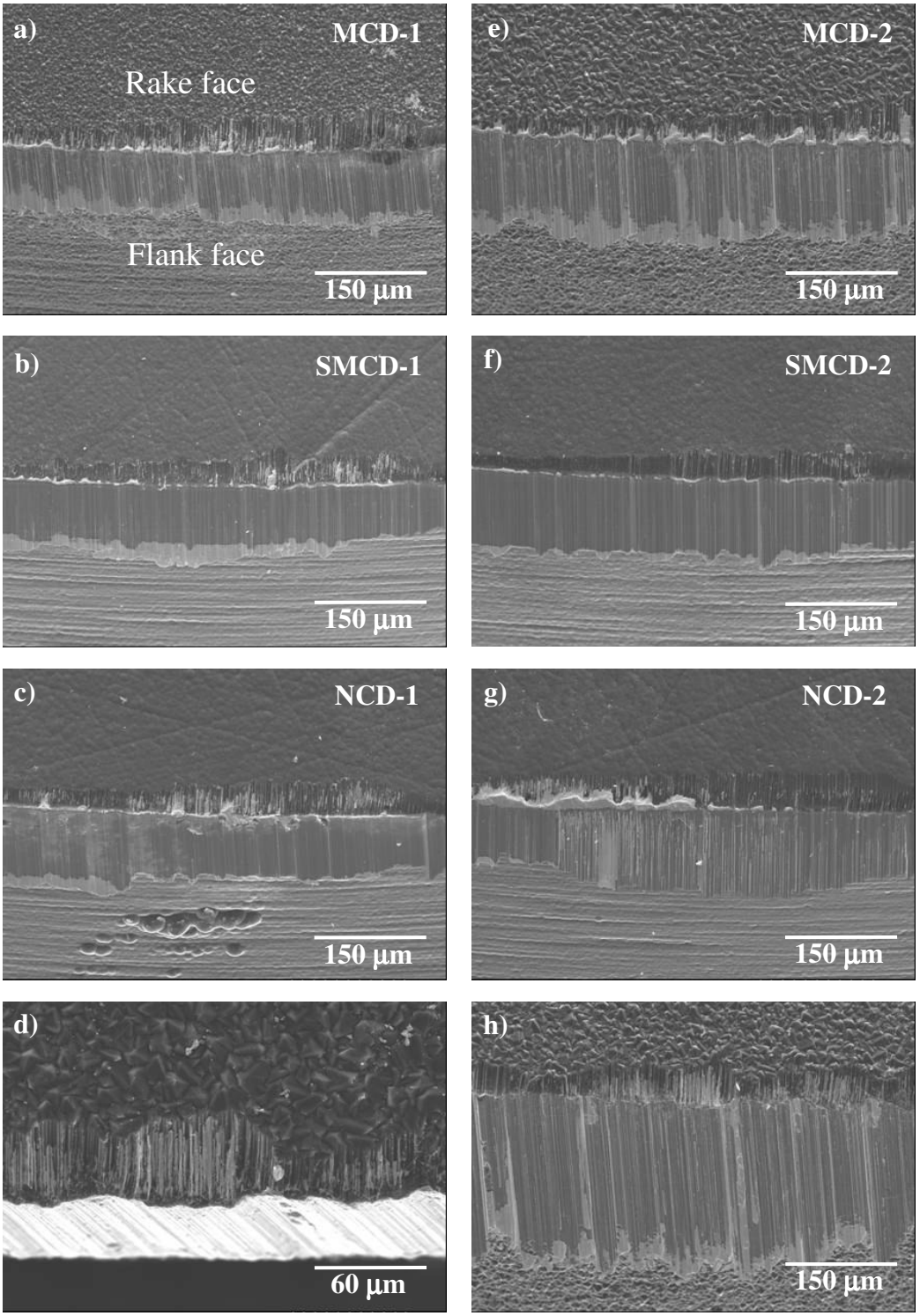

Fig. 3. Rake and flank faces of the distinct CVD diamond tools. a) to c) correspond to MCD-1, SMCD-1 and NCD-1 coatings, respectively, and e) to g) correspond to MCD-2, SMCD-2 and NCD-2 coatings, respectively, after one turning pass. Top (d) and inclined view (h) of MCD-2 cutting tool after three machining passes (~180 m cutting length, 12 min of cutting time).

A remarkable feature after all the turning tests was the absence of diamond film delamination at the cutting edge. In a previous work[3], the use of diamond coated tools for turning the same grade of hardmetal presented some drawbacks related to diamond adhesion on the flank face. In the present work, there was a significant increase of the adhesion strength by the improvement of the surface pre-treatments of the Si_3N_4 substrates, since all kinds of the tools upheld the strong compressive loading developed under cutting.

Differences on the edge quality, concerning to different roughness levels, affect the chip removal and workpiece surface finishing[17]. A rough surface may lead to built-up-edge (BUE) formation, weakening the cutting edge. In this work, BUE was not significantly developed, even for the roughest cutting tool. Nevertheless, a higher amount of adherent material was found in NCD-2 tool, as a consequence of the irregular wear at this cutting edge (Fig. 3g). The surface roughness influences the workpiece surface quality. Data in Fig. 4, measured after 4 min machining time, shows that there is a nearly linear correlation between the tool and hardmetal surface roughness. Good surface finishing could be achieved by the lower diamond crystallites sizes, SMCD and NCD, reaching the accepted industrial Ra of about 0.2 μm.

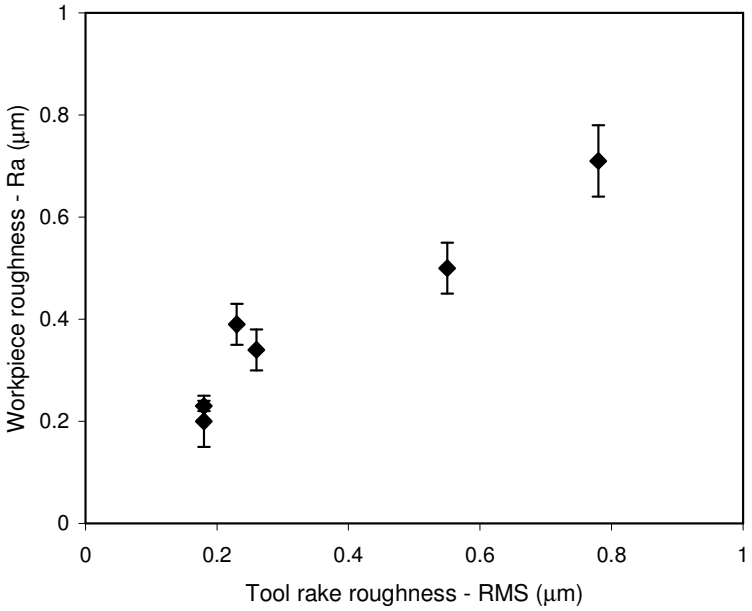

Fig. 4. Relationship between the tool surface roughness and the workpiece surface finishing for the different CVD diamond grades.

6. Conclusions

Silicon nitride inserts were successfully coated by CVD hot filament method with continuous and highly adherent diamond films of nano- (27 nm) and submicro- (43 nm) crystallite sizes, and conventional 5 and 12 μm micrometric grain size types. The respective coatings morphology and surface roughness resulted in dissimilar cutting performance in dry turning of WC–25 wt.% Co at 15 $m \cdot min^{-1}$ of cutting speed, 0.1 mm depth-of-cut and 0.1 $mm \cdot rev^{-1}$ feed. The submicrometric grade presented the best behaviour regarding cutting forces, tool wear and workpiece surface finishing. For this coating, the depth-of-cut, main and feed cutting forces attained the lowest values, respectively of F_d=150 N, F_c=100 N and F_f=15 N. The thinnest (23 μm) submicrometric coated inserts presented the best combination of types of wear (KM=30 μm, KT=2 μm and VB=110 μm) and workpiece surface finishing (Ra=0.2 μm), after 60 m cutting length. The performance of the nanometric grade was slightly inferior due to frictional interaction of surface ball-shaped agglomerates, although having a smaller crystallite size and a similar surface roughness (RMS < 0.26 μm). The conventional micrometric grade, featured by the presence of high asperities originated by the large crystals, suffered a higher abrasive action from the loose hard particles carried by the chip flow and from rubbing at the contact with the workpiece.

References

[1] Chou YK, Liu J. CVD diamond tool performance in metal matrix composite machining. Surf. Coat. Technol. 2005; 200: 1872-1878.

[2] Arumugam PU, Malshe AP, Batzer SA. Dry machining of aluminum-silicon alloy using polished CVD diamond-coated cutting tools. Surf. Coat. Technol. 2006; 200: 3399-3403.

[3] Almeida FA, Oliveira FJ, Sousa M, Fernandes AJS, Sacramento J, Silva RF. Machining hardmetal with CVD diamond direct coated ceramic tools: effect of tool edge geometry. Diam. Relat. Mater. 2005; 14: 651-656.

[4] Haubner R, Lux B. Deposition of ballas diamond and nano-crystalline diamond. Int. J. Refract. Met. Hard Mater. 2002; 20: 93-100.

[5] May PW, Smith JA, Mankelevich YA. Deposition of NCD films using hot filament CVD and Ar/CH_4/H_2 gas mixtures. Diamond Relat. Mater. 2006; 15: 345-352.

[6] Toprani N. Catledge SA, Vohra YK. Interfacial adhesion and toughness of nanostructured diamond coatings. J. Mater. Res. 2000; 15: 1052-1055.

[7] Gupta S, Weiner BR, Morell G. Synthesizing nanocrystalline carbon thin films by hot filament chemical vapor deposition and controlling their microstrucutre. J. Mater. Res. 2002; 17: 1820-1833.

[8] Catledge SA, Borham J, Vohra YK, Lacefield WR, Lemons JE. Nanoindentation hardness and adhesion investigations of vapour deposited nanostructured diamond films. J. Appl. Phys. 2002; 91: 5347-5352.

[9] Vojs M, Veselý M, Redhammer R, Janík J, Kadlecíková M, Danis T, Marton M, Michalka M, Sutta P. Double bias HFCVD multilayer diamond films on WC-Co cutting tools. Diam. Relat. Mater. 2005; 14: 613-616.

[10] Amaral M, Oliveira FJ, Belmonte M, Fernandes AJS, Costa FM, Silva RF. Hot-filament chemical vapour deposition of nanodiamond on silicon nitride substrates. Diam. Relat. Mater. 2004; 13: 643-647.

[11] Almeida FA, Fernandes AJS, Silva RF, Oliveira FJ. Re-sharpenable thick CVD diamond-coated Si_3N_4 tools for hardmetal turning. Surf. Coat. Technol. 2006; 201: 1776-1782.

[12] Köpf A, Feistritzer S, Udier K. Diamond coated cutting tools for machining of non-ferrous metals and fibre reinforced polymers. Int. J. Refract. Met. Hard Mater. 2006; 24: 354-359.

[13] Salvadori MC, Martins DR, Cattani M. DLC coating roughness as a function of film thickness. Surf. Coat. Technol. 2006; 200: 5119-5122.

[14] Brühne K, Kumar KVK, Fecht HJ, Gluche P, Flöter A. Nanocrystalline HF-CVD grown diamond and its industrial applications. Rev. Adv. Mater. Sci. 2005; 10: 224-228.

[15] Cullity BD. Elements of X-ray Diffraction, 2a ed., Addison-Wesley Series in Metallurgy and Materials, Addison-Wesley, 1978.

[16] Abreu CS, Amaral M, Fernandes AJS, Oliveira FJ, Silva RF, Gomes JR. Friction and wear performance of HFCVD nanocrystalline diamond coated silicon nitride ceramics. Diam. Relat. Mater. 2006; 15: 739-744.

[17] Oles EJ, Inspektor A, Bauer CE. The new diamond-coated carbide cutting tools. Diam. Relat. Mater. 1996; 5: 617-624.

Acknowledgements

F.A. Almeida's work is supported by Programme Alban, European Union Program of High Level Scholarships for Latin America, identification number E03D06378BR. M. Amaral acknowledges FCT for the grant SFRH/BD/9272/2002. Funding from FCT project POCI/CTM/59449/2004-"NANODIAM" is gratefully acknowledged.

4.4 *The machining of EDM graphite with CVD diamond direct coated Si_3N_4*

Micro- and nano-crystalline CVD diamond coated tools in the turning of EDM graphite

F. A. Almeida[1], J. Sacramento[2], F. J. Oliveira[1], R. F. Silva[1]

[1] Department of Ceramics and Glass Engineering, CICECO, University of Aveiro, 3810-193 Aveiro, Portugal

[2] High School of Technology and Management, Águeda, Portugal

(Journal of Nanoscience and Nanotechnology, submitted)

Abstract

Electrical discharge machining (EDM) is a widely used technique, namely in metal mould shaping. High quality EDM graphite is the foremost choice as electrode material but the random oriented graphite aggregates cause an abrasive action over the tools used in its machining. In order to guarantee tight tolerances and good surface finishing, wear-resistant diamond tools are the best option. In this work, microcrystalline (MCD) and nanocrystalline (NCD) CVD diamond coated inserts are used in turning operations. Cutting forces were always very low (< 20 N) within the cutting speed (200-800 $m \cdot min^{-1}$) and feed (0.02-0.2 $mm \cdot rev^{-1}$) ranges. Long turning tests of at least 15 minutes reached a KT ~ 22 μm (the coating thickness) for 10 km of cutting length, although without affecting the cutting performance. Another important result is the absence of diamond film delamination showing the high adhesion level offered by the silicon nitride ceramic substrates for CVD diamond coating. The smoother NCD coatings allowed to obtain a better workpiece surface roughness (Ra ~ 0.23 μm) than MCD ones (Ra ~ 0.37 μm)

Keywords: *Cutting tools, Diamond film, Hot filament CVD, EDM graphite.*

1. Introduction

Electrical discharge machining (EDM) is used to shape high-performance, intricate and accurate parts in leading aeronautical, automotive and moulds manufacturing companies. Graphite is the most widely used material for EDM electrodes due to its low cost and especially because of its high temperature resistance in the spark arc when compared, for instance, with copper [1]. High quality EDM graphite is fine grained and has low porosity content. The different C-C bond strength in the basal planes and between adjacent layers confers to graphite anisotropic mechanical and electrical properties, namely a considerable high strength and electrical conductivity in the basal plane [2]. An important consequence of the strong variation of mechanical strength with direction is the difficult machinability of graphite. In graphite machining, the random oriented graphite aggregates lead to a very abrasive powdery chip. This feature explains why diamond tools became the best solution for this application. The first option was the polycrystalline diamond (PCD) grade: the benefits of using PCD inserts comparing to conventional cemented carbide ones in turning of graphite were proved at high cutting speeds, such as $500 m \cdot min^{-1}$, where the tool life increased almost three-fold [3]. However, the graphite debris created by machining abrade the cobalt binding phase of the PCD tools, leading to diamond particles loosening and, consequently, tool wear. An improving solution is the use of binderless CVD diamond coatings. A tool-life gain of more than 10 times was reported in milling operations with CVD diamond cemented carbide coated tools, comparing to uncoated ones [4]. An EDM graphite producer reported an improved life of 25 to 30 times of diamond coated cemented carbides tools comparing to TiN-coated ones in turning operations [5]. An impressive gain of 242 percent in cost per graphite part produced is estimated by Myers [6] in an economic comparison projection between CVD diamond coated and uncoated cemented carbide end mills. In the same work, a few examples of parts machining, like EDM electrodes milling for making injection molds, attested the real benefit of CVD diamond showing 15 times gains in tool life and tight accuracies.

This work consists in the evaluation of the cutting performance of hot filament CVD diamond coated silicon nitride (Si_3N_4) ceramic tools in turning of EDM graphite. This substrate is the best choice regarding the inferior risk of film delamination due to the

chemical compatibility and low thermal expansion mismatch to diamond [7]. The influence of cutting parameters (cutting speed: 200 to 800 $m \cdot min^{-1}$ and feed: up to 0.2 $mm \cdot rev^{-1}$) on the cutting forces and tool wear were evaluated for different cutting tool geometries (round and triangle cutting tips) and different CVD diamond coatings (micro- and nano-crystallite sizes).

2. Experimental

The Si_3N_4 ceramic cutting tools were full densified by pressureless sintering at a dwelling temperature of 1750ºC for 2 hours, in an atmosphere of 0.1 MPa N_2, using aluminium and yttrium oxides as densification additives. The weight percentages were: 89.3% α-Si_3N_4 (Starck grade M11), 7.0% Y_2O_3 (Starck grade C) and 3.7% Al_2O_3 (CT-3000SG, Alcoa). The sintered ceramic parts were ground to standard normalized geometries of round (RNMN1003M0FN) and triangle (TNMN160308FN) shaped inserts. The rake face was lapped with 15 μm diamond slurry in an iron/polymer plate, followed by dry etching with CF_4 plasma for a controlled micro-roughening purpose. Before diamond deposition, the ceramic inserts were ultrasonically seeded in a *n*-hexane suspension of diamond powder (0.5-1 μm) during 1 hour.

Micro- (MCD) and nano- (NCD) crystalline diamond depositions were made in a hot filament chemical vapour deposition (HFCVD) reactor, using 4 straight and parallel tungsten wires as gas activators. Almost all the MCD and NCD deposition parameters were similar: filament temperature = 2300 ºC; substrate temperature = 850ºC; total pressure = 2.5 kPa; total gas flow= 100 sccm; deposition time = 7.5 hours. The unlike deposition parameter was the methane/hydrogen volume ratio. To deposit MCD diamond, a volume ratio of 0.02 (CH_4/H_2) was used, while in the case of NCD, this ratio was 0.03. The film thickness of both diamond grades was 22 ± 2 μm and the rake face surface roughness RMS values were 0.55 μm, for the MCD grade, and 0.18 μm, for the NCD one.

Dry turning tests were done in an industry facility, using a CNC lathe (Mori Seiki). The ISO code of the tool holders were as follows: CRSNR2525M 06 and CTGNR2525M

16. A three-axis piezoelectric dynamometer platform (Kistler 9257BA) was coupled into the lathe, where the tool holder is fixed. In this way, the signals were amplified in a Kistler 5011 apparatus and connected to a PC by coaxial cables and an acquisition board (PCMCIA, Keithley). The analogical signals were converted and filtered in real time using dedicated software. The variable cutting parameters were the cutting speed (200-800 $m \cdot min^{-1}$) and feed (0.02-0.2 $mm \cdot rev^{-1}$), while the depth-of-cut was fixed to 0.5 mm. The overall set of performed tests is given in Table I. The main resultant wear modes, flank wear (VB) and crater depth wear (KT), were measured accordingly with the ISO 3685 standard[8].

Table I. Overall set parameters used in the graphite turning.

Coating	Geometry	v ($m \cdot min^{-1}$)	f ($mm \cdot rev^{-1}$)	L (m)	t (min)	n (rpm)
MCD	Round	200	0.02	1499	7.5	754
		400		1481	3.7	1526
		600		1464	2.4	2316
		800		1446	1.8	3126
NCD		200		1375	6.9	822
		400		1393	3.5	1623
		600		1410	2.4	2404
		800		1428	1.8	3165
MCD		400	0.05	394	1.0	2297
			0.1	193	0.5	2339
			0.2	95	0.2	2383
NCD			0.05	415	1.0	2179
			0.1	204	0.5	2217
			0.2	100	0.2	2256
MCD	Triangle	600	0.02	1357	2.3	2498
				10075*	17.8*	2832*
NCD				1339	2.2	2531
				8936*	14.9*	3214*

* Values corresponding to the long cutting tests after 8 passes. The spindle speed (n) is at the last pass.

The initial dimension of the EDM graphite cylindrical bar used in the turning tests was ∅85.46 mm × 113 mm. The density of the graphite workpiece was 1.88 $g \cdot cm^{-3}$, as measured by immersion in ethylene-glycol, and falls in the upper limit of the densities range available in the market (1.6-1.9 $g \cdot cm^{-3}$) [9,10]. Nominal mechanical characteristics are:

Shore hardness = 62; flexural strength = 80 MPa; compressive strength = 112.6 MPa. The grain size is about 10 μm. The ASTM D1762-84 standard [11] was used to determine moisture, volatile matter and ash content in wood charcoal, and so the fixed carbon. The analysis of carbon content revealed the high purity of the workpiece, with a value of about 98 wt.%. A volatile matter amount of about 1.7 wt.% was detected and may be constituted by residues of hydrocarbons, resulted from the graphite manufacturing [2]. Low values of moisture (0.2 wt%) and ash content (0.14 wt%) were found. The last one has an important effect on the graphite machinability, since it is formed by metallic oxides that have a high abrasive nature [3].

3. Results and Discussion

The diamond coated Si_3N_4 round tools were employed in a first set of turning tests, Table I, due to the large number of cutting locations available in the cutting edge of each insert (from 4 to 8, depending on the depth-of-cut). Figs. 1a) and 1b) present the values of the three components of the cutting force as a function of the cutting speed when using MCD and NCD coated tools, respectively. It can be seen that, irrespectively of the diamond grain size, the cutting forces are very low and do not show a clear dependence on the cutting speed. This behaviour markedly differs from that observed in metal machining, where higher speeds lead to an overheating of the workpiece/tool contact point, with net effects on the cutting forces. In that case, cutting forces can decrease due to the higher metal ductility, but, conversely, they may rise if the tool wear rate increases. Indeed, in the machining of graphite the absence of heating and high forces at the tool cutting edge is a common evidence [12,13]. Unlike metals, when graphite is machined a continuous chip does not shear off from the workpiece. This is because brittle fracture of the polycrystalline aggregates takes place instead of plastic deformation. Also, the energy required for the initiation and propagation of the cracks is much lower [12,13]. A combination of crushing, by compressive stresses action, and flaking, from tensile stresses, occurs. Flaking leads to larger fragment particles and it is undesirable, particularly in finishing operations. Using of insert geometries with negative rake angles, such as in the present work, increases the

compressive stresses, leading to finer graphite soot formation and better workpiece surface finish [12].

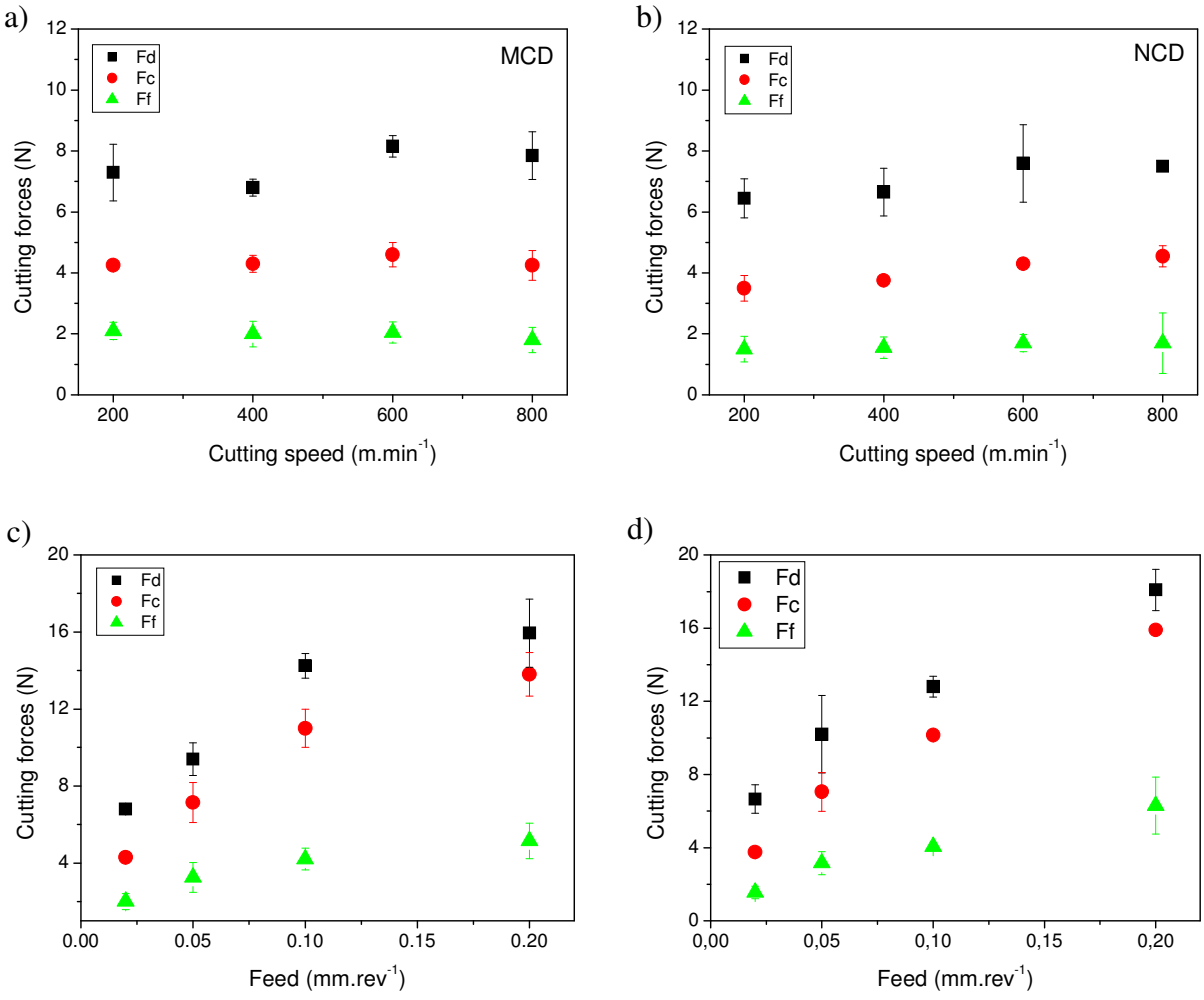

Fig. 1. Cutting forces in function of: a-b) cutting speed (at f = 0.02 mm·rev^{-1}); c-d) feed (at v = 400 m·min^{-1}) for MCD and NCD silicon nitride coated tools.

The graphite particulate aggregates cause a grooving abrasive action on the cutting edge, leading to a very narrow regular depression on the rake face of the tool (crater wear), Fig. 2. Figs. 2a),b) and 2c),d) are SEM micrographs of the MCD and NCD diamond tools after testing at lower and upper cutting speed limits of 200 and 800 m·min^{-1}, respectively. Besides crater wear, another wear mode is visible: the small notch at the entrance of the tool on the workpiece. No significant differences among the behavior of the diamond coatings at different cutting speeds could be detected. Nevertheless, a closer inspection and the measurement of the crater depth (KT) show that there is an almost linear decrease of

KT with increasing cutting speed, as plotted in Fig. 3. Again, no considerable difference between MCD and NCD diamond coatings was noticed confirming that the rake face roughness did not influence neither the cutting forces nor the wear parameters. This behavior is very distinct from that reported in a previous work on hardmetal machining, where the large surface roughness of the MCD coatings led to increased friction with the chip, higher cutting forces and larger tool wear with compared with NCD coatings [14]. The reduction on tool wear with cutting speed in graphite turning is probably due the easier fragmentation of such a brittle material at high impact rates. As particle aggregates sizes diminish, not only the abrasive action on the rake face is lesser but also dust is more effectively evacuated from the machining area. The improvement of the cutting performance, namely of the tool life, for higher cutting speeds was also reported by other authors [12].

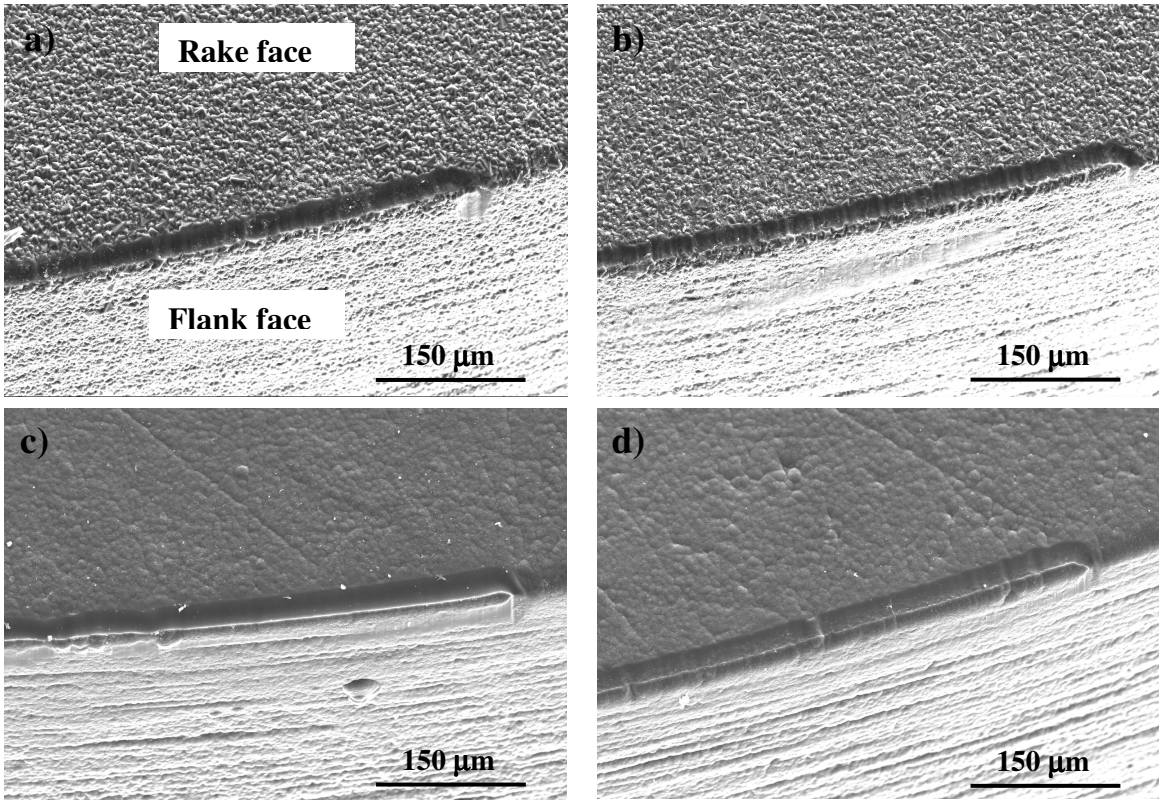

Fig. 2. Crater and notch wear for: a-b) MCD and c-d) NCD at the lowest (200 m·min^{-1}) and highest (800 m·min^{-1}) cutting speed, respectively (f = 0.02 mm·rev^{-1}; L ~ 1400 m).

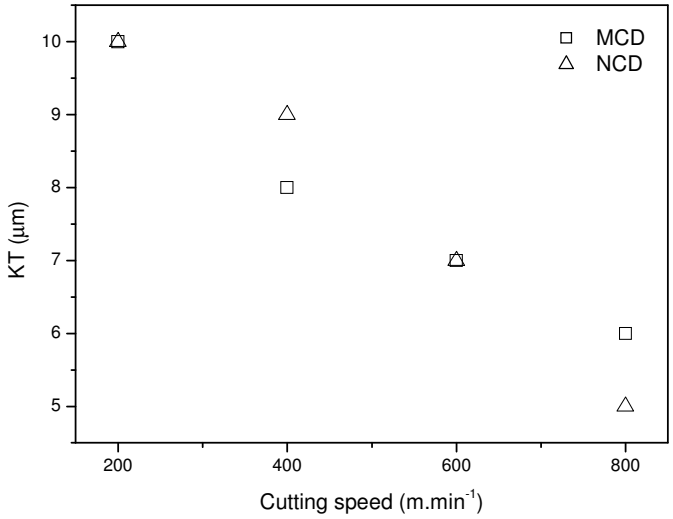

Fig 3. Crater depth (KT) in function of cutting speed (f = 0.02 mm·rev^{-1}; L ~ 1400 m).

Another important feature visible in Fig. 2 is the absence of flank wear at the main tool/workpiece contact area, resulting in the preservation of the cutting edge. This assured that the tolerances are kept within a hundredth of a millimeter throughout the workpiece length. Only at the minor cutting edge/workpiece contact, a small wear land on the flank face (VB_C of about 40 to 49 μm) was formed, as can be seen in Fig. 4. The machined workpiece, which may have an irregular surface due to the fracture events during turning, rubs this area and causes a small abrasive effect on the cutting tool. Here, some differences are seen when using MCD and NCD diamond tools, since the workpiece rubs the top asperities of the diamond crystals, in the case of MCD, while a more polished area results, in the case of the smoother NCD one, Figs. 4a) and 4b respectively. This was reflected on the workpiece finishing, with Ra values of 0.37 ± 0.04 μm using MCD coated tools and 0.23 ± 0.05 μm using NCD ones.

Regarding the influence of the feed value when passing from 0.02 to 0.2 mm·rev^{-1}, an increment of about 2 to 3 times of the cutting forces occurred for both the MCD and NCD tools, Figs. 1c) and 1d), although their magnitude remained very low. Generally, the increase of feed leads to higher compressive stresses and, as consequence, generates higher cutting forces [15]. The wear of the tools was negligible in all cases, meaning that the

machining of graphite by diamond tools can be done in a wide range of parameters, accordingly with their function and geometry. For instance, when machining a thin and intricate wall section in a brittle material, the use of small feed values is recommended to avoid any risk of breakage and chipping by the tool pressure [3].

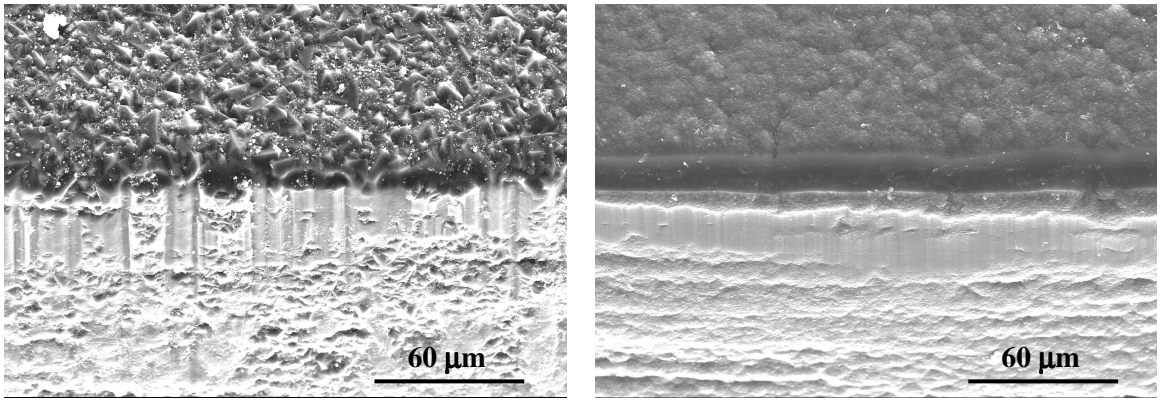

Fig. 4. Flank wear at the end of the minor cutting edge of a) MCD and b) NCD tools (v = 800 m·min^{-1}, f = 0.02 mm·rev^{-1}; L ~ 1400 m).

For turning of complex profiles, more flexible tool geometries than round ones are required and so triangular shaped inserts were also tested. The relatively high fracture toughness (about 6 MPa·m$^{-1/2}$) of silicon nitride ceramics [16] successfully allowed the use of this less resistant edge geometry, and no signs of cracks or edge breakage were observed after the turning tests. Fig. 5 presents values of the cutting forces for these tools and compares them with the round shaped ones when turning at the same cutting parameters of speed= 600 m·min^{-1}; feed= 0.02 mm·rev^{-1}; depth-of-cut= 0.5 mm. Corner and edge radius, clearance, rake and tool entrance angles are some of the key factors that influence the progression and magnitude of the cutting forces [17,18]. It can be seen that the magnitude of the F_d component of the cutting force is much smaller for the triangular tool comparing to the round shaped one. This is a consequence of the smaller included angle and corner radius of the former, by diminishing tool/workpiece contact area, and so, the pushing back force reaction exerted by the workpiece over the cutting tool. The relative magnitude of the other cutting forces also changed. The entrance angle of the triangular shaped tool of 91º, given by the tool holder, implies that the depth of cut is performed mostly by the main cutting edge, while in the case of the round tools the cut is isometric, and the depth of cut

is distributed over the main and minor cutting edges. Such differences could account for the higher relative value of the feed force (F_f) in the case of the triangle tools in comparison with the round ones. In the case of chip formation, the increase of feed force also means an increase in the shear stress acting on the rake face [18]. As a result of the different force behaviour, the wear features of the triangular tools (VB_C≈36 μm and KT≈5 μm) were slightly less than the reported values for the round ones in the same cutting conditions.

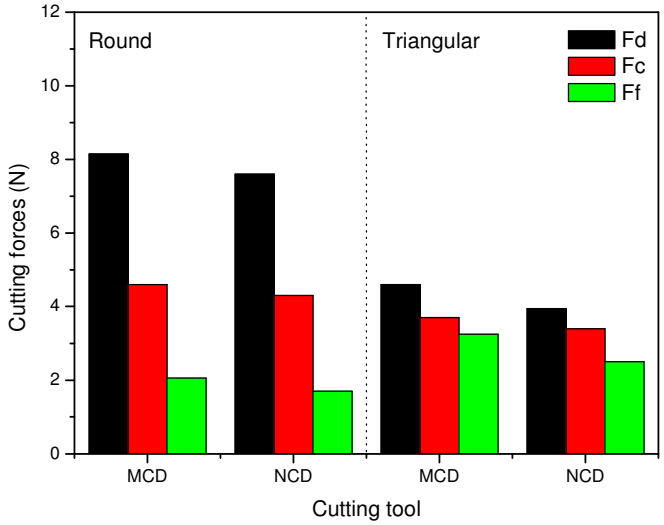

Fig. 5. Cutting forces in function of the different tool geometries and diamond coatings (v = 600 m·min^{-1}, f = 0.02 mm·rev^{-1}).

The triangular shaped tools were finally tested in long turning operations (8 passes, Table I). Representative SEM micrographs of the MCD and NCD edges (30º tilted and top view) are shown in Figs. 6a),b) and 6c),d), respectively. The development of flank wear at the end of the edge and the crater formation is clearly seen on both kinds of diamond grades. The measurements of VB_C showed values of 113 and 158 μm and KT values of 21 and 24 μm for the MCD and NCD diamond tools, respectively. The crater in the NCD tool reached the Si_3N_4 substrate, as can be seen in Fig. 6d, but without affecting the cutting forces and cutting ability. The inset in Fig. 6d shows the revealed Si_3N_4 microstructure by the polishing action of the abrasive graphite particles, where the hexagonal β-Si_3N_4 grains

are clearly discernible contrasting to the light gray vitreous intergranular phase. Due to the high spindle speed (~3000 rpm) used in these tests, vibrations and workpiece bending were sensed which lead to a variation on the workpiece Ra value from 1.29 μm near the chuck to 3.04 μm at the end. Nevertheless, the workpiece tolerances were maintained in both MCD and NCD long turning cases.

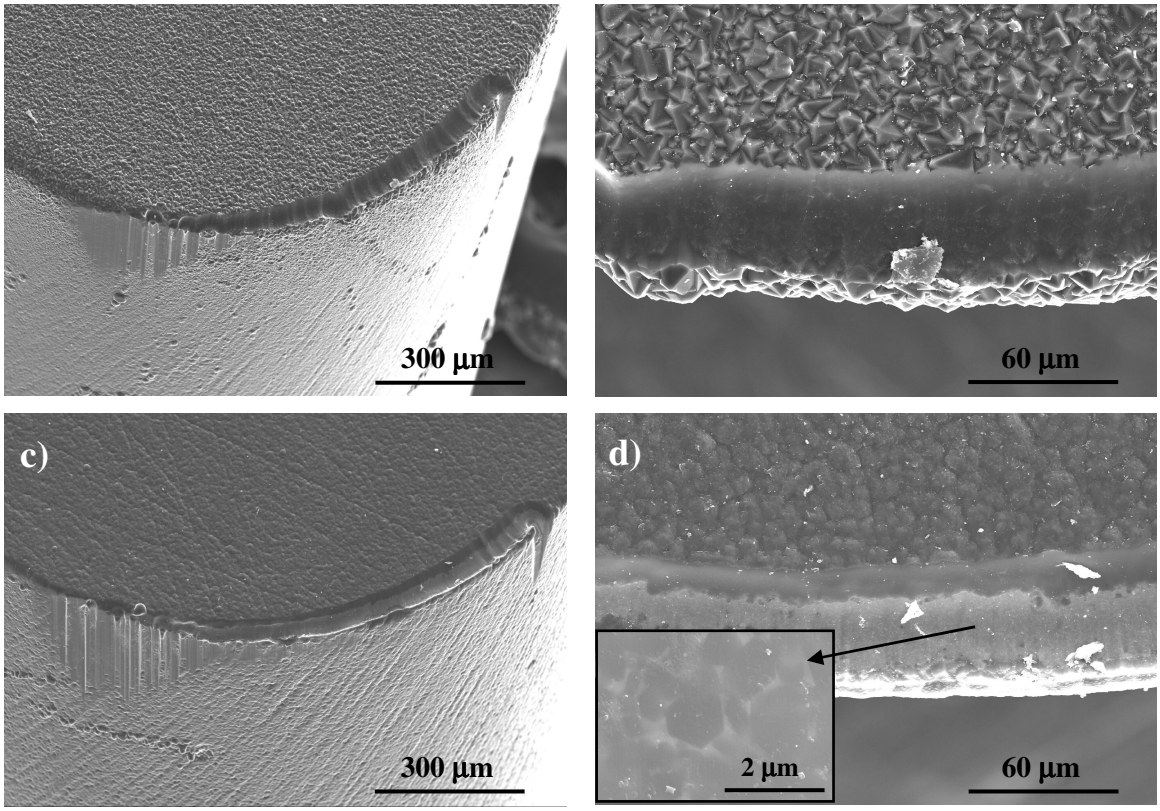

Figure 6**.** Rake and flank faces of a) MCD and c) NCD tools; b) and d) are the respective top view, where the crater on the rake face can be seen. The inset on Fig. c) presents the high magnification of the polished silicon nitride by the graphite particles on the surface of the NCD coated tool ($v = 600\ m \cdot min^{-1}$, $f = 0.02\ mm \cdot rev^{-1}$; L ~ 10 km).

These tests showed the potential of both MCD and NCD diamond coated cutting tools, even at situations where vibrations takes place. A coating endurance life of at least 45 minutes or 30 km of machined length can be achieved by these tools, considering the 3 edges per tool. The absence of diamond film delamination is an important point and confirms that silicon nitride ceramic tool is a superior substrate for CVD diamond coatings than hardmetal. A recent work published on EDM graphite machining with different

diamond coatings on hardmetal tools shows that, regarding the different diamond crystal sizes, delamination of the coatings at the rake face occurred between 80 and 1480 m of cutting length [13]. In that work, the cutting speed varied in the range 100-400 $m \cdot min^{-1}$, the depth of cut and feed were fixed at 0.3mm and 0.05 $mm \cdot rev^{-1}$, respectively, and a lower corner radius was used (0.4mm) than that of the present experiments (0.8mm).

4. Conclusions

Microcrystalline (MCD) and nanocrystalline (NCD) diamond coated Si_3N_4 ceramic inserts were successfully used to turn EDM graphite electrodes for the mould industry.

Although the cutting forces were very low (< 20 N), the abrasive action of graphite aggregates caused small crater and flank wear lands. The crater depth values (5 μm <KT<10 μm) after tests in the cutting speed range of 200-800$m \cdot min^{-1}$ showed that there is a linear inverse relationship between these parameters. This is attributed to the easier fragmentation of graphite aggregates at high speed values. Flank wear occurred only at the end of the cutting edge/workpiece contact with small magnitude (max. 49 μm).

No significant differences were observed between MCD and NCD films, except the small advantage of the smoother NCD coatings on the workpiece finishing: for the same cutting parameters, a workpiece roughness of Ra ~ 0.23 μm was obtained with NCD tools, while a Ra of ~ 0.37 μm was achieved by MCD ones.

Long turning tests of at least 15 minutes reached a KT ~ 22 μm (the coating thickness) after about 10 km of cutting length, although without affecting the cutting performance as the cutting edge and the flank face kept their integrity. The absence of diamond film delamination is a key point and shows the superiority of silicon nitride ceramics as substrate material for diamond coated tools.

Acknowledgements

F.A. Almeida's work is supported by Programme Alβan, European Union Program of High Level Scholarships for Latin America, identification number E03D06378BR. Funding from FCT project POCI/CTM/59449/2004-"NANODIAM" is gratefully acknowledged.

References

[1] Xueling Y, Zhengzhong Z, Jinliang C. Electrode erosion of a high energy impulse spark gap switch. Plasma Sci. Technol. 2005; 7: 3157-3160.

[2] Pierson HO. Handbook of carbon, graphite, diamond and fullerenes: properties, processing and applications. Noyes Publications, New Jersey. U.S.A. (1993).

[3] Cook MW. A guide to machining carbon and graphite with syndite PCD. Ind. Diam. Review 1994; 54: 174-178.

[4] Kanda K, Takehana S, Kanda K, Takehana S, Yoshida S, Watanabe R, Takano S, Ando H, Shimakura F. Application of diamond-coated cutting tools. Surf. Coat. Technol. 1995; 73: 115-120.

[5] Mucha T. Machining graphite. EDM Today November/December 2003. http://us.gfac.com/intech/newsroom/documents/graphite1.pdf

[6] Myers D. Machining graphite using diamond-coated tools - Part 3: Machine tool considerations and application results. MoldMaking Technology Online. http://www.moldmakingtechnology.com/articles/129905.html

[7] Almeida FA, Belmonte M, Fernandes AJS, Oliveira FJ, Silva RF. MPCVD diamond coating of Si_3N_4-TiN electroconductive composite substrates. Diam. Relat. Mater. 2007; 16: 978-982.

[8] International Standard ISO 3685 (1993). Tool life testing with single-point turning tools.

[9] Cross-reference guide to comparing brands & grades of EDM graphite. Intech EDM. http://www.intech-edm.com/newsroom/documents/graphite.pdf

[10.] Characteristics of isotropic graphite. Toyo Tanso Co. Ltd. http://www.toyotanso.co.jp/Products_SpecialGraphite_detail_en.html

[11] Standard test method for chemical analysis of wood charcoal, ASTM D 1762-84 (reapproved 2001).

[12] Schroeter RB, Kratochvil R, Gomes JO. High-speed finishing milling of industrial graphite electrodes. J. Mater. Proc. Technol. 2006; 179: 128-132.

[13] Cabral G, Reis P, Polini R, Titus E, Ali N, Davim JP, Grácio J. Cutting performance of time-modulated chemical vapour deposited diamond coated tool inserts during machining graphite. Diam. Relat. Mater. 2006; 15: 1753-1758.

[14] Almeida FA, Amaral M, Oliveira FJ, Silva RF. Machining behaviour of silicon nitride tools coated with micro-, submicro and nanometric HFCVD diamond crystallite sizes. Diam. Relat. Mater. 2006; 15: 2029-2034.

[15] Dahlman P, Gunnberg F, Jacobson M. The influence of rake angle, cutting feed and cutting depth on residual stresses in hard turning. J. Mater. Proc. Technol. 2004; 147: 181-184.

[16] Almeida FA, Bóia H, Santos C, Monteiro J, Oliveira FJ, Silva RF. Electroconductive ceramic composites for cutting tools. Mater. Sci. Forum 2006; 514-516: 638-642.

[17] Trent EM, Wright PK. Metal Cutting. 4th ed., Woburn: Butterworth-Heinemann, 2000.

[18] Kopac J. Cutting forces and their influence on the economics of machining. J. Mech. Eng. 2002; 48: 121-132.

Conclusions

Chapter 5

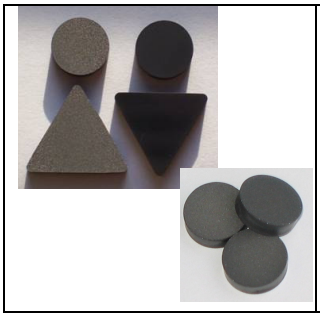

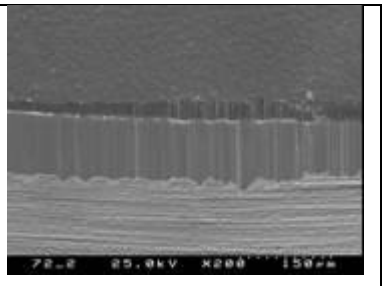

CVD diamond cutting tools with high quality and promising behaviour in machining of hard and abrasive materials were developed. The results showed that Si_3N_4 and Si_3N_4-TiN ceramic are effective substrates, attaining high adhesion levels to the diamond coating. The addition of TiN to Si_3N_4 matrix presented a slight decrease in hardness of about 3% but an increment of the fracture toughness of approximately 20%, corresponding to values up to 7.5MPa·$m^{1/2}$ for the composite with 30vol.% TiN An effective electroconductive network was achieved with TiN content above 23 vol.%, making possible the use of electrodischarge machining. TiN has a higher coefficient of thermal expansion (CTE) than Si_3N_4, consequently, the CTE values increase with the increment of the TiN content, and so does the thermal expansion mismatch between the substrate and the diamond film. The estimated thermal stresses were found to be low and tensile (0.90 GPa) for the monolithic Si_3N_4 substrate, changing to a compressive nature for the Si_3N_4–TiN composite substrates (−1.90 GPa for Si_3N_4–30 vol.% TiN). Brale imprints demonstrated that the subsurface radial cracks decreased in number and length when TiN was added to Si_3N_4, this behaviour being related to increasing fracture toughness of the composite. No CVD diamond film delamination took place at 600 N for every kind of substrate, but at 1000 N partial or full circumferential cracking was observed for the monolithic Si_3N_4 sample or the high content TiN grades. The optimal behaviour (no film delamination under 1000 N), which corresponds to the minimal residual stress magnitude, was observed for the Si_3N_4–9 vol.% TiN substrate.

Three different diamond structures could be developed in the HFCVD reactor: nano – NCD - (27 nm), submicron- SMCD - (43 nm) crystallite sizes, and conventional 5-12 μm micrometric – MCD - grain size types. A low surface roughness was attained by the nano and submicron grades (RMS 0.18-0.26 μm), comparatively to the microcrystalline (RMS 0.55-0.78 μm) one. Optical and SEM observations of Brale indentation imprints in the range 50-1700N, and measurements of the corresponding circumferential crack radii, allow the ranking of the different diamond grades as NCD→SMCD→MCD, from the lowest to the highest adhesion resistance. The lowest graphitic phase content and the highest hardness explain the best behaviour of the MCD grade. On the contrary, the deposition conditions for the NCD coating, cause a less effective chemical bond to the ceramic substrate. The MCD coating supported a normal load of 1600N without spalling-off and presented an interfacial crack resistance of 12.0 N·μm^{-1}. The SMCD presents a value of

interfacial crack resistance of 8.3 $N \cdot \mu m^{-1}$ and NCD of 6.8 $N \cdot \mu m^{-1}$. The enhanced adhesion level of these films when compared with the literature comes from the more effective mechanical interlocking provided by CF_4 plasma etching of the substrate prior to the deposition.

The coatings morphology and surface roughness of the different diamond grades resulted in dissimilar cutting performance in dry turning of WC–25 wt.% Co at 15 $m \cdot min^{-1}$ of cutting speed, 0.1 mm depth-of-cut and 0.1 $mm \cdot rev^{-1}$ feed. The submicrometric grade presented the best behaviour regarding cutting forces, tool wear and workpiece surface finishing. For this coating, the depth-of-cut, main and feed cutting forces attained the lowest values, respectively of F_d=150 N, F_c=100 N and F_f=15 N. Also, it presented the best combination of wear modes (KM=30 μm, KT=2 μm and VB=110 μm) and workpiece surface finishing (Ra=0.2 μm).

With respect to the effect of the cutting edge geometry, the cutting forces increased with the bluntness of the cutting edge in the following order: sharp<chamfer<hone. Although wear of the cutting edges increases by aggravating the machining conditions, sharp edge tool integrity could be kept for a machining speed of 15 m min^{-1}, depth of cut of 0.1 mm for feed rates up to 0.15 $mm \cdot rev^{-1}$. A good workpiece finishing was obtained for the same cutting speed and depth of cut but for the lowest feed rate of 0.03 $mm \cdot rev^{-1}$. Film delamination and edge fracture occurred for honed edge tools at all tested conditions. Rough machining was performed in turning of three hardmetal compositions with a thick diamond film (150 μm). The machining parameters were adjusted to suit different hardmetal grades, the speed and feed being respectively reduced to 20 $m \cdot min^{-1}$ and 0.1 $mm \cdot rev^{-1}$ for the lowest Co binder grade (18 wt.%), while for the coarser WC grades containing larger amounts of Co, the speed and feed were kept at 30 $m \cdot min^{-1}$ and 0.15 $mm \cdot rev^{-1}$, keeping the depth of cut at 0.2 mm. The lower Co content hardmetal grade, GD40, yielded the largest cutting force and wear when the same machining parameters for GD50 and GD60 were used. The higher Co content grade induced easy formation of built up edge resulting in discontinuities in the cutting force. Due to the wear, the cutting edge recession occurs and flank wear increases. This change of the cutting edge geometry increases the cutting force and reaches a threshold value corresponding to Fd~700 N above which the tool fails. Wear of the CVD diamond tool occurs due to abrasion of the rake and

flank faces mainly by diamond debris. Diamond microchipping, enhanced by the adherent Co built-up-edge (BUE), and transgranular fracture are the source of the loose diamond particles. A tool life criterion of VB≈diamond thickness was considered allowing cutting lengths of 2000 m per tool under optimised dry turning conditions. When using cutting fluids, increased tool life is easily achieved due to reduction of Co adhesion and enhancement of diamond debris removal from the cutting edge.

In the turning of EDM graphite, the cutting forces were very low (< 20 N), but the abrasive action of graphite aggregates caused small crater (5 μm <KT<10 μm) and flank (max. 49 μm) wear lands in the cutting speed range of 200-800m·min^{-1}. No significant differences were observed between MCD and NCD films, except the small advantage of the smoother NCD coatings on the workpiece finishing: for the same cutting parameters, a workpiece roughness of Ra ~ 0.23 μm was obtained with NCD tools, while a Ra of ~ 0.37 μm was achieved by MCD ones. Long turning tests of at least 15 minutes reached a KT ~ 22 μm (the coating thickness) after about 10 km of cutting length, although without affecting the cutting performance as the cutting edge and the flank face kept their integrity. Once more, the absence of diamond film delamination showed the superiority of silicon nitride ceramics as substrate material for diamond coated tools.

Chapter 6

Perspectives and future work

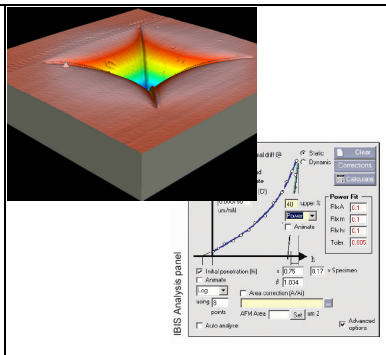

The following works are thought to be made to better characterize and test the cutting tools developed during this thesis:

- Study of the interface nature and microstructure between the diamond grains and between the film and substrate by high resolution transmission electron microscopy TEM.

- Evaluation of the mechanical properties (compression and flexural strengths) of the bare ceramic cutting tools and coated with the different diamond coatings at room and high temperatures (about 500ºC) using an universal mechanical testing machine equipped with a furnace with controllable atmosphere.

- Thermo-mechanical tests applying a cyclic force upon the surface of the coatings to evaluate the fatigue response and diamond film adhesion.

- Study of polishing procedure of microcrystalline thick diamond coatings, evaluation of the resulted surface quality by Raman spectroscopy, X-Ray diffraction and optical, electronic and atomic force microscopy.

- Deposition bilayered coatings (thick nanocrystalline diamond onto thin microcrystalline diamond coatings) and comparison with the polished ones in terms of surface quality as well as in cutting action.

- Study of multi-layered nano-micro diamond coatings and evaluation in order to improve fracture toughness.

- Use of different tool inserts geometries (square, rhombic) and angles (neutral and positive) in machining tests.

- Evaluation of the scaling up possibilities of the diamond coated cutting tools manufacture by the hot filament technique.

- Machining tests on other important materials, such as: carbon fiber reinforced plastics, alluminium silicon alloys and metal matrix composites.